Physik Department

Dynamic structure formation of DNA-coated colloids guided by enzymatic reactions

Dissertation
von

Henry Dehne

Technische Universität München

Physik Department

Lehrstuhl für Zellbiophysik-E27

Dynamic structure formation of DNA-coated colloids guided by enzymatic reactions

Henry Dehne

Vollständiger Abdruck der von der Fakultät für Physik der Technischen Universität München zur Erlangung des akademischen Grades eines

Doktors der Naturwissenschaften (Dr. rer. nat.)

genehmigten Dissertation.

Vorsitzender: Prof. Dr. Martin Zacharias

Prüfer der Dissertation: 1. Prof. Dr. Andreas Bausch

2. Prof. Dr. Friedrich C. Simmel

Die Dissertation wurde am 19.02.2020 bei der Technischen Universität München eingereicht und durch die Fakultät für Physik am 01.07.2020 angenommen.

Abstract

Self-assembly of colloidal particles is a powerful concept to build functional materials, as a wide range of material properties can be addressed by the choice of the single building blocks and their interactions. DNA-coated colloids have proven to be well suitable, as the programmability and specificity of pre-crafted DNA allows a precise control of the colloidal interactions and results in the formation of a diverse set of structures. In this thesis, a binary system of micrometer-sized DNA-coated colloids is used to control the process of diffusion-limited cluster aggregation. The specific control of the binding affinities was deployed to study the impact of colloidal structure formation on the mechanical properties of a colloidal-hydrogel. It was shown that the colloidal gelation results in an increased toughness of the hydrogels of approx. 35, indicating that the colloidal structure formation yields access to significant synergetic effects in polymer–colloid hybrid gels. In addition, the binding affinities of the colloids were controlled dynamically by using enzymatic reactions. An antagonistic set of enzymatic reactions was used to polymerize and degrade RNA strands in order to achieve autonomous and transient colloidal aggregation, which was modulated in terms of lifetime and cluster size. Moreover, local restriction of enzymatic activity was used to gain spatiotemporal control of the colloidal aggregation, resulting in propagating aggregation waves, unattainable for passive diffusion systems. Finally, an oscillating reaction network was utilized in order to guide the mesoscopic structure formation over time and facilitate the development of active and switchable materials.

Acknowledgments

An erster Stelle möchte ich mich bei meinem Doktorvater Professor Dr. Andreas Bausch bedanken, der mich während meiner gesamten Promotion unterstützt hat und immer ein offenes Ohr für neue Ideen hatte.
Weiterhin danke ich allen Mitarbeitern von E22/27 für die Unterstützung im Labor, die Diskussionen und Ratschläge und besonders für die lockere Arbeitsatmosphäre. An dieser Stelle möchte ich mich speziell bei Fabian Hecht bedanken, der mich als Neuling super aufgenommen hat und mich in jeglicher Sache unterstützt hat. Ebenso danke ich meinen langjährigen Kollegen Benedikt Buchmann und Alfredo Sciortino. Dank euch hatte ich selbst an stressigen und frustrationsreichen Tagen eine lustige Zeit in der Arbeit und auch darüber hinaus. Auch bei anderen Leidensgenossen und Weggefährten möchte ich mich bedanken, wie Andreas Reitenbach, der mich als Bachelor und Masterstudent immer unterstützt hat sowie Philip Bleicher, Thomas Suren und Katharina Dürre.
In diesem Zuge möchte ich auch meinen langjährigen Freunden aus Schule und Studium, sowie meiner Familie danken. Besonders bei meinen Eltern, die mir das alles erst ermöglicht haben und mir in jeder Situation zur Seite standen. Zu guter Letzt bedanke ich mich bei meiner Frau Julia. Danke, dass du in jeder Lebenslage für mich da bist und mir immer beistehst.

Contents

1. Introduction

Self-assembly describes the process of a disordered system to organize itself without external direction. Single components assemble depending on their interactions into higher ordered structures by minimizing the free energy of the system. The organisation of the single subunits is able to facilitate synergistic effects with unique functionality and emerges on all different scales. It ranges from the atomic organisation of molecules, the formation of cell-membranes by the assembly of phospholipids and the molecular folding of chains of amino acids into functional proteins.
Moreover, the process of self-organisation is actively driven by the consumption of energy and is the basis of most natural structures and cellular functions. In order to guide the complex organisation of a cell dynamically, biochemical reaction networks are used to control the interplay of biological molecules by tuning their interactions. They are able to orchestrate the random motion of the single subunits and guide the dynamic assembly of versatile macromolecules, by regulating the gene activity and protein expression. Thus, a variety of integrated cellular processes is realised like the organisation of the cytoskeleton, which is responsible for the cell motility and the movement of organelles and vesicles through the cytoplasm. Especially the autonomous and periodic characteristics of a reaction network are of huge interest, since they enable the capacity of the system to adapt to environmental changes and respond to external stimuli. The circadian clock is a famous example of an oscillating reaction network in living systems, in which periodic reactions like the gene expression are regulated within a rhythm of 24 hours. Beside the importance of biological relevant networks, also chemical oscillating reactions like the Belousov-Zhabotinsky reaction gained much attention, since the periodic changes of the chemical compounds seemed to be in contradiction with the laws of thermodynamics. These networks are the basis for many theoretical descriptions of the mechanisms, which are necessary to enable sustained oscillations.
In addition, biochemical reaction networks can be used for the development of technological applications, by exploiting the reaction kinetics of a network to control a desired mechanism. The circadian cycle of drosophila was reconstituted in vitro and used to achieve the periodic expression of specific proteins. Furthermore, synthetic reaction networks have been used to facilitate active materials, like the transient assembly of synthetic molecules, resulting in the gelation and the tuning of the viscoelastic properties over time.
Moreover, the colloidal self-assembly proved to be useful in order to realise the development of functional materials. A wide range of material properties can be targeted by the choice of the single building blocks and their organisation. Colloids of different materials and sizes from the nano- up to the micro-scale have been developed and can be

manipulated in their arrangement. In equilibrium self-organisation, the colloidal systems are able to reach the thermodynamic equilibrium state, resulting in colloidal crystals with tunable lattice structures. In contrast, out of equilibrium systems are dominated by kinetic traps, which result in self-similar fractal gels or colloidal clusters with distinct sizes. Depending on the colloidal size, material and organisation, different applications can be realised like seen for biosensors and optoelectronics. In addition, the manipulation of the colloidal surface chemistry can be used for drug delivery and medical sensing. Especially the colloidal functionalisation with DNA strands gained much attention, as the interactions can be controlled precisely by the selectivity and manipulation of the DNA strands. In multicomponent systems, versatile materials have been developed by using selective binding partners in order to achieve hierarchical assembly. Moreover, the external manipulation like seen for the temperature controlled aggregation, which exploits the different melting temperatures of the colloidal species, was used to realise complex meta-materials.

It is the aim of this thesis to combine the highly adaptable structure formation of DNA-coated colloids, with the dynamic control, mediated by enzymatic reaction networks in order to broaden the spectrum of autonomous acting materials. Therefore, a binary set of 1µm sized polystyrene colloids is used, which is functionalised with two kinds of docking DNA. The colloidal interaction can be controlled by DNA/RNA linker strands which bridge between the two colloids and induce the diffusion-limited cluster aggregation. The specific control of the colloidal aggregation was used to investigate the influence of the colloidal organisation on the viscoelastic properties of a colloid-polyacrylamide hybrid gel. It was shown that the colloidal aggregation increases the elasticity and yield-strain simultaneously, leading to an enhanced toughness and extended linear response of the hydrogel. Thus, proving the importance of the colloidal structure formation for the mechanical performance.

In addition, we aimed to control the dynamic structure formation of DNA-coated colloids in order to create autonomous and transient materials. So far, the temporal control of DNA-coated colloids was only achieved using external stimuli like chemical interventions or temperature ramps. We report, the enzymatic mediated colloidal structure formation, which is able to control the binding affinities of the colloids by polymerizing and degrading RNA strands. The transient colloidal structure formation was realised by using fuel consumption and was modulated in terms of lifetime and cluster size. Beside the temporal control of the aggregation, the local restriction of enzymatic activity was used to manipulate the colloidal aggregation in space and resulted in the propagation of transient aggregation waves within a diffusion channel.

Finally, we expanded the dynamic control of the colloidal structure formation by utilizing an oscillating reaction network in order to guide the mesoscopic structure formation over time. Therefore, an enzymatic system was used, which is able to generate DNA in an oscillating manner at constant temperature. The DNA concentration peaks during these oscillations were exploited by further reactions in order to produce an additional DNA species with higher DNA binding affinities, able to bridge between colloids. Thus, we were able to couple the oscillatory reaction network with the colloidal structure formation, demonstrating the active and switchable characteristics of the system.

2. Theoretical Framework

2.1 Colloidal structure formation

2.1.1 Molecular self-assembly

The molecular self-assembly is a fundamental part in science in order to understand the complex and autonomous organisation in nature. It is defined as a process, in which a disordered system is able to organize the single subunits without external direction into higher ordered structures. The structure formation depends only on the interactions of the single compounds and is driven by the reduction of free energy[1]**.** The aggregation of the single subunits enables synergistic effects, like seen for the organisation of phospholipids into vesicles, lipid bilayers and cell membranes or the correct three-dimensional conformation of proteins[2–4] (Fig. 2.1). In addition, the molecular self-assembly is also of huge interest for the technological development of materials, which rely on compounds, that are simply too small for an external manipulation[5,6]. Here, the assembly of DNA gained much attention, because of the selective and sensitive hybridisation interactions[7]. In DNA origami, the programmability of DNA is used to realise complex structures on the nano- and micron-scale with different geometries and functions[8,9]. Moreover, self-assembly in colloidal science is used to combine the precise control of structure formation with programmable functionality, given by the properties of the single building blocks. A variety of complex meta-materials can be realised like seen for optoelectronics and medical sensing[10–12]. In the following chapters the principles of colloidal structure formation and the control of aggregation by the colloidal interactions are discussed.

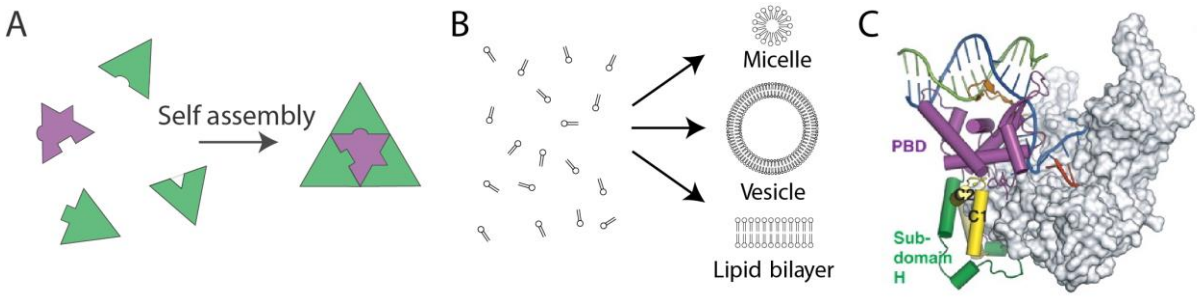

Figure 2.1: Molecular self-assembly. A) The interactions of the single building blocks predefine the formation of higher ordered structures. B) Self-assembly of phospholipids results in a variety of complex structures, ranging from bilayers to vesicles and micelles. The organisation is due to hydrophobic and hydrophilic interactions of the single phospholipids. C) The complex folding of proteins is given by the interactions of the single amino-acids and defines the three dimensional shape and the functionality of the protein. The image shows the 3D structure of the *T7 RNA polymerase*, which is used in chapter 5.[13]

2.1.2 Colloidal self-assembly

Colloidal systems are commonly composed of nano- to micron-sized particles which are dispersed in a liquid media. They can be found in nature as seen in milk and blood, but are also used for technological applications like ink, paint and integrated electronics[14,15]. The organisation of the colloidal particles plays an important role for the versatile material properties and is predefined by the interactions of the single building blocks. Starting with a single colloid in suspension, the movement of the particle is given by the Brownian motion[16]. The collisions of molecules of the surrounding media are pushing the particle into random trajectories resulting in an arbitrary movement. This passive diffusion process determines the speed of colloidal aggregation and is defined by the mean square distance x^2 of the colloid. For the one-dimensional movement, it is described by Einstein, Smoluchowski and Langevin:

$$x^2 = \frac{k_B T}{3r\pi\eta} t \tag{2.1}$$

with k_B the Boltzmann's constant, T the absolute temperature, r the radius of the particle and η the viscosity of the surrounding media.
The colloidal aggregation can be described by the model system of "hard spheres". It is characterised by impenetrable spheres, which can't overlap and have no interactions. Therefore, the interaction potential of the single colloids excludes the attraction and repulsion of colloids (Fig. 2.2A)[17]. Although the movement of the single components is random and no direct interactions exist, colloidal systems are able to form higher organized structures. This can be explained by an entropic description of the free energy F [14,18,19] :

$$F = U - TS \tag{2.2}$$

with U the internal energy, T the temperature and S the entropy. The internal energy is defined as $U = Nk_BT$ with N the total number of particles and k_B the Boltzmann constant. Since, the colloidal system will minimize the free energy, the colloidal solution is going to remain in a dispersed state at equilibrium[18–20]. However, ordered phases arise for higher colloidal volume fractions (Fig. 2.2B). For colloidal volume fractions above 54%, a disorder-order transition takes place and hard spheres are able to form face-centred cubic crystals and glasses[21]. In this configuration, the particles have more effective room to move and the reduction of the configurational entropy compared to random packing can be compensated by the enhanced free volume entropy. In the intermediate liquid-solid phase, a strong increase of the viscosity of the system is noticeable. This is due to the confinement of colloid space and results in a strong increase of friction. Here, also non-Newtonian effects emerge like shear thickening[22,23], were the viscosity increases with the rate of shear strain.

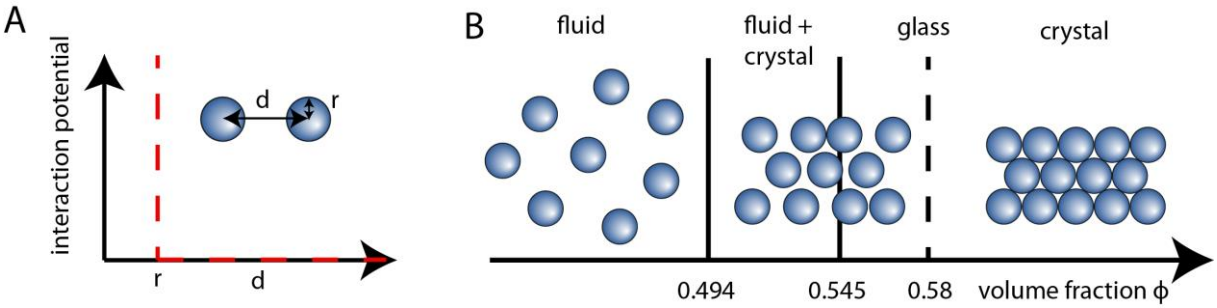

Figure 2.2: Organisation of hard spheres. A) Hard spheres have no attractive and repulsive interactions and are impenetrable. Thus, the interaction potential is zero for colloidal distance d above the colloidal radius r, and infinite for d equals r. B) The colloidal organisation of hard spheres mainly depends on the volume fraction ϕ of the system. Below the characteristic value of ϕ< 0.494, the colloids are dispersed and randomly distributed and show fluid behaviour. In contrast, colloids are able to form colloidal crystals for volume fractions above ϕ< 0.545. In between (0.494>ϕ<0.545), the intermediate phase exists with properties of the fluid and crystal regime.

However, colloidal interactions play a significant role in the colloidal aggregation and arise due to chemical events like repulsive surface charge groups and attractive van der Waals forces. The superposition of all interparticle forces is given by the DLVO theory and can be described by the interaction potential (Fig. 2.3A). Due to the short range attractive and long range repulsive forces, energy barriers between two colloids arise[24]. If these barriers are too high compared to the thermal fluctuation, particles can't attach and the system will remain in a dispersed and random distributed configuration. For lower energy barriers, the thermal motion is high enough to overcome the energy barrier, leading to a colloidal aggregation caused by the attractive forces. Here, complex and higher ordered structures can form, even at low colloidal volume fractions. Depending on the strength of the attractive forces, different kinds of colloidal organisations arise. Low attractive forces allow the colloidal system to rearrange after aggregation. The system can minimize the free energy and reach

the thermodynamic equilibrium, resulting in colloidal crystals below the volume fraction predicted for the hard spheres[25]. Higher attraction forces prevent the rearrangement, leading to colloidal systems which are out of equilibrium and kinetically trapped[26]. These structures commonly show self-similar behaviour and are defined as colloidal fractals. The formed structures are scale free, meaning that they have the same statistical properties on different scales (Fig. 2.3B), like it can be seen for snowflakes and coastlines. Self-similar systems can be characterised by the scaling behaviour during the growth process. While the area of a rectangular and the volume of a sphere scale quadratic and cubic with increasing radius respectively, self-similar systems scale with a rational number D_f in between[27]:

$$E_i = E_{i-1} \cdot \kappa^{D_f} \tag{2.3}$$

with E the arbitrary euclidean measure (e.g. volume) of the growth process, i the iteration step and κ the scaling factor.
The colloidal fractals can be characterised by the exponent D_f of the scaling factor. Moreover, the fractal dimension of a given system can be analysed using the "box counting dimension". Here, a lattice with lattice constant ε is used to cover the fractal structure and the covered parts $N(\varepsilon)$ of the fractals are counted. For decreasing ε, D_f converges to the fractal dimension of the system[28]:

$$D_f = \lim_{\varepsilon \to 0} \frac{\log N(\varepsilon)}{\log \frac{1}{\varepsilon}} \tag{2.4}$$

The fractal dimension of the colloidal aggregation is defined by the strength of the colloidal interactions and can be described by different coagulation theories. For high binding affinities, an irreversible binding of two colloids at first contact can be assumed. Thus, the assembly of the colloidal system is only limited by the diffusion of the single colloids and can be described by the diffusion limited cluster aggregation (DLCA)[29]. The formed structures are highly branched and characterised by a fractal dimension of $D_{f,DLCA} = 1.78 \pm 0.1$. Moreover, weaker colloidal interactions result in an aggregation process, which is limited by the reaction times and thus referred to as reaction limited cluster aggregation (RLCA)[30], with a fractal dimension of $D_{f,RLCA} = 2.1 \pm 0.5$. The energy barriers of the interaction potentials are in the range of $k_B T$ or larger. The probability to overcome the energy barrier is therefore reduced, but increases for multiple binding partners. This leads to a slower aggregation process and denser packing of the colloids (Fig. 2.3C)[31].
Since the colloidal aggregation relies on electrostatic interactions, colloidal systems can be controlled by the surface chemistry of the colloids. Hence, the salt concentration of the media can be used in order to neutralize the electrostatic repulsion and induce colloidal aggregation[32]. On the other hand, colloidal interactions can also be controlled by using uncharged polymers. In solution, polymers are able to cause depletion forces, while the functionalisation of polymers on the colloidal surface can be used to control the repulsive forces by acting as entropic springs[33,34]. In the following chapter, we will discuss the precise control of colloidal interactions enabled by DNA-coated colloids.

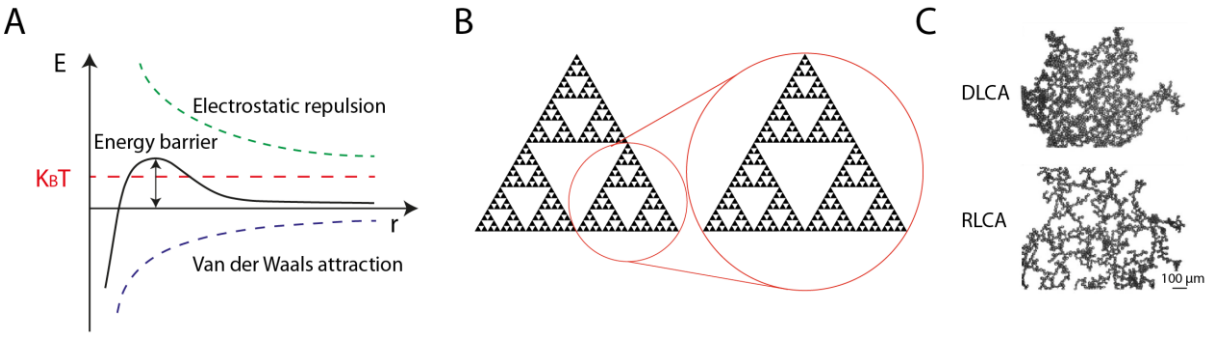

Figure 2.3: Self-similarity. A) The interaction potential of the colloids is according to the DLVO theory the superposition of attractive and repulsive forces. Here, the repulsive forces are given by electrostatic interactions, while attractive forces arise because of van der Waals forces. The short range attractive forces and long rang repulsive forces result in energy barriers, which define the aggregation process. B) Self similar objects have the same statistical properties on different scales. This can be demonstrated by the Sierpinski triangle, which can be subdivided into identical triangles. C) Colloidal structure formation of polystyrene particles for different interaction potentials controlled by the salt concentration of the media. Sticky particles with strong attractive forces show highly branched fractals (DLCA, for $20\ \mathrm{mM}\ CaCl_2$), while higher energy barriers result in denser packed structures (RLCA, for $10\ \mathrm{mM}\ CaCl_2$)[35].

2.1.3 Colloidal self-assembly via DNA hybridisation

The first realisation of DNA-coated colloids (DNAcc) was reported in 1996, by the functionalisation of single stranded DNA to 10 nm sized gold particles via thiol chemistry[36,37]. It gained much attention in the scientific community, because of the precise control of the colloidal interaction caused by the selectivity of DNA hybridisation and the versatile design principles facilitated by the different combinations of complementary DNA. Since that, different kind of surface functionalisations like the streptavidin-biotin bond was used to coat DNA on colloids consisting of materials like gold, silver and polystyrene from the nano- to micron-scale. In order to study the interaction potentials of the colloids, methods like optical tweezers were used. The attractive forces in a colloidal system depend on the surface density of the DNA strands on the functionalised colloids and the binding energy G_i of a single bond between two complementary DNA strands, which is mainly defined by the length of the complementary DNA (Fig. 2.4A). In addition, non-complementary spacer are used to dictate the colloidal distance of bound particles. The length of the spacer defines the configuration space of the single DNA strands, which is important for the amount of possible bonds between two colloids, sterical effects and the probability of two colloids to encounter[38,39]. Although the prediction for the equilibration of DNA hybridisation is very precise, it is not straightforward to determine the colloidal interactions via DNA hybridisation. In the regime of small binding energies, the attractive forces F_{att} are predicted by the “Poisson” approximation[40]:

$$F_{att} = -K_B T \ < n >$$ (2.5)

Here, the attractive forces are simply defined as $K_B T$ multiplied with <n>, the number of bridges that form in chemical equilibrium for a given spacer. In addition, repulsive forces arise due to the compression of DNA strands (Fig. 2.4B) and the reduction of configurational space between two bound colloids (Fig. 2.4C).

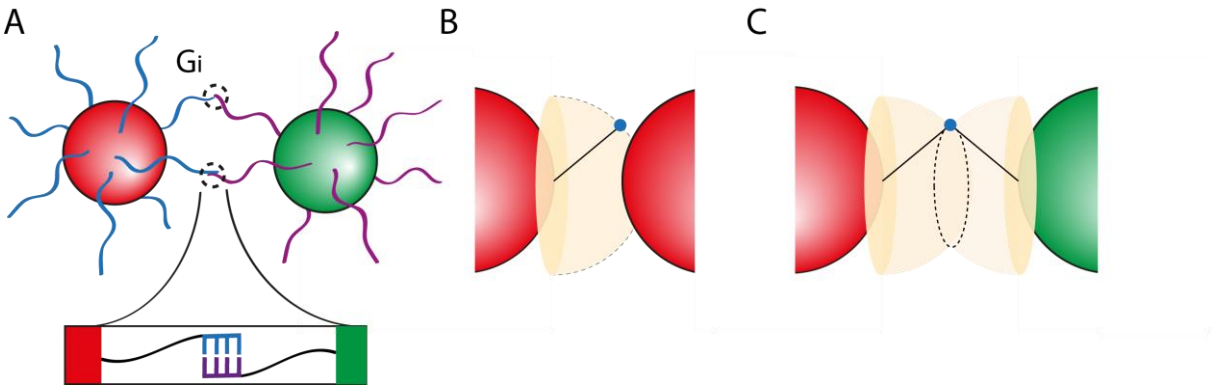

Figure 2.4: DNA-coated colloids. A) The attractive forces of DNA-coated colloids are defined by the length of the complementary DNA and the amount of bonds G_i. The non-complementary spacer (black) defines the colloidal distance and is important to prevent sterical effects. B) The repulsive forces arise due to the compression of DNA and the decrease of configurational space, schemed by the limitation of the hemisphere. C) In the case of aggregated particles, repulsive forces arise, because of the reduction of configurational space of the linked docking strands (dotted circle).

Since the binding affinities can be controlled precisely by the choice of pre-crafted DNA, a wide range of colloidal structures was realized. For weak interactions, colloidal crystallisation was achieved at low volume fraction. Moreover, it was possible to control the lattice structures of the crystals by using different sized colloids (Fig. 2.5A)[41]. In addition, patches of DNA on the colloidal surface were utilized for the formation of finite sized clusters with tuneable geometries (Fig. 2.5B)[42]. In multicomponent systems, the different melting temperatures of colloids can be exploited in order to create hierarchical self-assembly by using temperature ramps and enable colloidal scaffolds (Fig. 2.5C)[43].

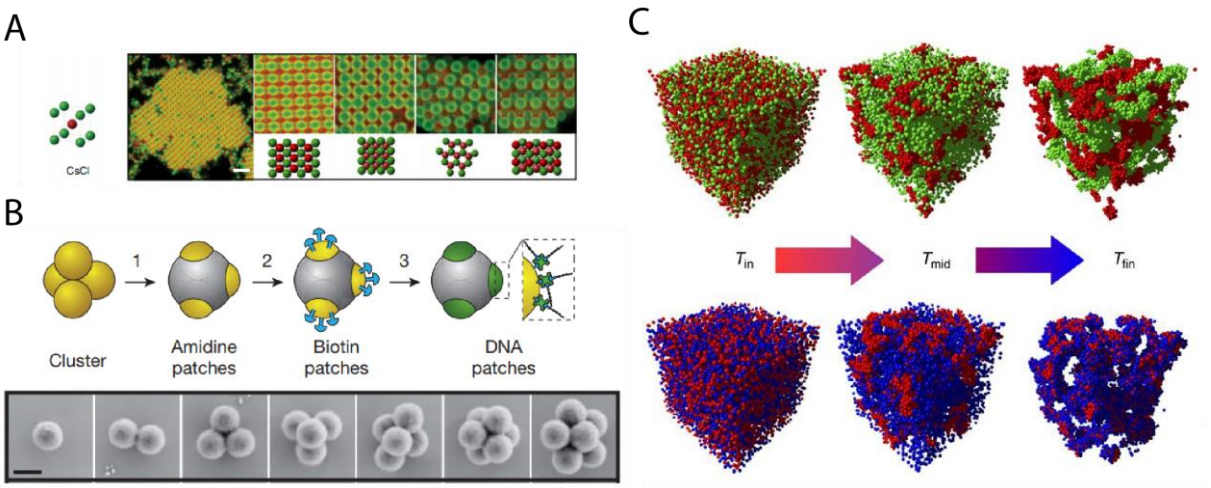

Figure 2.5: Structure formation of DNA-coated colloids. A) Colloidal crystallisation is realised by weak DNA interactions and the minimization of free energy of the system. Different sized colloids can be used to define the crystal lattice.[41] B) Patches of DNA on the colloids lead to the formation of finite sized structures. The DNA patches define the amount of possible binding partners.[42] C) The different melting temperatures of multicomponent systems can be exploited to control the aggregation of colloidal species separately. Thus, hierarchical assembly and aggregation scaffolds can be realised.[43]

2.2 Dynamic structure formation

2.2.1 Biochemical reaction networks

In contrast to the passive process of self-assembly, the dynamic structure formation is driven by the consumption of energy. The molecular self-organisation is commonly guided by biochemical reaction networks, which are defined as complex circuits of coupled reactions and can be described as the central processing units of life (Fig. 2.6A). In living cells, enzymatic controlled metabolism pathways regulate the gene activity, protein expression and perform integrated cellular functions[44]. While biological networks can be observed in living organisms, the control and manipulation in vivo is quit challenging and barely possible. Consequently, bottom up approaches for the in vitro reconstitution are helpful to understand the complex interactions which are responsible for mechanisms like the periodic protein expression and trigger waves. The circadian clock is one example for a complex organisation process. It was shown, that the gene expression of flies follows a periodic rhythm of 24 hour[45](Fig. 2.6B). The network was reconstituted in vitro and the crucial mechanism were identified, which were responsible for the sustained oscillation of protein expression[46]. In addition, reconstituted networks can be coupled to further reactions in order to control a desired mechanism[47,48] and create smart materials which control certain material properties like seen for the gelation of synthetic molecules (Fig. 2.6C)[49]. The

detailed description of biological processes within a biochemical reaction network is very complex and includes many single events. Therefore it is necessary to simplify the underlying processes and reduce the system to the essential parts of the reaction network. For enzymatic reactions, this is realised by using Michalis-Menten kinetics:

$$\frac{d\,c_P}{dt} = v_{max}\frac{c_S}{K_M + c_S} \tag{2.6}$$

with c_P the concentration of the product, c_S the concentration of the substrate, v_{max} the maximum speed of the reaction, which is given by the enzyme concentration and catalytic rate and K_M the Michaelis-Menten constant, which defines the speed of the saturation. In addition, the diffusion of the single components plays an important role in out of equilibrium systems to describe pattern formation. These systems can be described by the reaction-diffusion equation (RDE):

$$\frac{d}{dt}c_i = f\,(c_i) + D \cdot \frac{d^2}{d\,x^2}c_i \tag{2.7}$$

with $f(c_i)$ the reaction term and $D \cdot \frac{d^2}{d\,x^2}c_i$ the diffusion equation with the diffusion constant D. The reaction-diffusion equations can be used to simulate complex pattern-formation like seen for turing instabilities[50], which are caused by a combination of non-linear reactions and chemical compounds with different diffusion constants. In bistable systems, RDE's can be used to describe the appearance of trigger waves[51]. Here, the propagation of chemical compounds exceeds the speed of passive diffusion processes as seen for mitotic waves in *Xenopus* eggs[52] and the action potentials in the axon of a neuron[53]. A promising approach for the realisation of complex and functional reaction circuits are DNA based networks which are coupled to enzymatic reactions[54]. Programmable DNA replacement reactions can be used to control enzymatic activity[55]. One example of these networks is the molecular predator-prey system[56], which will be discussed in chapter 2.2.2.2.

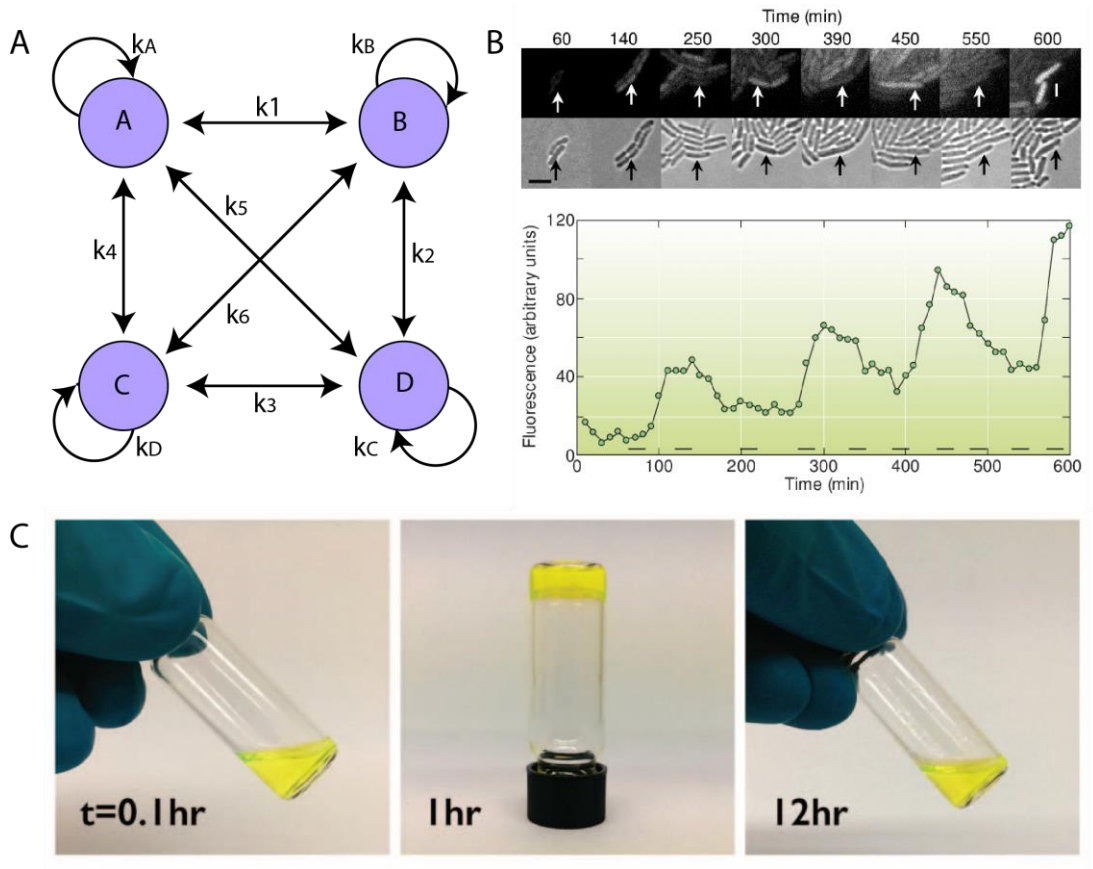

Figure 2.6: Biochemical reaction networks. A) A biochemical reaction network is used to describe a system of coupled reactions. Here, the compounds A-D are connected with reaction rates k_i. B) In vitro reconstruction of the circadian cycle in *E.coli*, demonstrating the oscillatory expression of GFP[45]. C) A reaction network is used to control the transient polymerisation of synthetic molecules and control the material properties of the system[49].

2.2.2 Oscillations in biochemical reaction networks

2.2.2.1 Conditions and Theory

A chemical reaction is defined as a process, in which reactants are converted into certain products due to the reduction of free energy. This process is usually characterised by an asymptotical and unidirectional progression of product formation and takes place until a system remains in thermodynamic equilibrium[57]. Thus, the periodic changes of the chemical compounds seen in the Belousov-Zhabotinsky reaction[58], presented in 1959, gained much attention in the scientific community. The sustained oscillations seemed to be in contradiction with the second law of thermodynamics, which predicted irreversible reaction pathways in closed systems due to the decrease of entropy over time. In this chapter, we will discuss the conditions, required for sustained oscillations and finally simulate the kinetics of the oscillating molecular predator-prey system. In general, four conditions can be formulated for an oscillating system[59]:

- **Far from equilibrium**
- **Open system**
- **Non-linear kinetics**
- **Feedback mechanism**

In order to prevent a unidirectional reaction pathway, the oscillatory reaction network needs to be far from thermodynamic equilibrium[60]. Enough energy supply is required to create closed reaction trajectories and prevent a stationary state. In the case of ideal sustained oscillations, the system needs a constant supply of energy and the removal of occurring side products. Consequently, an open system is needed to enable the transfer of energy and material[61]. However, this condition is only required to facilitate sustained oscillation on very long time scales. In addition, the closed trajectories are always based on non-linear reaction kinetics, like autocatalytic reactions, which cause an exponential amplification of chemical compounds[62]. However, a variety of non-linear reaction mechanisms are sufficient, like the appearance of time delays between two different reactions, caused by activation thresholds or transportation mechanisms[63]. Finally, an oscillating network is always characterised by certain feedback mechanisms. The reaction products are able to regulate the kinetics of the network,[64] which can cause the bistability of a system[65]. The discussed conditions are the minimum requirements to enable sustained oscillation and can be demonstrated by the Lotka-Volterra equation, which describe the population dynamics of prey and predator species[66]:

$$\frac{dx}{dt} = \alpha x - \beta xy \tag{2.8}$$

$$\frac{dy}{dt} = \delta xy - \gamma y \tag{2.9}$$

With x the concentration of the prey and y the concentration of the predator, α the rate of the prey amplification, β the consumption term of the prey by the predator. The amplification rate of the predator is given by δ and γ represents the rate of the predator extinction. The prey species is characterised by an unlimited and exponentially growth, which is coupled to a negative feedback caused by the predator amplification. The negative feedback is able to stop the prey amplification, which is followed by a regulation of the predator amplification. Subsequently both species are going to decline. After the population of the predator drops below a critical value, the system is able to recover and facilitate sustained oscillations of the predator and prey species.

2.2.2.2 Simulation of the molecular predator-prey system

In this chapter we simulate the molecular predator-prey system, described in chapter 6. The mathematical model is a simplified description of the chemical reaction network and is based on the equilibration of DNA hybridisation and the enzymatic reactions, which are described by Michaelis-Menten kinetics. The interaction of the predator and prey can be modelled with a two-variable mathematical model of non-dimensionalized equations[56]:

$$\frac{dn}{dt} = \frac{g\ n}{1 + \beta\ g\ n} - p\ n - \ \lambda\ \delta\ \frac{n}{1 + p} \tag{2.10}$$

$$\frac{dp}{dt} = p\ n - \ \delta\ \frac{p}{1 + p} \tag{2.11}$$

With g the rate of the prey amplification, β the saturation of the prey production, defined by equilibrium constants of the DNA species, $\delta = \frac{rec}{pol}$ the ratio of DNA degradation (rec) and amplification (pol) and $\lambda = \frac{k_N}{k_P}$ the ratio of prey and predator degradation. The detailed derivation of the equations and absolute values of the parameters can be found in the supplements of the "Predator-Prey molecular ecosystems" [56]. The coupled reactions (eq. 2.10 and 2.11) are able to facilitate sustained oscillations of the prey and predator species (Fig. 2.7A, B). The reaction network is characterised by a fast prey and predator amplification, which is followed by the slow and exponential decay. At a certain point in time, the predator can't suppress the prey amplification anymore and the reaction network restarts the cycle. The mathematical models of oscillating reaction networks are often based on the unlimited autocatalytic amplification. This can be realised for very small values of β. In this case, the equations $\text{eq } 2.10 \text{ and } 2.11$ are simplified to the classic model of the Lotka-Volterra equations (Fig. 2.7E, F). However, the sustained oscillations of the molecular predator-prey system are based on the competing degradation of the prey and predator, which leads to the saturation of the degradation term. This is demonstrated by assuming a first order degradation, because of low concentrations of the predator (p<<1). This leads to the following equations:

$$\frac{dn}{dt} = \frac{g\ n}{1 + \beta\ g\ n} - p\ n - \ \lambda\ \delta\ n \tag{2.12}$$

$$\frac{dp}{dt} = p\ n - \ \ \delta\ p \tag{2.13}$$

The first order degradation prevents sustained oscillation and the prey and predator reach a coexistence steady state, after some damped oscillations (Fig. 2.7C, D).

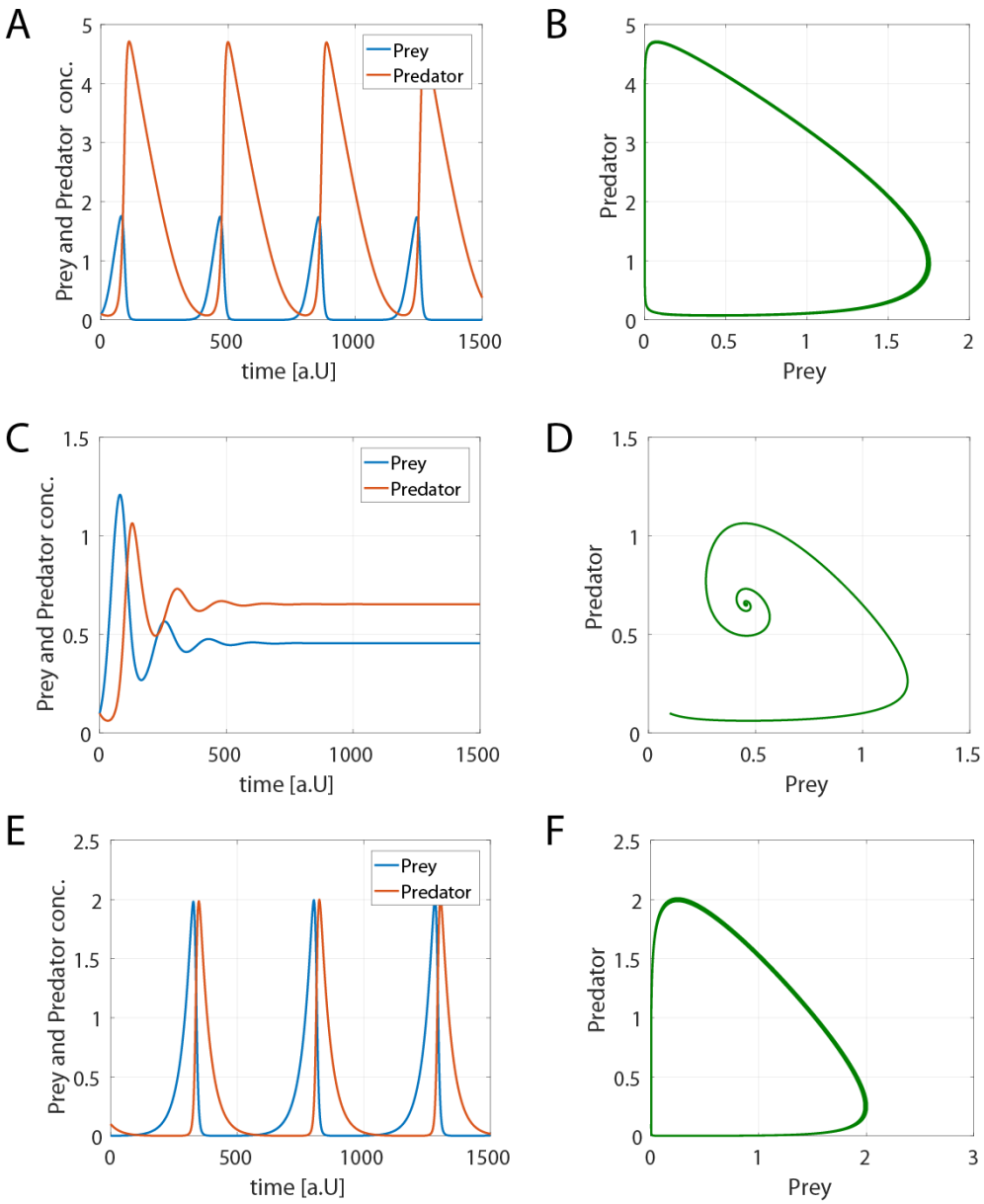

Figure 2.7: Simulation of the predator-prey system. A) The molecular predator-prey equation according to eq. 2.10 and 2.11 result in sustained oscillations. A saturated degradation is assumed, because of the competing degradation of prey and predator. B) Assuming a first order degradation (eq. 2.12 and 2.13) of prey and predator prevents sustained oscillations. The reaction network reaches a steady state, possibly after some damped oscillation. C) The assumption of unlimited prey amplification changes the molecular predator-prey system to the classic Lotka-Volterra equations described in chapter 2.2.2.1.

2.3 Rheology

Rheology is the study of flow and deformation of materials in order to characterise their viscoelastic behaviour. A classic elastic material can be described by Hooks law and reacts to an applied deformation with a proportional stress. In contrast, an ideal Newtonian liquid reacts with a stress which is proportional to the rate of the applied strain. However, most materials have elastic and viscous material properties and can therefore be described by models consisting of series of Hookean springs and Newtonian dashpods (Maxwell/Voigt-elements). In order to extract the elastic and viscous part of materials, oscillatory shearing rheometers are used, which apply an oscillatory shear deformation $\gamma(t)$ to a material and measure the resulting shear stress $\sigma(t)$ of the material.

$$\gamma(t) = \gamma_0 \, sin(\omega t) \tag{2.14}$$

$$\sigma(t) = \sigma_0 \, sin(\omega t + \delta) \tag{2.15}$$

with $\gamma_0$the amplitude of the oscillatory shear and ω the angular frequency. Since, the response to the applied sinusoidal deformation between an ideal elastic solid and a Newtonian liquid differs (Fig. 2.8)[67], viscoelastic materials can be characterised by the phase delay δ and the amplitude attenuation.

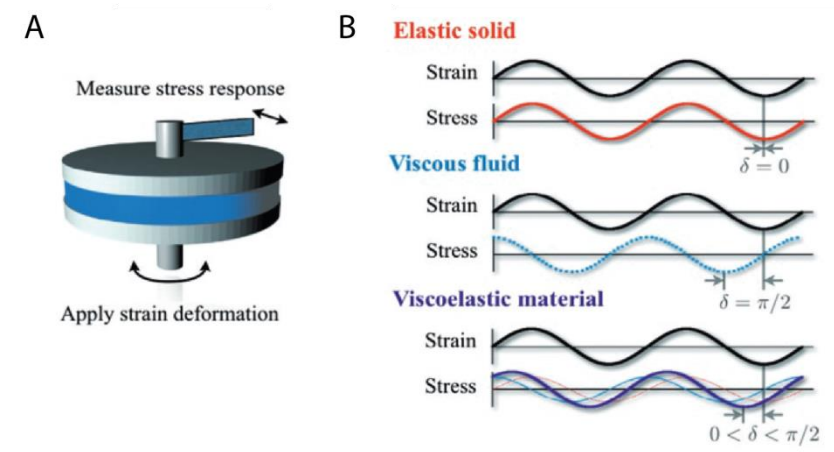

Figure 2.8: Oscillatory shear rheology. A) Oscillatory shear strain is applied to a material and the responding stress is measured. B) The phase delay of strain and stress indicates the viscoelastic behaviour of the material.[67]

The viscoelastic material can be described by the complex shear modulus G^*:

$$G^* = G' + iG'' \tag{2.16}$$

$$\tan(\delta) = \frac{G''}{G'} \tag{2.17}$$

The elastic part of the material is given by the storage modulus G' and is defined by the ratio of stress to strain ($\frac{\sigma}{\gamma}$). The loss modulus G''represents the viscous behaviour of the material and the dissipative loss of energy due to the shear process[68]. Moreover, the response of colloidal materials and polymers depend on the speed of the applied strain, due to jamming

and entanglement. Therefore, it is necessary to determine the material properties on different timescales. This is realised by frequency sweep experiments, which measure G^*depending on the applied angular frequency ω (Fig. 2.9B). Untangled polymer networks tend to behave liquid for slowly applied strains and solid for faster deformations. In addition, materials can be characterised by their capacity to resist applied deformations. In strain-stress experiments increasing deformations at a constant deformation rate $\dot{\gamma}$ are used to determine the linear regime of the material, were no plastic deformation occurs (Fig. 2.9A). Furthermore, the yield stress is defined as the turning point after the linear regime. The slope in the linear regime corresponds to the storage modulus, since it is the ratio of strain and stress. Deformations above the elastic regime result in irreversible plastic deformations and a finally rupture of the material.

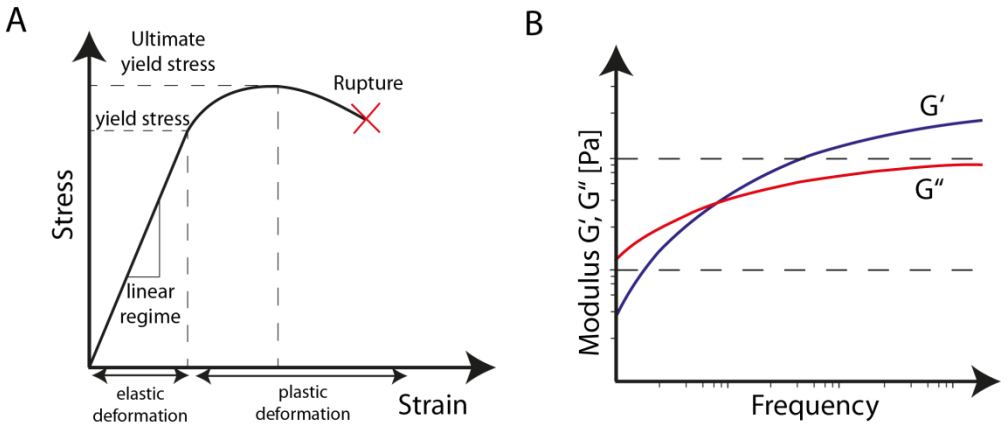

Figure 2.9: Viscoelastic measurements. A) In strain-stress experiments, constant shear deformation is applied and the elastic and plastic regime is determined in order to analyse the capacity of the material. B) Frequency sweeps are used to analyse the material response on different time scales. G' and G'' are measured over a certain range of ω to determine the relaxation of the material.

3. Material and Methods

3.1 DNA-coated colloids

3.1.1 Sample preparation

All chemicals used in this thesis were obtained from *Sigma-Aldrich*, unless otherwise specified. The oligonucleotides were purchased from *biomers* and *Integrated DNA Technology*. The DNA sequences used in every chapter are listed in Table 3.1, 3.2 and 3.3 and were designed using "*NUPACK*" in order to analyse the hybridisation in equilibrium and the secondary structures. The streptavidin coated colloids are 1 µm sized fluorescent polystyrene microspheres (ex/em: 660/690 nm and ex/em: 480/520 nm) and were purchased from *Bangs Laboratories.* The microspheres (1% v/v) are functionalised with ssDNA by incubating the colloidal stock solution with biotinylated docking DNA for at least 12 hours on a rotator at 4°C. The concentration of DNA defines the density of DNA on the colloidal surface. For the rheological measurements, it was chosen, such that one colloidal particle is covered with $\approx 6 \cdot 10^4$ DNA strands and for the enzymatic measurements $\approx 12 \cdot 10^4$ DNA per colloid was used. The unbound docking DNA was removed after the incubation step by centrifuging the samples at 1200 relative centrifugal force and replacing the supernatant with a low-Tris-salt buffer (150 mM NaCl, 10 mM Tris, pH 8.8). The washing procedure was performed for three times, while 450 mM sucrose was used in the final step to match the density of the colloids and the buffer and avoid sedimentation. The final colloidal solution was sonicated for 30 min to prevent non-specific aggregation and stored at 4°C on a rotator. To guarantee reproducibility of the experiments, the colloids were used not longer than 5 days.

3.1.2 Microscopy

The colloidal structure formation of the DNA-coated colloids was observed using confocal microscopy in order to exclude non-specific interactions. A Leica TCS SP5 was used with a HCX PL APO 63x/1.40-0.60 oil CS objective. For the excitation, a 488 nm Argon- and a 633 nm Helium-Neon laser was used at 100% intensity. For the detection, the bandwidth of two photomultiplier was set to 490-560 nm and 660-710 nm. Since light scattering at high

particle concentration leads to a reduction of the intensity within the samples, the Leica software tool “linear compensation mode” was used to ensure a homogenous signal. In addition, bright-field optical images and videos were obtained using a Leica DMI600B and a HCX PL APO 40x/1.25-0.75 oil CS objective.

3.2 Rheology

3.2.1 Sample preparation of colloidal hybrid-hydrogel

The colloidal samples were prepared in a buffer of 450 mM sucrose, 150 mM NaCl, 10 mM Tris and 10 mg/ml BSA. For the polyacrylamide gels, Acrylamide 4K solution (29:1) was used containing 0.1% ammonium persulfate and 140 µM Tris(2,2’biprydidyl) dichlororuthenium(II) as a photoactivatable catalyzator. Two species of DNA-coated colloids were prepared using biotinylated DNA strands *Dock C* and *Dock D* (see table 3.1). The Docking strands consist of a 40 nT poly T spacer and a DNA sequence which is complementary to the linker CD. Already a small amount of linker (~10 nM) is sufficient to induce colloidal aggregation. To ensure reproducible experiments, the ratio of linker strands to total docking strands (1:13) was kept constant for all experiments. Before the polymerisation of the polyacrylamide is induced, the DNA-linkers are added in order to produce colloidal gels. Each sample was prepared with a final concentration of 10 µl and incubated for one hour at room temperature to enable the colloidal structure formation. The samples were transferred on the lower plate of the rheometer with a cut off pipette in order to minimize the destruction of the colloidal gels by shear forces. In a next step, the upper plate is lowered to working distance, followed by a second incubation step of one hour to ensure the complete gelation of the colloids. Finally, the polymerisation of PAM is induced using a *Schott KL 1600* light-emitting diode lamp.

Name	**Sequence** (5’→3’)	**Modification**
Dock C	CACCCACCCACACCAACCAACTTTTTTTTTTTTTTTTTTTTTTTTTTTTTTTTTTTT	3’-BiotinTeg
Dock D	TTTTTTTTTTTTTTTTTTTTTTTTTTTTTTTTTTTTTTTTTTATCTAATACATTAC	5’-BiotinTeg
Linker CD	GTTGGTTGGTGTGGGTGGGTGTTTGTAATGTATTAGAT	

Table 3.1: DNA sequences used in chapter 4.

3.2.2 Rheological analysis

The rheological experiments in this thesis were performed using an *Anton Paar Physica MCR 301* plate rheometer. The upper measuring plate *PP08* with a diameter of 8 mm was used in order to minimize the required sample volume. Since the polymerisation of the polyacrylamide gel is induced by light, a self-made lower plate was used, containing a transparent acryl glass, which is surrounded by a water reservoir in order to prevent evaporation (Fig. 3.1). All experiments were performed in a darkened room to exclude the uncontrolled polymerisation of the PAM gel. The polymerisation of the hybrid gels was monitored using oscillatory shear experiments with deformations within the linear regime. The storage modulus G' and the loss modulus G'' was analysed over time to ensure the complete gelation of the samples. Afterwards, frequency sweeps were performed in order to analyse the frequency dependent viscoelastic behaviour. Finally, the resistance of the gels was investigated using strain-stress experiments. The gel was deformed at a constant shear rate and the linear regime and the yield stress of the gel was determined. All experiments were monitored and evaluated using *Rheoplus* and *Matlab*.

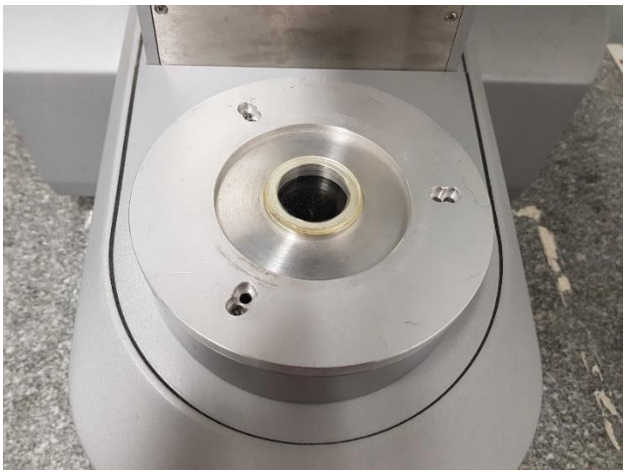

Figure 3.1: Oscillatory shear rheometer. The rheometer was equipped with a self-made plate, with a transparent acryl-glass to enable the illumination of the samples and the subsequent polymerisation of the polyacrylamide. In addition, a water reservoir was used to avoid evaporation.

3.3 Dynamic structure formation

3.3.1 Sample preparation

The *T7 RNA polymerase* (200 U/µl) and *RNaseH* (5 U/µl) were purchased from *ThermoFisher Scientific* and used undiluted at their stock solution concentration. The experiments were performed with buffer conditions, which were optimized for the enzymatic activity as well as the colloidal structure formation. The buffer contains 450 mM sucrose, 10 mM Tris, 5mg/ml BSA and 30 mM $MgCl_2$. The NaCl used in the previous chapter was replaced with $MgCl_2$,

because of the *T7 RNA polymerase*. The DNA-coated colloids were prepared according to chapter 3.1.1 and used at a concentration of 0.15% v/v. The samples were observed within self-made *parafilm* chambers with 10 µl volume size. The working temperature of 37°C was achieved by using an *IBIDI*-heating chamber and a copper objective warmer. The used DNA sequences are listed in table 3.2. In contrast to the docking DNA strands used in chapter 4, the DNA strands don't have the 40 nT long poly T spacer. Here, only the complementary part of the docking strands was used, because of nonspecific interaction caused by the *T7 RNA Polymerase.* It turned out, that the polymerase is able to induce colloidal structure formation in the absence of DNA-linker and template DNA. In addition, this effect is enhanced in the presents of *NTP*. This effect was prevented by lowering the total length of the docking DNA and consequently decreasing the binding sites of the polymerase. The reduction of the accessibility for the RNA-linker was compensated by increasing the docking DNA density on the colloidal surface($\approx 12 \cdot 10^4$ DNA per colloid). The diffusion chambers were produced by cutting a *parafilm* in the shape seen in Fig. 5.12A using a laser cutter**.** The reservoir of the chambers were incubated with BSA-Biotin and streptavidin for 30 min and functionalised with biotinylated template DNA afterwards.

Name	Sequence (5'→3')	Modification
Dock A	CCACACCAACCAAC	3'-BiotinTeg
Dock B	ACTTACTATATAAC	5'-BiotinTeg
Linker AB	GTTGGTTGGTGTGGGTGGGTGTTTGTTATATAGTAAGT	
RNA-threshold	ACUUACUAUAUAACAAACACCCACCCACACCAACCAAC	
Template	CACCCACCCACACCAACCAACAAAACTTACTATATAACCCCTATAGTGAGTCGTATTAG	
Comp-Template	CTAATACGACTCACTATAGGGGTTATATAGTAAGTTTTGTTGGTTGGTGTGGGTGGGTG	3'- Biotin (optional)

Table 3.2: DNA/RNA sequences used in chapter 5.

3.3.2 Enzyme kinetics of *T7 RNA Polymerase* and *RNaseH*

The *T7 RNA Polymerase* is a DNA dependent single-subunit RNA polymerase from the *T7 bacteriophage*. It has a molecular weight of 99 kDa and catalyses the polymerisation of RNA from a dsDNA Template in the 5'→3'direction by using *NTP* as a substrate. It is widely used in biotechnological application for the expression of recombinant proteins (pET-series), because of the selective activation by the *T7* promoter sequence (TAATACGACTCACTATAGGG) and the low basal transcription rate. It is characterised by a dissociation constant of $K_D = 10\,\mathrm{nM}$ and has transcription rate of 200-260 nucleotides/s.

The polymerase requires Mg^{2+} ions as cofactors for the synthesis of RNA and has a working temperature of 37°C.[69,70]
The *Ribonuclease H* (*RNaseH)* has a molecular weight of 17.6 kDa and is part of the sequence independent endonucleases that catalyse the cleavage of RNA strands of a RNA/DNA substrate. Homologs of the enzyme can be found in many organisms like E.coli, yeast and archaea bacteria[71,72]. In biotechnology it is widely used for the degradation of (nonspecific) RNA residuals and primers during the DNA amplification of a polymerase chain reaction[73]. The degradation of RNA is realised by the cleavage of the phosphodiester backbone via a hydrolytic mechanism, producing a 5'-phosphate and 3'-hydroxyl termini with a turnover rate of 7.1 cleavages/s per monomer[74].

3.3.3 Fluorescence measurements

The enzymatic activity of the polymerase and ribonuclease were analysed using a *Jasco FP-8500 spectrofluorometer*. For the visualisation of the RNA, the RNA/DNA intercalator *SYBR Green II* (*ThermoFisher, ex/em: 497/520 nm*) was used at 0.19% of the stock solution. 50 µl samples were pipetted into quartz ultra-micro cuvettes (*Hellma analytics*) and placed in a temperature controlled multi sample holder. The samples were excited with 497 nm and a spectral width of 1 nm by a Xe-lamp and the emitted light was detected at an angle of 90° at 530 nm with a spectral width of 5 nm. To avoid contamination, the cuvettes were incubated with 2% *Hellmanex III* at 70°C for 30 min, subsequently washed with millipore water and sonicated for additional 30 min. The fluorescence signal of the samples was transferred to the total RNA concentration. Therefore, the dependency between fluorescent signal and DNA concentration was determined (Fig. 3.2). The dye obeys a linear dependency of up to 10 µM without saturation. For the measurements, the minimum of the signal was determined and computed to be the DNA template concentration, because no RNA was produced so far. This allows a direct conversion to RNA concentration.

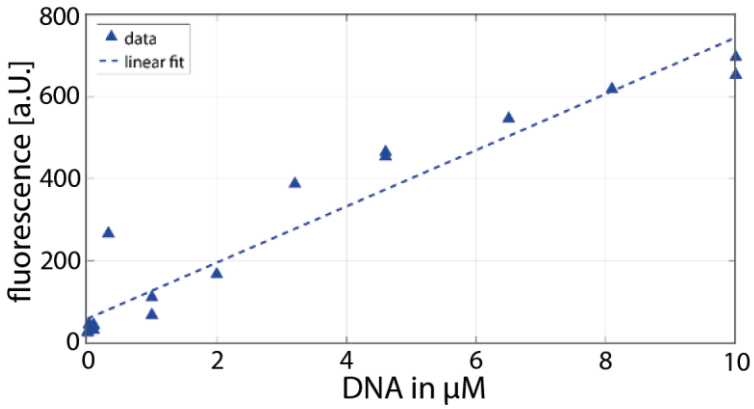

Figure 3.2: Fluorescence measurements of SYGRII. Different concentrations of prebuild DNA were measured using fluorescent spectroscopy at a constant concentration of SYGRII. A linear response of signal and DNA concentration can be observed up to 10 µM of DNA.

3.3.4 Image analysis

The average cluster size of the colloidal structure formation was determined by thresholding the bright field images in order to generate a binary mask for each image. The obtained masks of the colloidal aggregation was than analysed in terms of size and total amount using the software tool “analyse particle” of *ImageJ*. Since, the fluorescence microscopy does not allow the exact tracking of the particles, the cluster size is determined in arbitrary units using the background information of the single images. The obtained data were transferred and analysed using *Matlab*.

3.3.5 Simulation reaction-diffusion

The RNA production and degradation was simulated using differential equation with enzymatic rates which were obtained from fluorescence measurements on the basis of Michaelis-Menten kinetics. The experiments of the reaction-diffusion experiments were simulated using Gaussian filter functions, which are commonly used in image processing and allow a fast computation of diffusive processes. The diffusion of RNA and the colloidal aggregation was simulated separately within rectangular matrices using periodic boundary conditions for the colloids and repulsive conditions for the RNA. The RNA production was restricted to distinct parts of the rectangular in order to simulate the reservoir of the diffusion chamber. The *Matlab* script can be found in A1.

3.3.6 Gel electrophoresis

DNA/RNA hybridisation reactions were observed using native polyacrylamide gel-electrophoresis in a polyacrylamide TBE gel (89 mM Tris, 89 mM boric acid and 2 mM EDTA, pH 8.0). The separating gel was prepared with the following buffer concentrations: 18% acrylamide, 0.3% APS, 3.7 µM EDTA, 8 mM TEMED, in TBE buffer. The collecting gel contained: 3.6% acrylamide, 1 µM EDTA, 0.3% APS and 10 mM TEMED. The loading dye *Qiagen gelpilot* was added to the samples and the ladder with a final concentration of 5 µM. In the gel-electrophoresis, 100 V were applied to the gel for 1.5 hours, which was stained afterwards using SYBR Green II (1:1500) for additional 1.5 hours.

3.4 Oscillating reaction network

3.4.1 Sample preparation

The enzymes *Bst. Polymerase large fragment* and the nicking enzyme *NB.Bsmi* were obtained from *New England Biolabs*. The degradation reaction was realised by the exonuclease *ttRecJ* from *Thermus Thermophilus*, a 5'->3' processive exonuclease, which was purified in our lab (details in A2). All experiments were performed in a reaction buffer containing 20 mM Tris-HCl, 10 mM $(NH_4)_2SO_4$, 10 mM KCl, 50 mM NaCl, 8 mM $MgSO_4$, 400 µM *dNTP* Mix (*NEB*) and a pH of 8.8. In addition, 0.1% *SynperonicF108* (*SigmaAldrich*), 4 mM DTT, 100 µg/mL BSA (*NEB*) and 2 µM *Netropsin* (*Sigma Aldrich*) are used as stabilizing agents for the enzymatic reactions. The extremely thermostable single strand binding protein *ETSSB* (*NEB*) was used at 5 ng/µL in order to prevent the formation of weak secondary structures of the DNA species. The nickase *Nb.Bsmi* was used at 6% of the stock solution mix, unless otherwise specified and all experiments were performed at T= 46.5°C. In addition, the *T4 gene 32 protein* (gp) was used to prevent the exponential growth of arbitrary DNA sequences. The reaction (ab initio amplification) arises for long time periods in the presents of the polymerases and restriction enzymes, like the *Bst. Polymerase* and the nicking enzyme *NB.Bsmi* (Fig. 3.3).

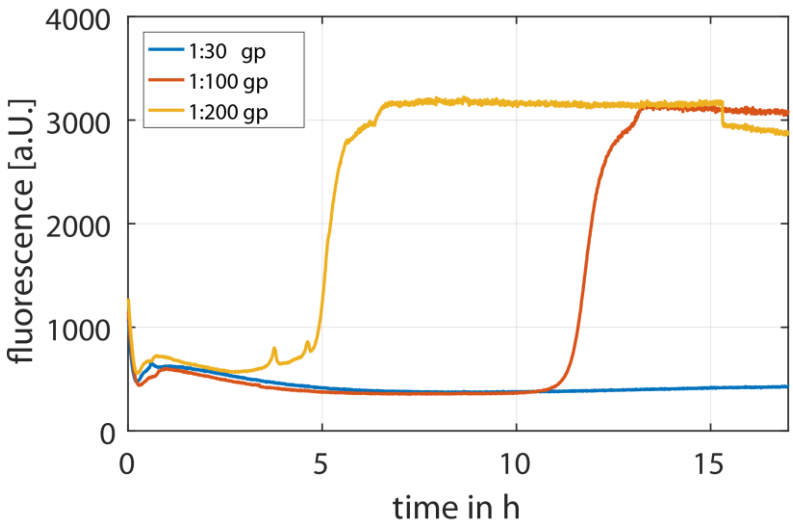

Figure 3.3: Ab initio amplification. The ab initio amplification leads to an exponential amplification of random DNA sequences which interferes with the predator-prey reaction. The protein *T4gp32 (stock concentration: 1 mg/ml)* is used to prevent this reaction. It is a single stranded binding protein and used in PCR reactions in order to decrease the non-specific amplification of polymerases.

The imaging of the colloidal aggregation was realised by using a self-made copper chamber which was calibrated to be 46.5°C by using a temperature sensor. Besides the monitoring of the structure formation, experiments were performed using a PCR machine at constant working temperature. Multiple samples were observed and the reactions were stopped individually by cooling down the samples to 4°C.

3.4.2 DNA sequences of the predator-prey system

All oligonucleotides used in this chapter were obtained from *biomers*. The design of the molecular ecosystem (N, P and G) is based on the work of Fujii and Rondelez[56]. Several modifications of the oligonucleotides are necessary to enable the stability of the reaction network. Phosphorothioate backbones ("*") are used to block the exonuclease digestion. Phosphate at the 3' end of the DNA was used to prevent the elongation of the strands by the polymerase. The C18 spacer in the *Dock C-P* sequence was used to prevent the elongation of the bound linker.

Name	Sequence (5'→3')	Modification
Prey (N)	CATTCGGCCG	
Predator (P)	CATTCGGCCGAATG	
Template (G)	C*G*G*CCGAATGCGGCCGAATG	3'-Phosphat
Dock A Gen 2 mod10	C*A*C*CCGAATGTTTTTTTTTTTTTTTTTTTTTTTTTTTTTTTTTTTTTTTT	3'-Biotin
Dock C-P	TTTTTTTTTTTTTTTTTTTTTTTTTTTTTTTTTTTTTTTT **X** ACTTACTATATAAC	5'-Biotin, 3'-Phosphat X="C18spacer"
Link ac mod 10	CATTCGGGTGGTTATATAGT	
Prey-converter	A* C*T*ATATAACCACCCGAATGCGGCCGAATG	3'-Phosphat
Predator-converter	A*C*T*ATATAACCACCCGAATGCATTCGGCC	3'Phosphat

Table 3.3: DNA sequences used in chapter 6.

3.4.3 Fluorescence measurements

The fluorescent measurements in this chapter were performed with the platereader *SpectraMax M5* (*Molecular devices*) using the *MICROPLATTE, 384 WELL, PS, F-BODEN, µCLEAR®* by *Greiner Bio-One*. A sample volume of 15 µl was used and additional 15 µl of mineral oil was used to prevent evaporation during the measurements. To visualize the production and degradation of the oscillating network, the DNA intercalator *EvaGreen* (*Biotium*, *ex/em: 500/530 nm*) was used undiluted at 1x concentration (stock concentration: 20x in water).

4. Viscoelastic properties of a colloidal-hydrogel

In this chapter, we investigate the mechanical influence of colloidal structure formation within a hydrogel. The aggregation of DNA-coated colloids (DNAcc) and the polymerisation of a polyacrylamide gel can be controlled independently, resulting in identical materials which only vary in their colloidal arrangement. Hydrogels are a biocompatible class of materials characterized by a hydrophilic polymer matrix able to hold water without dissolution[75]. They are used in many biomedical applications, because of characteristics like permeability and bio adhesion. In addition, the incorporation of colloidal systems proved to be useful to create synergetic hybrid materials with unique and superior material properties[76]. Moreover, the modification and multifunctionality of the colloids opens up a new set of possibilities ranging from drug delivery to biological/medical sensing[77,78]. Due to the major importance of biomedical hydrogels to resist shear forces and ablation, the mechanical performance and tuneability of hydrogels is of special interest[79–81]. However, the colloidal interactions and arrangement often remains unattained leaving behind possible synergetic effects[82–84]. We mechanically characterize a polyacrylamide-colloid hybrid hydrogel in a colloidal monodisperse and a colloidal gelated state. We show, that the elasticity of the polyacrylamide (PAM) hydrogel can be increased by an order of magnitude by the incorporation of monodisperse DNAcc. In addition, the gelation of colloids almost doubles the elasticity reached for the monodisperse state, while the yield strain is enhanced simultaneously. Thus, the toughness and the related resistance of the hybrid material in the gelated state is increased by a factor of 35, proving the relevance of colloidal structure formation for the mechanical performance. Most data and scientific findings of these chapter have been published[85].

4.1 Production of polyacrylamide-DNA-coated colloids hybrid gels

Colloidal interactions and the resulting structure formations are often coupled to the surrounding media and the chemical characteristics. Tuning the colloidal arrangement without changing the mechanical properties of the surrounding hydrogel is mostly out of reach for polymer-colloid hybrid networks[86,87]. Hence, we developed a system, where the colloidal structure formation and the polymerisation of the hydrogel can be induced individually at different points in time and under the same buffer conditions (Fig. 4.1). Therefore, we functionalized two species of 1 µm sized polystyrene colloids with different

single stranded DNA. The sequences are designed in such a way, that the microspheres remain monodisperse under hybridisation condition, while the structure formation can be induced by the addition of a 38 nT ssDNA-linker strand. The fast heterocoagulation can be monitored by confocal imaging and results in the fractal gelation of the colloids. The fractal dimension was determined as D~1.8, which is in accordance with the diffusion limited cluster aggregation[88]. The polymerisation of the polyacrylamide gel can be triggered afterwards by light exposure using a light-sensitive catalyst. Subsequent imaging of the samples proves that the polymerisation does not deform the colloidal gel and the fractality remains. Consequently, polyacrylamide-DNA-coated colloids hybrid hydrogels can be obtained in a colloidal gel or monodispersed state and analysed in rheological means.

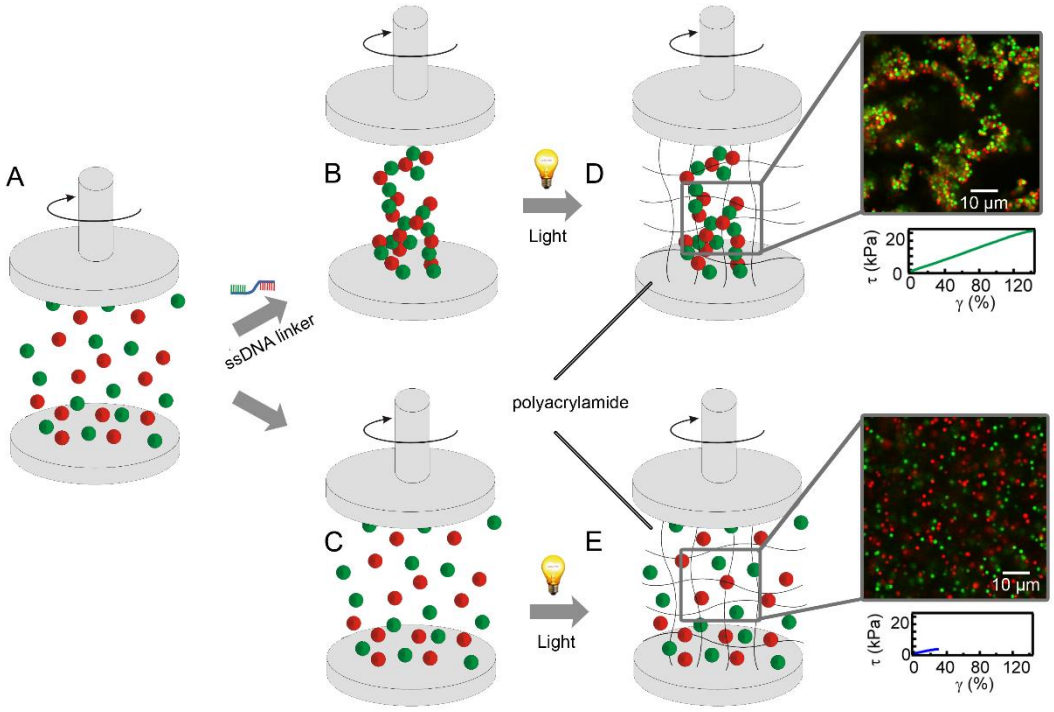

Figure 4.1: Production of the different colloidal hydrogels. A) The DNAcc are dispersed in the unpolymerized polyacrylamide and stay monodisperse, because of the non-complementary DNA docking strands. B) The colloidal structure formation can be induced by the addition of ssDNA-linker, or C) remains in the dispersed state. D), E) The polymerization of PAM is triggered by a light-sensitive catalyst, yielding polymer–colloid hybrid hydrogels, which differ in their colloidal organisation. Confocal imaging confirms that the colloidal structure formation is not influenced by the PAM polymerisation (here: DNAcc 2% (v/v)). The strain-stress experiments show the increased brittleness for the monodisperse system and are discussed in more detail in chapter 4.3.

4.2 Reinforcement of monodisperse DNA-coated colloids on the polyacrylamide hydrogel

Polyacrylamide is a hydrogel with a wide range of viscoelastic properties and is therefore used in many different applications. The polyacrylamide monomer and crosslinker concentration will define the mesh size and the corresponding elasticity of the network. The hydrogel matrix is the dominant compound in the system and was therefore investigated separately without the addition of colloids[89]. The elasticity of the polyacrylamide networks was analysed for different PAM concentrations, while the ratio of monomers to crosslinker (29:1) was kept constant. To this end, we performed constant frequency measurements over time, to determine the duration of the different networks to complete the gelation. While the high PAM networks completely polymerize in a few seconds, lower PAM networks are characterized by a distinct lagphase and a relative slow polymerisation curve (Fig. 4.2).

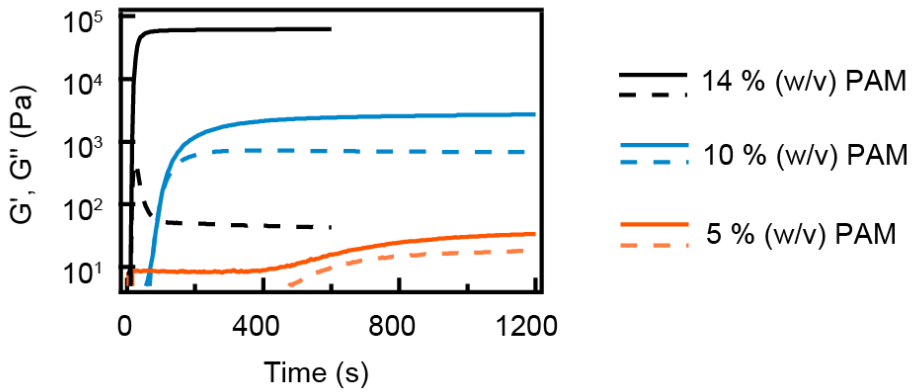

Figure 4.2: Polymerization measurements. The Polymerization of pure polyacrylamide was monitored by measuring G' (lines) and G'' (dashed lines) at $f = 1$ Hz and $\gamma = 0.1$ for different PAM concentrations. The asymptotic value G'_{max} of G' for the lowest PAM concentration is approximately reached at $t = 20$ min.

After identifying the polymerization time, it is possible to analyze the storage modulus (G') of the different concentrated PAM networks by using frequency sweeps (f=0.1-10 Hz and $\gamma = 0.1$). As expected from literature, the elasticity of the network has a power law dependency on the PAM concentration. The storage modulus ranges from 30 Pa to 5.5 kPa for the different concentrations (Fig. 4.3). While the elasticity of the network increases with the PAM concentration, the system also tends to get more brittle. To this end, we performed strain-stress experiments (Fig. 4.6 and 4.8A) and determined the yield strain when the network tends to fail and the network is plastically deformed.

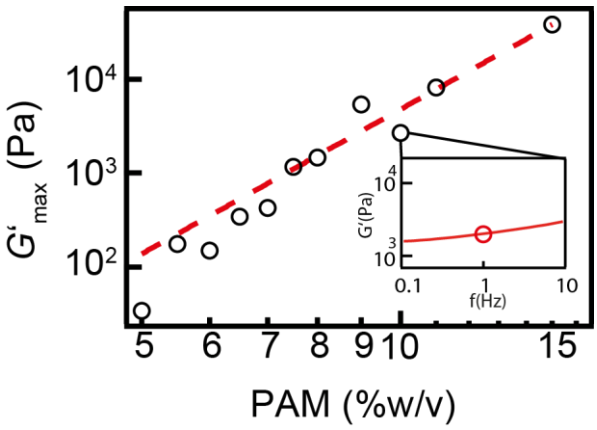

Figure 4.3: Mechanical properties of the polyacrylamide gel. The storage modulus G'_{max} of pure PAM increases with the monomer concentration as a power-law function ($0.036 * x^{5.13}$). The elasticity of the gels was analysed using frequency sweeps (inset). G' was determined at f=1Hz (red circle).

In a next step, we investigated the interplay of the PAM gel and freely distributed colloids. The PAM concentration was kept constant (10%) and the volume fraction of the colloids was increased successively (Fig. 4.4A). A strong increase of the storage modulus can be detected. At 4% colloidal volume fraction, the storage modulus increases from 200Pa to 1000Pa. This strong relationship is in accordance with the increased elasticity seen for filler materials in composite networks[90]. In addition, we analyzed the influence of the colloidal reinforcement for different concentrated PAM networks. We determined the ratio between hybrid gels with 4 vol.% colloids and the corresponding pure PAM without colloids (Fig. 4.4B). It has shown that the colloidal reinforcement is especially prominent for weak PAM gels. The incorporation of colloids increases the storage modulus by 15-fold. However, the ratio of G' decrease with the PAM concentration and vanishes for very stiff PAM gels.

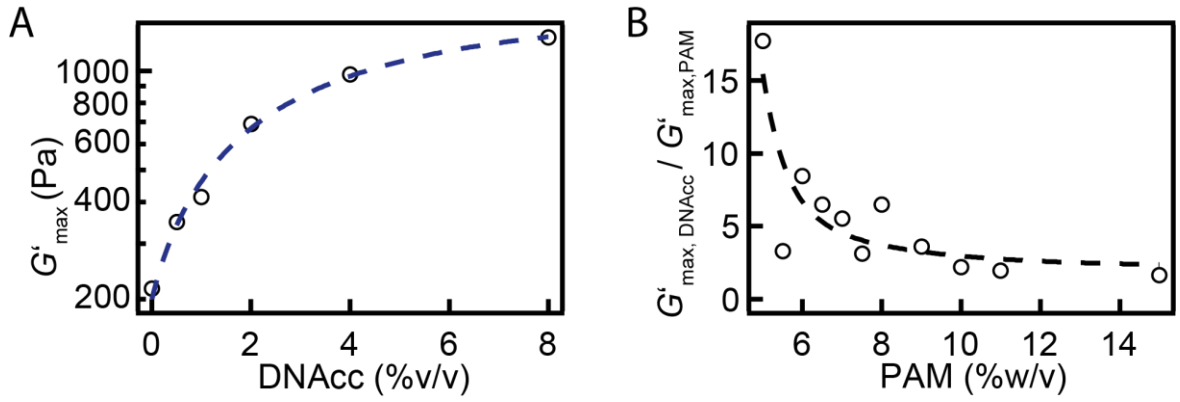

Figure 4.4: Influence of monodisperse colloids within a polyacrylamide gel. A) The storage modulus of the hybrid gel was analysed for different concentrations of monodisperse DNAcc at a fixed PAM concentration (5% w/v). The colloids lead to a continuous increase of G' by approximately an order of magnitude ($476.43 * x^{0.48}$). B) Comparison of colloidal hybrid gels (4% (v/v) of monodisperse colloids) and pure PAM gels. The influence of the monodisperse colloids on the storage modulus is especially prominent at low PAM concentrations and strongly suppressed at PAM concentrations above 8% (w/v).

It is reported that the reinforcement of such composite materials is based on colloid-colloid interactions, which have a long-range for weak surrounding gels, which decreases with the stiffness of the surrounding gel[91]. The colloids act as polymerization seeding points, which create coronas of higher PAM concentration around the single colloids with distinct concentration gradients. The overlap of these coronas results in increased particle interaction, effectively enhancing the elasticity of the network (Fig. 4.5). In higher concentrated networks, the gradient around the particles is reduced, because of the complete gelation of the PAM network. This leads to a reduction of the reinforcement of the filler particles. It is noticeable, that the addition of colloids also increases the effective PAM concentration by the displacement of the media. Nevertheless, this effect is very small and negligible. The PAM concentration of a 5% w/v network will only increase by 0.2% using 4% (v/v) of colloids.

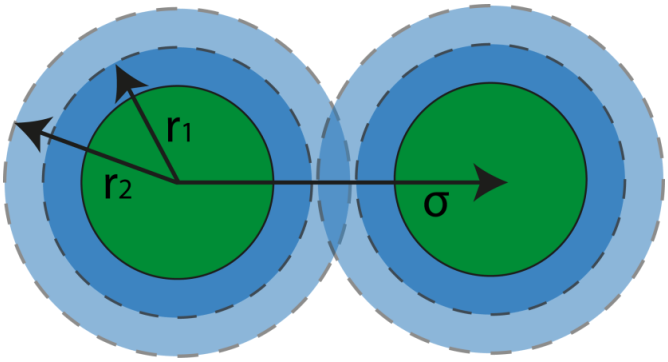

Figure 4.5: Interaction of colloids within a hydrogel. The colloids (green) act as polymerisation seeding point, resulting in a gradient of PAM concentration around the single colloids. The intersection of the increased PAM results in particle-particle interactions, which depend on the distance (σ) between two colloids and the present gradient of the surrounding PAM network, which is schemed by the colour strength (blue) for coronas at distances of $\mathbf{r_1}$ and $\mathbf{r_2}$.

Similar to the PAM network, which is getting more brittle for stiffer gels, the increased G' caused by the colloids is also connected to a reduction of the yield stress. This can be seen in the direct comparison of the strain-stress experiments (Fig. 4.6) and over the complete range of PAM concentrations (Fig. 4.8A). This effect is also in accordance with the model of coronas around the colloids. The single colloids and their concentration gradients lead to an increased inhomogeneity of the system resulting in the formation of crack tips at higher deformations. These defects will propagate through the system leading to a premature collapse of the system.

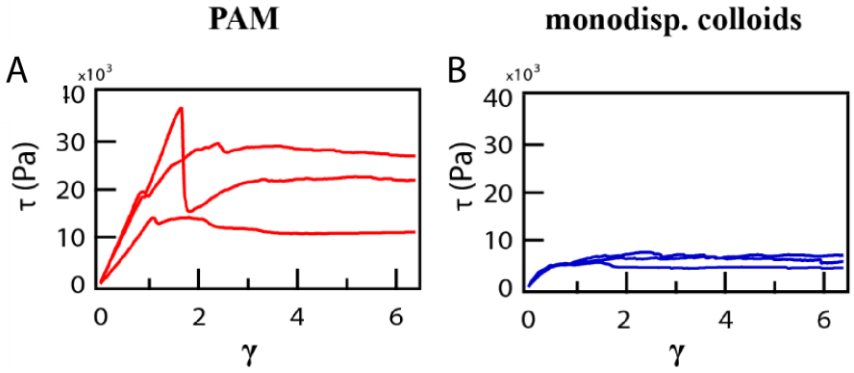

Figure 4.6: Strain-stress measurements of pure PAM and monodisperse colloidal hydrogels. A), B) The strain-stress curves of pure PAM (10%) and monodispersed colloids embedded in 10% PAM were analyzed. The yield strain γ_{yield}, which is defined as the first turning point in the strain-stress curve, equivalent to the second derivative to be zero was determined. The pure PAM $\left(\gamma_{\mathrm{yield}} = 84.0 \pm 11.2\right)$ reaches the highest value compared to the monodispersed system $(\gamma_{\mathrm{yield}} = 12.1 \pm 1.6)$.

4.3 Influence of the colloidal structure formation

The addition of monodisperse colloids leads to an increased storage modulus by more than an order of magnitude. In addition, the colloidal gelation results in an almost doubling of the stiffness at low PAM concentration. This can be seen by the direct comparison of G' of freely distributed colloids and gelated ones (Fig. 4.7). This effect persists for PAM concentration of up to 10% and vanishes for very stiff and brittle gels. The reinforcement caused by the gelated colloids can be explained by the increased colloidal interaction. The mean distance of colloids is drastically reduced once they aggregate. This results in a larger overlap of the PAM coronas leading to increased interactions. Once the elasticity of the network is dominating, the influence of the particle interaction reduces, as it can be seen for the monodisperse colloidal system.

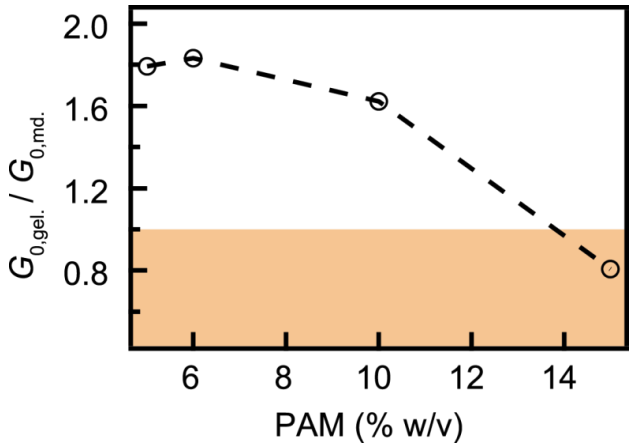

Figure 4.7: Comparison of gelated and dispersed colloids. Colloidal gelation results in an increased stiffness compared to the dispersed system. The gelation of the colloids within the hybrid gel (4% (v/v) DNAcc) increases the storage modulus, which can be seen by the ratio $G_{(0,gel.)}/G_{(0,md.)}$, with G_0 the shear moduli for hybrid hydrogels containing gelated or monodisperse colloids. This effect is especially prominent at low PAM concentrations and suppressed at high PAM concentrations (orange area).

In addition, the gelated colloids are also able to resist more stress than the randomly distributed colloids. The shear stress seems to distribute more homogenously which reduces the formation of crack tips prominent for the monodisperse colloids. This is in accordance with the behavior of the loss modulus, which indicates the dissipative loss of energy. The monodisperse system increases significantly with the colloidal concentration, while the gelated system stays constant over the measured range.

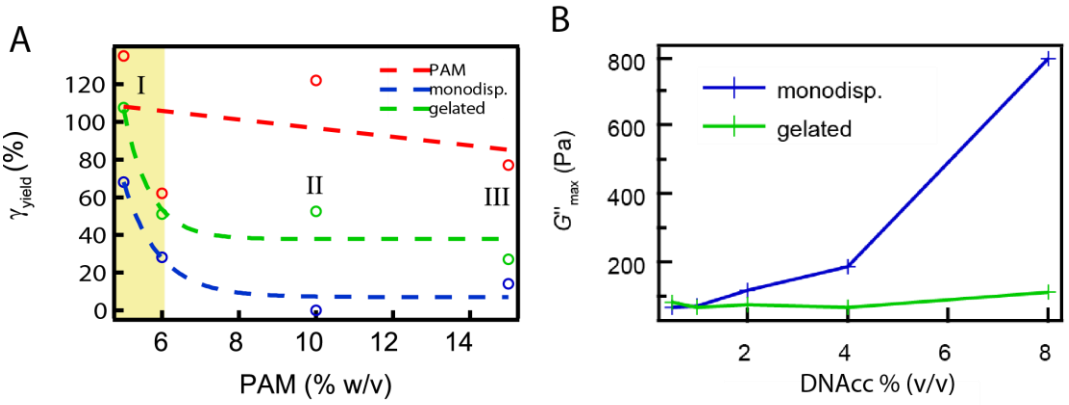

Figure 4.8: Mechanical stabilization of gelated hybrid gels. A) The yield strain of monodisperse DNAcc is drastically decreased compared to the pure PAM, even at low concentrations (yellow area). In contrast, the gelated DNAcc are able to mechanically stabilize the hybrid gel. B) The loss modulus of the gelated hybrid gel is constant for different concentrations of DNAcc. For monodisperse colloids, G'' increases significantly with higher DNAcc concentrations, which indicates an additional energy dissipation in the system.

For a more detailed analysis, we performed strain-stress ramps. We applied multiple shear steps with increased deformation to extract the different behaviour of the two systems (Fig. 4.9). It can be seen, that the monodisperse system is irreversible deformed after the first step of the strain-stress experiment (γ =15%). In comparison, the gelated system is able to resist 9 shear steps with a total deformation of γ=140%. In total, the increased elasticity and the additionally increased yield stress leads to a 35-fold increase in toughness, caused by the prolonged linear regime.

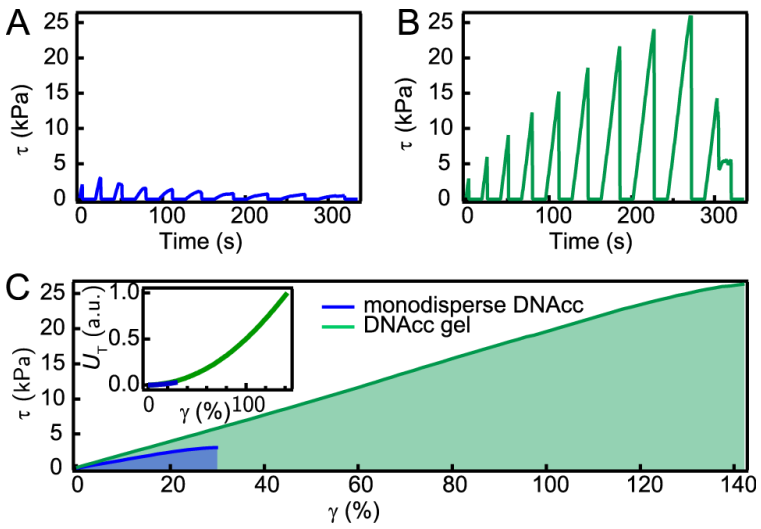

Figure 4.9: Extended linear response of gelated hybrid gels. A), B) Strain ramp protocols for the 4% (v/v) DNAcc – 10% (w/v) PAM hybrid hydrogel with monodisperse and gelated DNAcc, respectively. C) The detailed representation of the last linear strain response for monodisperse and gelated DNAcc shows the synergetic effects of the colloidal structure formation. The energy, which is required to overcome the linear regime is increased by a factor of 35 by the colloidal gelation. The enlarged linear response is responsible for the rescue of the toughness.

4.4 Discussion and Outlook

In this chapter it was shown, that the colloidal arrangement is a fundamental process to tune the viscoelastic behaviour of polymer-colloid hybrid gels. This was realised by developing a procedure to trigger the polymerisation of polyacrylamide hydrogel and the colloidal aggregation of DNA-coated colloids independently. Thus, it was possible to investigate the influence of the structure formation exclusively without changing the chemical environment of the system. We showed that the incorporation of monodisperse colloids has a strong influence on the stiffness of the hybrid gel, however results in a more brittle network. The colloidal gelation is able to increase the storage modulus and the yield strain, resulting in a reinforced toughness. However, the strengthening effects strongly rely on the surrounding media. Therefore, we defined three PAM regimes from soft, intermedia and stiff to summarize the influence of the colloidal structure formation. We compare the toughness of the pure PAM, the monodisperse and the gelated hybrid-gels for the different PAM regimes (Fig. 4.10). At low PAM concentration, the incorporation of monodisperse colloids results in an increased G'. Since these hydrogels tend to be more brittle, the toughness of the pure PAM and the monodisperse colloidal gel is almost identical. However, the elasticity of the gelated system is even more prominent and resists more deformation. Thus, the gelated system has a significant high toughness in this regime. In the intermedium regime, the toughness of the monodisperse system decays, because of the reduced yield strain. However, the gelated system is able to partially rescue the yield strain, leading to an identical toughness compared to the pure PAM network. In the regime of the high PAM concentration, the reinforcement of monodisperse and gelated colloids vanishes and the toughness of pure PAM network is dominating. In this experimental setup, the meshsize of

the PAM network is very small compared to the large colloids. Thus, the interactions always arise from the overlap of the concentration gradient caused by the coronas. Therefore, it would be interesting to investigate the influence of colloidal arrangement, for colloidal sizes which are comparable to the mesh size of the surrounding media. Here, different interaction of hydrogels and colloidal-gel arise with new synergetic effects, like seen in other double network materials. In addition the incorporation of the colloidal network can be tuned by a direct and controlled crosslinking between colloids and the hydrogel.

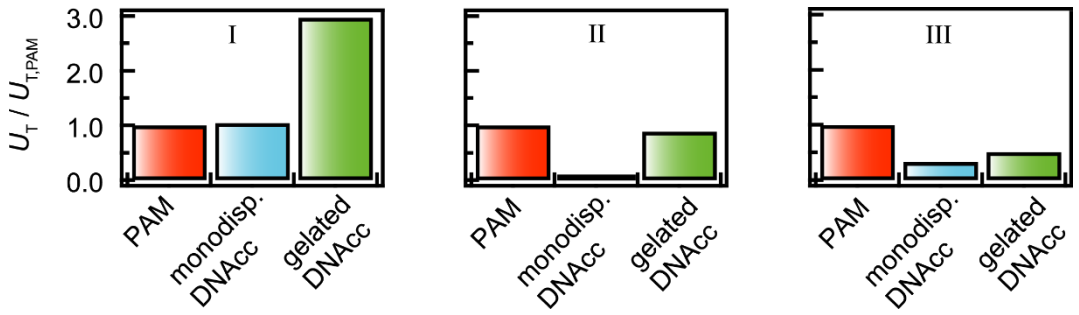

Figure 4.10: Toughness U_T for 3 different PAM concentrations. At low PAM concentration (I, PAM: 5%), the colloidal gelation significantly enhances the toughness. For higher concentrations of PAM (II, PAM:10%; III, PAM:15%), the toughness of the monodisperse hybrid gel is reduced. However, the gelation of DNAcc is able to rescue the toughness of the pure PAM network and facilitate tough gels with a significantly higher storage modulus.

5. Transient structure formation

In this chapter, we aim to control the dynamic self-organisation of DNA-coated colloids in order to make one step towards autonomously acting materials. Colloidal self-assembly is a powerful concept to build functional materials[92–97]. A wide range of different material properties can be addressed by the specific choice of the colloidal building blocks and their organisation[98–102]. In the previous chapter, we already showed that the mechanical performance of a colloidal hybrid hydrogel significantly relies on the colloidal arrangement. So far, mainly external stimuli like temperature ramps[103,104] or chemical interventions like phosphorylation[105] were used to control the temporal colloidal interactions. However, the autonomous and transient control of the colloidal structure formation was never accomplished using the potential of DNA-coated colloids (DNAcc). Here, interactions of the single building blocks can be tuned precisely by the proper choice of pre-crafted DNA [106,107], resulting in colloidal structures ranging from colloidal crystals[41,108] to fractal-gels[109,110]. In addition, the selectivity of DNA hybridisation enables hierarchical self-assembly in multicomponent systems[43]. The colloidal interactions can be activated at different stages resulting in aggregation scaffolds and the formation of a diverse set of structures. We report the dynamic control of the colloidal interactions by using an antagonistic set of enzymatic reactions. The *RNA polymerase T7* is used to produce RNA-linker strands which are able to bridge between two different species of DNAcc and induce the colloidal structure formation. The subsequent colloidal disintegration is realised by the degradation of the RNA-linker using the ribonuclease *RNaseH*. The transient and autonomous aggregation is realised by using fuel consumption. We show that the colloidal aggregation can be controlled in time and total cluster size by tuning the underlying enzymatic reactions. In addition, control of the time traces can be accomplished by using competing DNA hybridisation reactions. Finally, the spatio-temporal control of the colloidal self-assembly can be attained, by restricting the enzymatic activity locally, which results in traveling aggregation fronts. Most data and scientific findings of these chapter have been published[111].

5.1 Enzymatic setup

In the previous chapter we induced the colloidal structure formation by adding single stranded DNA-linker to the system, which are able to bind the complementary docking strands of the colloids and bridge between two different colloidal species. Here, we control the colloidal interaction dynamically by producing and degrading RNA-linker strands (Fig. 5.1). The production of the RNA-linker is realised by the *RNA polymerase T7,* which catalyses the production of single stranded RNA (ssRNA) by using a double stranded DNA (dsDNA) template. The polymerase binds to the 20nT recognition sequence of the template and transcribes the subsequent part into ssRNA, which are used as colloidal linkers. Finally, the disintegration of the colloidal structures relies on the degradation of the RNA-linker. This is realised by the ribonuclease *RNaseH*, which is able to catalyse the degradation of RNA of a RNA-DNA complex. Thus, the *RNaseH* degrades the RNA-linker strands, once they are bound to the colloidal DNA.

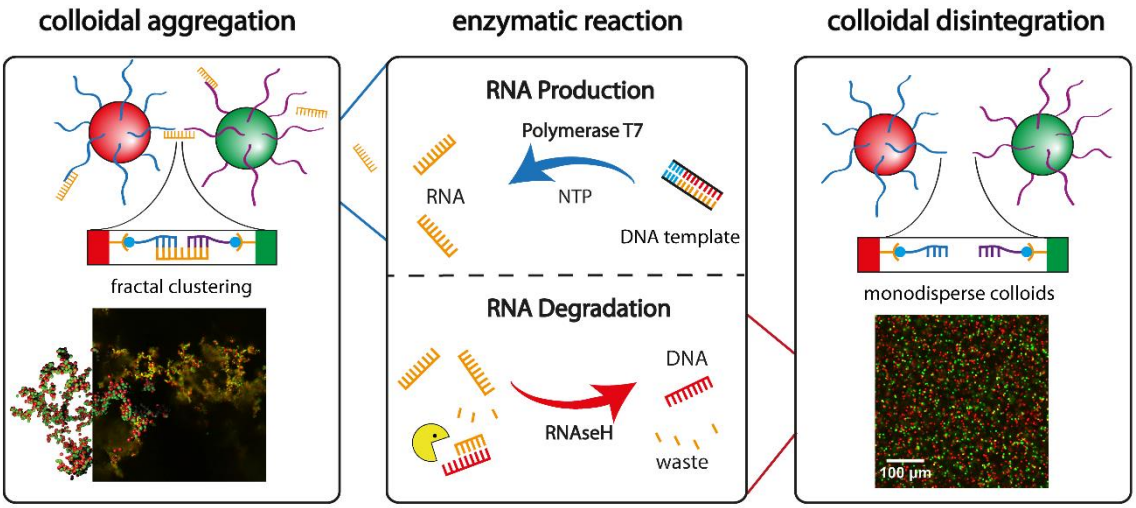

Figure 5.1: Scheme of enzymatic controlled structure formation. The 1 µm sized polystyrene colloids are functionalized with two sorts of ssDNA docking strands and can be distinguished via fluorescence. The structure formation is induced by complementary RNA-linker strands which link the two different colloidal species. The production of the RNA-linker is realised using a *T7 Polymerase,* free dsDNA templates and *NTP*s in solution. The disintegration process of the so formed colloidal clusters is achieved by the activity of the ribonuclease *RNAseH*, which degrades the RNA-linkers once they are bound to DNA.

5.2 Enzymatic mediated colloidal aggregation

The dynamic control of the colloidal structure formation requires a precise control of the underlying enzymatic reactions. Therefore, it is essential to determine the reaction rates of the enzymes and characterize their interplay. As a first step, the production of the RNA-

linker by the *T7 polymerase* will be modelled. The RNA production depends on the substrate *NTP*, the ds template and the total amount of enzymes. The resulting reaction can be described by a *Michaelis-Menten* model:

$$\frac{dRNA}{dt} = k_{T7} \cdot \frac{c_{T7}}{K_{M,T7} * c_{T7}} \cdot \frac{c_{NTP}(t)}{K_{M,NTP} + c_{NTP}(t)} \tag{5.1}$$

with c_{T7} and c_{NTP} the concentrations of *T7* and *NTP*, and $K_{M,T7}$ and $K_{M,NTP}$ the corresponding *Michaelis-Menten* constants. k_{T7} represents the effective catalytic rate of *T7* at a template concentration of 25 µM, which was kept constant in the following experiments. In a first step, fluorescence time-course measurements were performed to visualise and quantify the production of RNA-linker strands. By exclusively varying the *NTP* and *T7* concentration, the *NTP* and *T7* dependency of the production speed were quantified separately. In all experiments, a constant speed of RNA production can be observed (Fig. 5.2A and B). The fluorescence signal of the RNA was transferred into total RNA concentration according to chapter 3.3.3 and the production rate of the RNA was determined using linear fits. Here, the reaction speed shows a linear dependency towards *T7* and *NTP* (Fig. 5.2C and D).

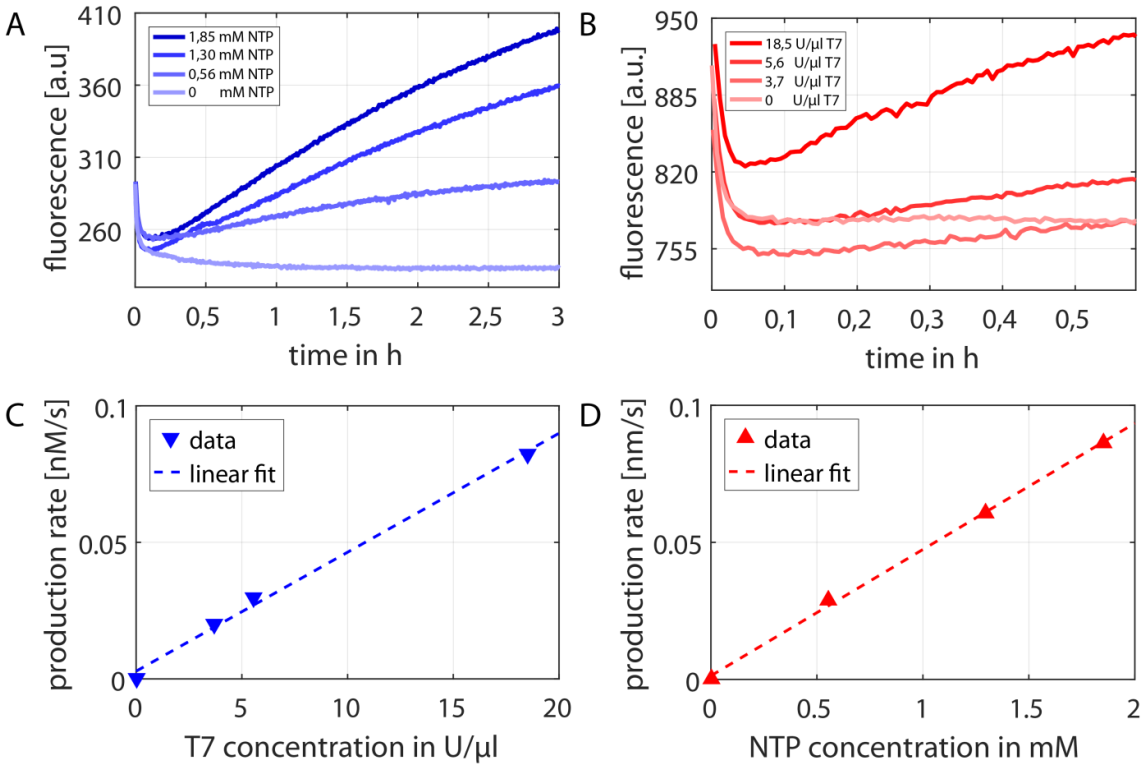

Figure 5.2: RNA production. The RNA production is monitored by fluorescence spectroscopy using the DNA intercalator *SYBR Green II*. A) The speed of RNA production is controlled by increasing the substrate *NTP* and is constant for the duration of the measurement. B) The same linear production can be achieved by controlling the amount of *T7 polymerase*. C),D) Here, the signal of A and B was transferred to the total RNA concentration (chapter 3.3.3) and the rates were obtained by linear fits. Both *NTP* and *T7* controlled experiments show a linear dependency towards the production speed.

The constant production rates indicate that the *NTP* is not depleted and the concentration stays constant for the duration of the measurements and can be approximated as:

$$c_{NTP}(t) \sim c_{NTP}(t = 0) = NTP = const. \tag{5.2}$$

Additionally, the linear dependency of *NTP* and *T7* leads to a simplification of the Michaelis-Menten model to a linear description:

$$\frac{dRNA}{dt} = k1 \cdot T7 \cdot NTP \tag{4.3}$$

Where *k1* describes the effective rate at a constant template concentration and $T7$ the dimensionless normalised concentration of c_{T7}. In subsequent experiments, confocal imaging was used to investigate the ability of the enzymatic reaction to induce structure formation (Fig. 5.3). The production of RNA-linker leads to an aggregation of the binary colloidal system (Dock A+B). The monodisperse state of the single colloidal compounds proves the selectivity of the produced RNA-linker.

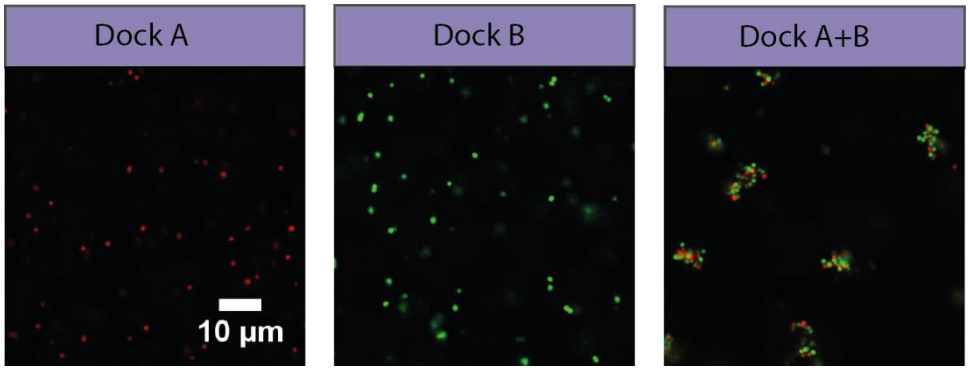

Figure 5.3: Polymerisation of RNA-linker with different colloids. The polymerisation of RNA-linker was performed in the presence of colloids functionalised with docking A, docking B and the combination A+B. Only the combination of both docking strands forms clusters. Thereby it is possible to prove the functionality of the produced RNA-linker and the selectivity of the DNA hybridisation.

As already shown in the fluorescence spectroscopy measurements, the speed of RNA production can be controlled precisely by tuning the enzymatic reactions. In a next step, we aimed to transfer this control to the colloidal aggregation. Thus, we monitored the structure formation in the presence of the enzymatic setup for different production rates by varying the *NTP* concentrations. We quantified the colloidal aggregation by calculating the average cluster size over time according to chapter 3.3.4. As expected, the speed of aggregation is directly coupled to the *NTP* dependent speed of RNA polymerisation (Fig. 5.4A). In addition, we monitored the aggregation after one hour of polymerisation to demonstrate the different occurring cluster sizes (Fig. 5.4B). The colloidal clusters for the low *NTP* concentration consist of only a few colloids, while the fast RNA production results in large colloidal clusters which already form colloidal gels. It is noticeable, that the aggregation speed can only be controlled, once the RNA production speed is below a certain limit. For

very high RNA production speeds, the amount of RNA at which the optimal aggregation conditions are fulfilled (~40 nM) is reached within a few minutes. Hence, the speed of aggregation is only limited by the diffusion of the colloids and it is necessary to stay below this regime, to enable the control of aggregation speed.

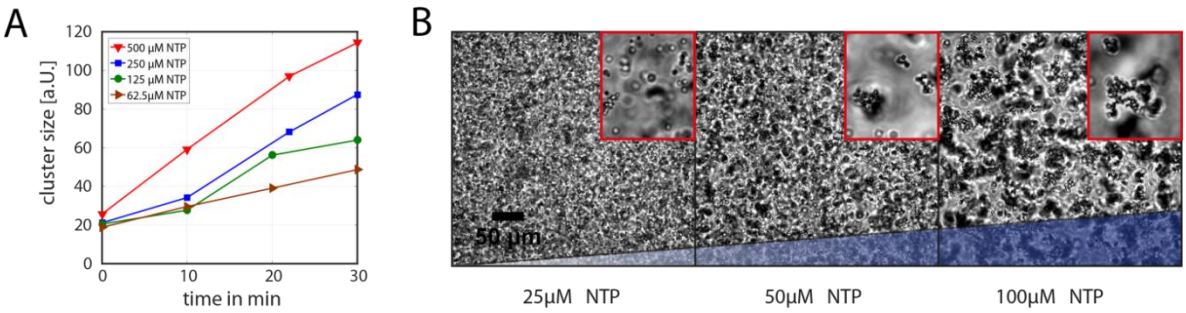

Figure 5.4: Colloidal aggregation over time for different RNA production rates. A) The colloidal clustersize was analysed over time for samples containing different *NTP* concentrations. The speed of aggregation is directly controlled by tuning the speed of RNA-linker production. B) Colloidal structure formation after one hour of RNA production for different *NTP* concentrations.

5.3 Enzymatic mediated colloidal disintegration

In a next step, we aimed to control the disintegration of colloidal clusters by using the ribonuclease *RNaseH*. The enzyme degrades RNA once it is bound to DNA and can consequently be used to disintegrate DNA-coated colloids which are linked by ssRNA-linker. The degradation of the RNA can be described by *Michaelis-Menten* kinetics:

$$\frac{d\,RNA}{dt} = -k_{RNaseH} \cdot c_{RNaseH} \cdot \frac{RNA}{K_{M,RNA} + RNA} \tag{5.4}$$

with k_{RNaseH} the catalytic rate of the *RNaseH* and $K_{M,RNA}$ the *Michaelis-Menten* constant. Since the ribonuclease needs a DNA-RNA substrate, we analysed the effective rate of degradation in the case of saturated ssDNA concentrations by varying the *RNaseH* concentration (Fig. 5.5A). The speed of degradation shows a linear dependency towards the enzyme concentration (Fig. 5.5B). This is in accordance with the typical K_M values known for ribonucleases ($K_M = 10^{-2} M$). The K_M is much higher than the produced RNA concentrations (~100 nM), which leads to the linear relation between *RNaseH* concentration and RNA:

$$\frac{d\,RNA}{dt} = -k_2 \cdot RNaseH \cdot RNA \tag{5.5}$$

with k2 the effective rate of degradation. Finally, the functionality of the *RNaseH* is demonstrated by monitoring the colloidal disintegration over time (Fig. 5.5C).

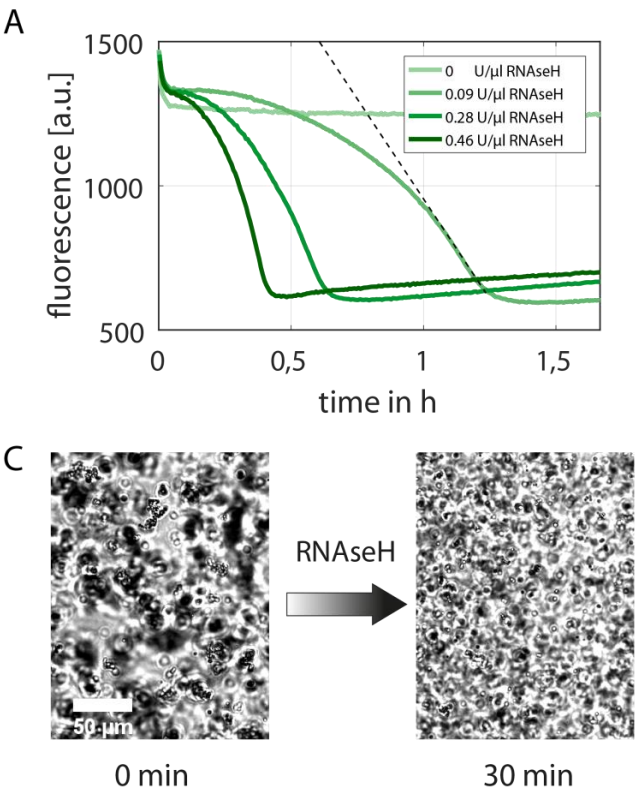

Figure 5.5: Colloidal disintegration. A) The degradation of 10 µM RNA strands was performed for different concentrations of *RNaseH* in the presents of 10 µM complementary DNA. B) The rates of RNA degradation were determined using linear fits at the greatest slope of the time traces (dotted line). C) The colloidal aggregation is induced by the addition of 100 nM RNA-linker strands. The complete disintegration of the colloidal structures was realised within 30 min using a *RNaseH* concentration of 0.1 U/µl.

5.4 Dynamic structure formation

5.4.1 Autonomous transient structure formation

Since the effective reaction rates of the RNA production and degradation were determined, it is possible to describe the interplay of both reactions by a linear coupled differential equation:

$$\frac{d\,RNA}{dt} = k1 \cdot T7 \cdot NTP - k2 \cdot RNaseH \cdot RNA \tag{5.6}$$

Thus it is possible to make prediction for the RNA production of the experiments (Fig. 5.6). As expected, the RNA production results in a linear production in the absence of the degradation term. With increasing *RNaseH* concentration, the RNA production and degradation equilibrates resulting in a steady state.

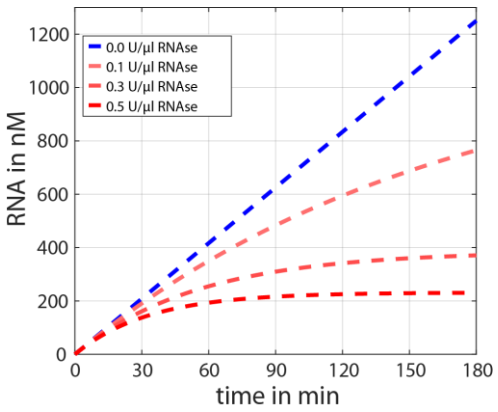

Figure 5.6: Simulation of the RNA production. The RNA production was simulated according to equation 5.6. The production term of the RNA was kept constant, while the *RNAseH* concentration was increased successively. It can be shown, that the coupled linear reaction results in a steady state and shows no transient behaviour.

The steady state does not allow the formation of a transient colloidal aggregation. Thus, it is necessary to avoid the regime of linear production and degradation speed. This can be realised by a reduction of the production speed caused by fuel consumption. This regime can be experimentally determined by using an increased ratio of *T7* and *NTP* concentration in the absence of *RNaseH* (Fig. 5.7A). Thereby, it is possible to extract the consumption term and couple a further differential equation to the RNA production (eq. 5.6):

$$\frac{d\,[NTP]}{dt} = -k3 \cdot NTP(t) \cdot T7 \tag{5.7}$$

with k3 the rate of *NTP* consumption. This rate relies on the amount of nucleotides which are used to produce one RNA strand. It can be seen, that the initial RNA production follows the linear production rate without fuel consumption according to eq. 5.6 (Fig. 5.7A, black dotted line). After 20 minutes the RNA profile differs from the linear equation, because of the reduced *NTP*. After identifying the degradation term, the coupled set of differential equations can be used to make predictions for the transient behaviour in the presents of a degradation term (Fig. 5.7B).

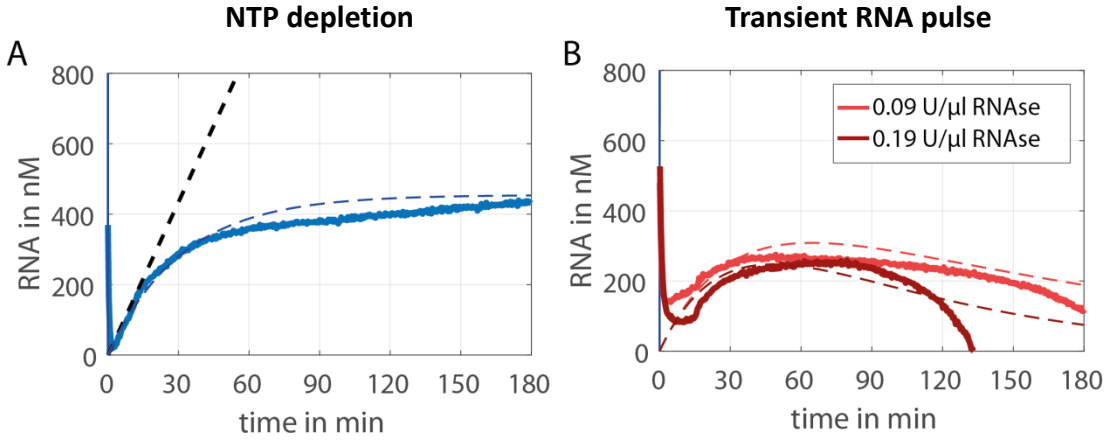

Figure 5.7: Simulation of RNA production. A) The blue curve shows the RNA production in the regime, were the *NTP* consumption is dominant. The RNA production stops without the presence of *RNAseH*. The black dotted line was simulated with eq. 5.6 and fits well with the increase in the beginning. The blue dotted line was achieved by adding a fuel consumption term (eq. 5.7) to the linear equation. Thereby, it was possible to extract the rate *k3*. B) Transient RNA production was achieved by adding *RNAseH* to the limited RNA production with the setup used in (A), the timescales can be controlled by using different *RNAseH* concentration. The dotted line represents the simulation (eq. 5.7), which considers the fuel consumption extracted from (A).

The meassured data and the simulations fit well and the transient behaviour of the RNA can be characterised by a relaxation pulse with a fast production and a consecutive slow degradation phase. In a next step, the enzymatic setup of the transient RNA pulse (0.09 U/µl *RNaseH*) was transferred to the colloidal system. As expected, the colloidal structure formation fits perfectly with the underlying RNA pulse (Fig. 5.8).

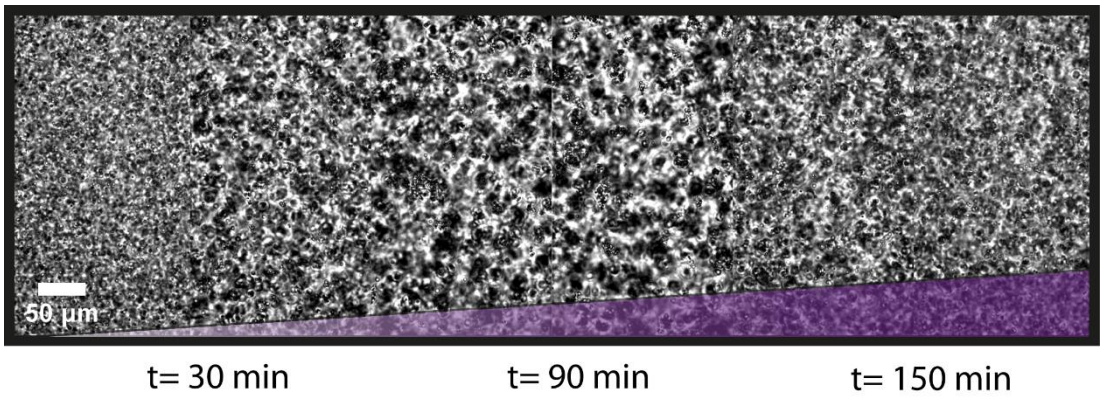

Figure 5.8: Transient colloidal aggregation. The enzymatic setup used in the experiment shown in figure 4.7B was applied to a setup containing DNA-coated colloids. The colloidal structure formation shows the same temporal profile as the RNA production.

5.4.2 Tuning of the transient structure formation

In a next step, we aimed to tune the time traces of the transient structure formation, by exclusively varying the *RNaseH* concentration (Fig. 5.9A). The structure formation can be controlled in time and total cluster size. The time point, when the disintegration of the colloids starts can be controlled (Fig. 5.9C) and is directly coupled to the maximum cluster size (Fig. 5.9B). The different cluster sizes are demonstrated by the insets, showing the complete colloidal gelation for the longest pulse, while the clusters during the short pulse consist only of several colloids. The characteristics of the transient RNA pulse are given by a fast production- and a slow subsequent degradation phase. Therefore, the most straight-forward and precise method to control the shape of the transient pulse, is the tuning of the degradation reaction. In addition, it is also possible to tune the production term of the reaction (Fig. 4.10A). Different *NTP* concentrations result in small variations of the temporal profile. It is noticeable, that the degradation phase of the highest *NTP* concentration (1000 µM) starts first. Thus, the transient clustering (Fig. 5.10B) does not exhibit the sensitive tuning of lifetime and cluster size, seen for the *RNaseH* controlled pulses.

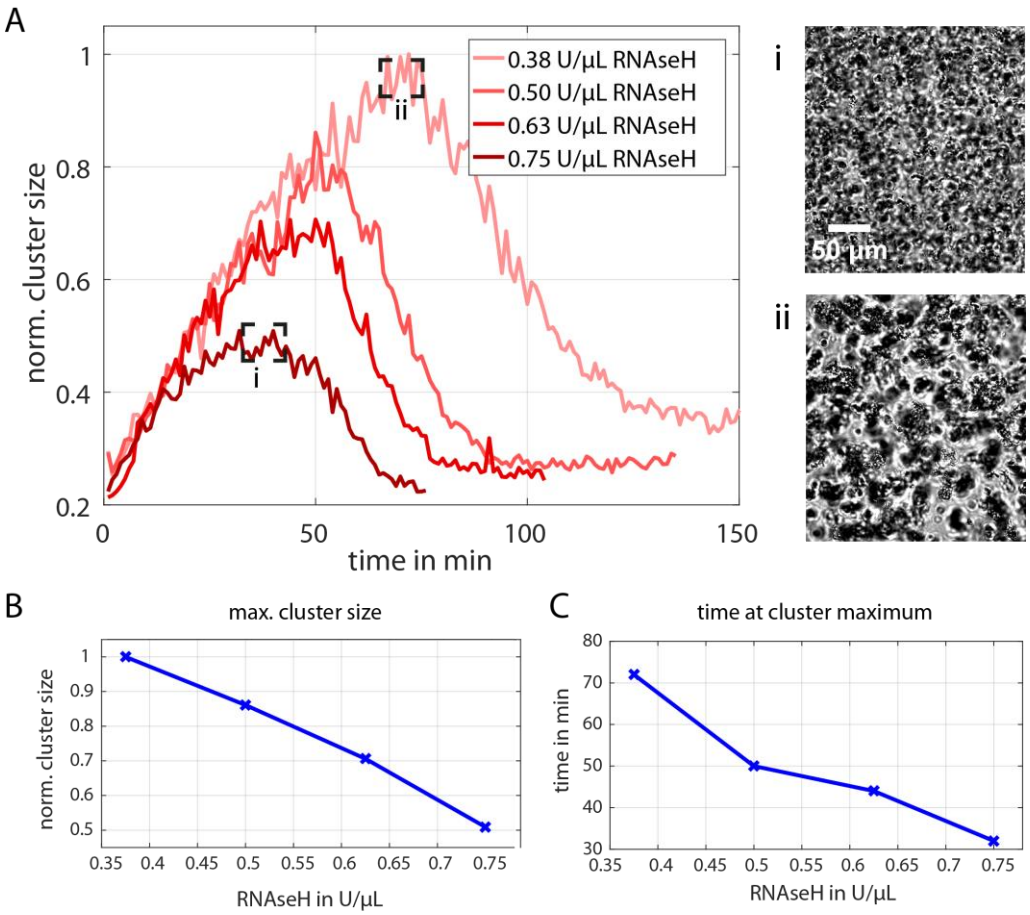

Figure 5.9: Tuning the transient colloidal aggregation. A) Transient colloidal aggregation is controlled by tuning the enzymatic reactions. The limited RNA production was kept constant, while the speed of degradation was varied using different concentrations of *RNaseH*. The insets show the bright field images of the maximum cluster sizes occurring for the shortest (i) and longest pulse (ii). B) The maximum cluster size of the different pulses can be controlled by the *RNAseH* concentration. C) The time point of disintegration is shifted by approximately 40 minutes between the longest and shortest pulse and allows the control of the temporal aggregation process.

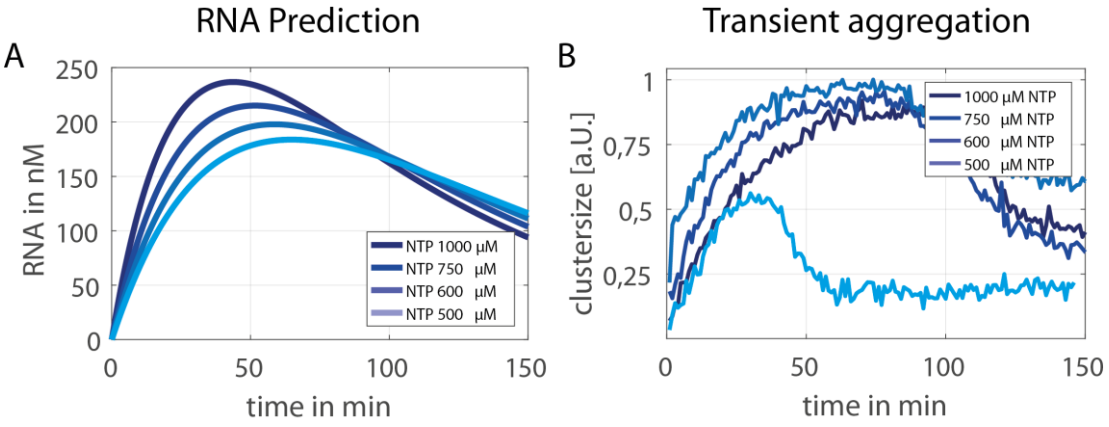

Figure 5.10: Tuning the transient colloidal aggregation by tuning the RNA production. A) Predictions of the RNA pulses for different *NTP* concentrations according to eq.5.6 and 5.7. B) Transient structure formation using the enzymatic setup of the predicted RNA production.

5.4.3 Tuning the transient structure formation by competing hybridisation reactions

So far, we controlled the temporal behaviour of the transient aggregation pulse by tuning the enzymatic reactions. In this chapter, we want to exploit the selectivity of DNA hybridisation to manipulate the structure formation. We introduce a ssRNA strand, which is complementary to the RNA-linker. Thus, the produced RNA-linker will bind the complementary RNA strand and form a RNA/RNA duplex which is protected from the *RNaseH* mediated degradation. The duplex is fully complementary and has therefore a higher affinity than the RNA/docking-DNA complex, which is only half complementary. Consequently, the RNA-linker will preferentially bind the complementary RNA strand. After the RNA strands are saturated with RNA-linker, the RNA can effectively bind the docking strands and induce the structure formation by effective RNA-linker (Fig. 5.11C). The prediction of the effective RNA-linker (Fig. 5.11A) shows a slow delay for transient pulses with the RNA threshold. This is because of the fast production phase in the beginning. The main difference can be seen in the total peak of RNA concentration and the difference in RNA concentration during the degradation phase. This is confirmed by the transient behaviour of the colloidal aggregation (Fig. 5.11B). The start of aggregation is slightly delayed by 5 minutes, while the main difference can be seen in the abrupt degradation phase. Here, the complementary RNA acts as an aggregation threshold.

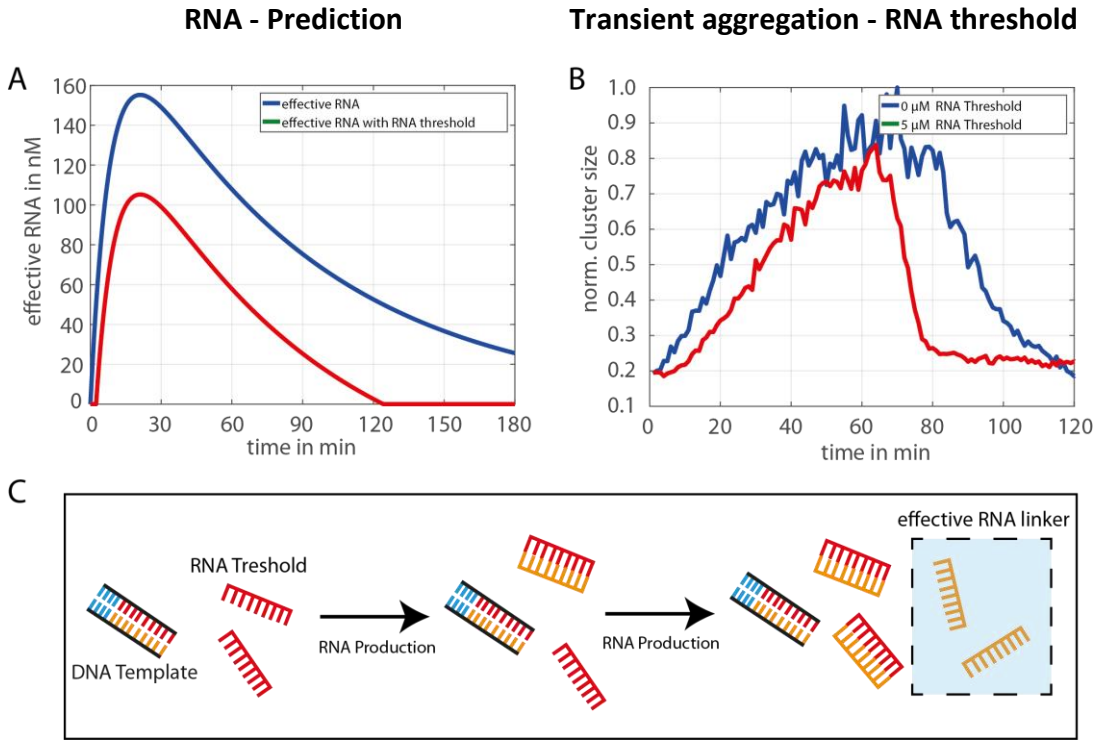

Figure 5.11: Controlling the colloidal structure formation by using threshold reactions. A) Predictions of the RNA profile with and without RNA thresholds. The effective RNA describes single stranded RNA-linker, which can bind colloidal docking DNA, because they are not bound to the RNA threshold. B) Transient colloidal structure formation using 5 µM of the RNA threshold. C) The produced RNA preferentially binds the fully complementary RNA strands. Once the RNA strands are saturated, the excess of RNA strands can effectively be used as linker strands.

5.4.4 Spatial control of the colloidal aggregation

In this chapter, we aim to control the spatio-temporal behaviour of the colloidal aggregation, by restricting the enzymatic activity locally. This was realized by using a microfluidic chamber containing a reservoir, which was functionalised with dsDNA templates (Fig. 5.12A). Thus, it is possible to exclusively produce RNA-linker in the reservoir, while the RNA degradation takes place globally.

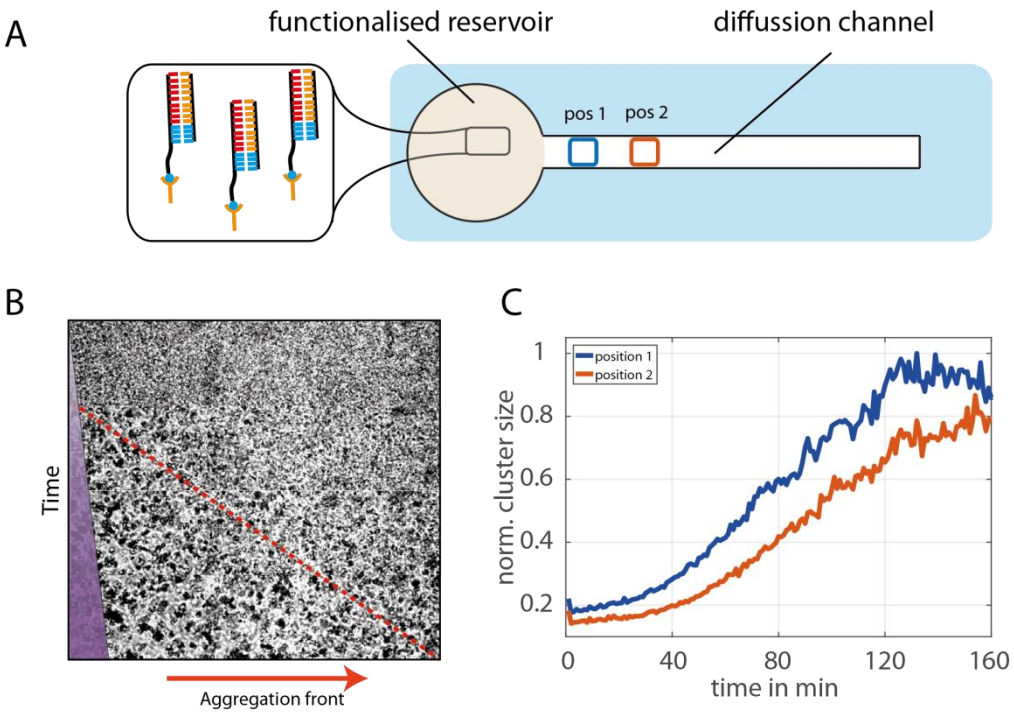

Figure 5.12: Diffusion channels with template-functionalised reservoirs. A) Scheme of the diffusion channel. The reservoir is functionalised with DNA templates via biotin-streptavidin bonds to enable a restricted RNA production. Position 1 and 2 demonstrate the position of the colloidal monitoring. B) The colloidal structure formation propagates from the reservoir into the channel, because of the diffusing RNA strands, which were produced in the reservoir. C) The average clustersize over time for two different positions along the channel.

In a first step, the restricted RNA production was observed in the absence of a degradation reaction. As expected, the colloidal aggregation starts in the functionalised reservoir, while the aggregation within the diffusion channel is delayed. The RNA-linkers diffuse into the channel, resulting in a propagating aggregation front (Fig. 5.12B). The propagation of this aggregation was quantified by measuring the average cluster size at two different positions in the diffusion channel (Fig. 5.12C). Here, the speed of propagation is given by the diffusion constant of the RNA-linker and the speed of the RNA production. A fast RNA production results in an increased RNA gradient, which leads to an enhanced diffusive flux, according to Fick's first law. Thus, we can only observe the propagation of an aggregation front near the reservoir for lower production rates. In addition, it is also possible to apply the enzymatic

conditions of the transient pulse to the diffusion chamber. In this case, a homogenously aggregation takes place near the reservoir, because of the fast RNA production. Subsequently, a degradation front can be detected, which propagates from the reservoir into the channel (Fig. 5.13). Surprisingly, the observations are in contradiction with regular reaction-diffusion systems. It is expected, that the highest concentration of RNA is always at the position of the production source (reservoir). Consequently, there should be a decreasing gradient of RNA and colloidal clusters along the diffusion channel. However, the colloidal clusters start to disintegrate near the reservoir, resulting in a disintegration front propagating along the channel.

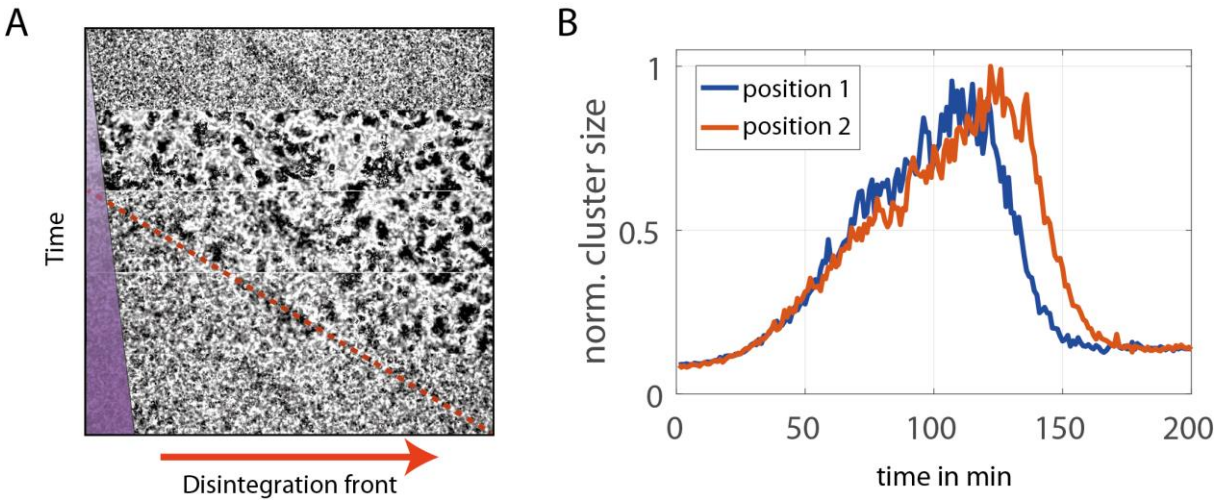

Figure 5.13: Transient RNA pulse within a diffusion channel. A) The colloidal structure formation is measured over time in the diffusion channel, by applying a transient RNA pulse at the reservoir. A fast aggregation can be observed, which is followed by a propagating disintegration front. B) The average cluster size was determined over time for two positions along the channel. A homogenous aggregation can be seen, which is followed by a disintegration, starting at position 1 (positions defined in Fig. 4.12 A).

To analyse this in more detail, we adapted the simulations of the transient behaviour with a reaction-diffusion equation:

$$\frac{d\,RNA(x,t)}{dt} = RNA(x,t) + D \cdot \frac{d^2\,RNA(x,t)}{dx^2} \tag{5.8}$$

with D the diffusion coefficient of the RNA-linker. The RNA production was simulated on a 16x128 matrix according to the already introduced reaction-model (eq. 4.6). In order to simulate the restricted reaction of the reservoir, the production only takes place in the first part of the channel (16x10 matrix) and was set to zero at the rest of the channel. The diffusion of the RNA was simulated using a gaussian filter function. In addition, the colloidal aggregation was simulated by a colloidal binding rate under consideration of the local RNA concentration (more details in chapter 3.3.5). Thus, it is possible to predict the concentration gradients of the RNA pulse and the resulting colloidal aggregation in the diffusion channel

over time. As expected, applying the transient RNA production leads to the diffusion of the RNA into the channel and a subsequent degradation, were the highest concentration always occurs at the position of the reservoir (Fig. 5.14). Therefore, the RNA dependent colloidal aggregation shows the same behaviour. Consequently, a direct transfer of RNA concentration to colloidal aggregation is not sufficient to describe the observed behaviour.

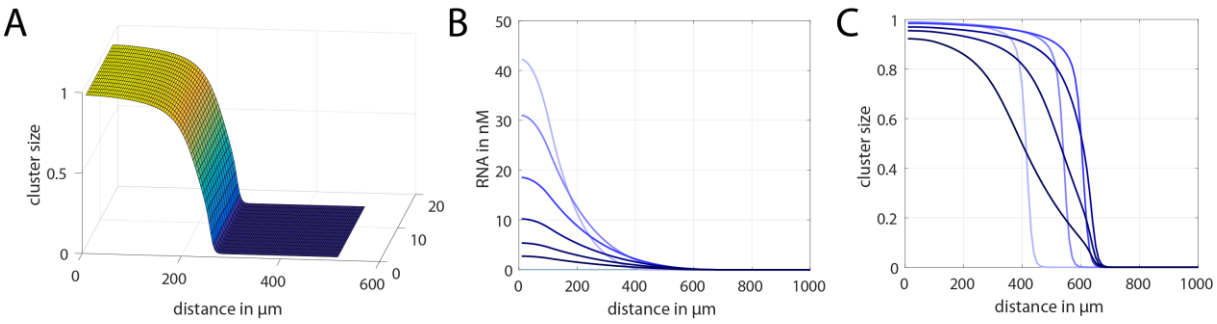

Figure 5.14: Simulation of diffusion channel for a transient RNA production. A) Snapshot of the colloidal clusters during the aggregation process. B) RNA concentration profile along the middle of the channel at different points in time. c) The colloidal cluster sizes for the same time steps, showing a forward aggregation front and a backward disintegration front.

In order to investigate this phenomenon, the binding affinity of the colloids before and after disintegration by the *RNaseH* was observed. These measurements showed, that the binding affinity of the colloids is reduced, once they are disintegrated (Fig. 5.15). This can be explained, by the operation of the *RNAseH*, which only degrades RNA once it is bound to DNA. In the colloidal setup, the majority of the RNA-linker is bound to one species of the colloidal docking DNA. Hence, only this partially complementary part of the RNA can be degraded, while the remaining part of the RNA is free to bind to the second colloidal DNA species. This temporal side-product blocks remaining full length linker strands from bridging between two types of colloids. Computing the equilibration of all competing DNA/RNA hybridisation reactions confirm that the temporary side-products result in a reduction of the colloidal DNA – linker complex.

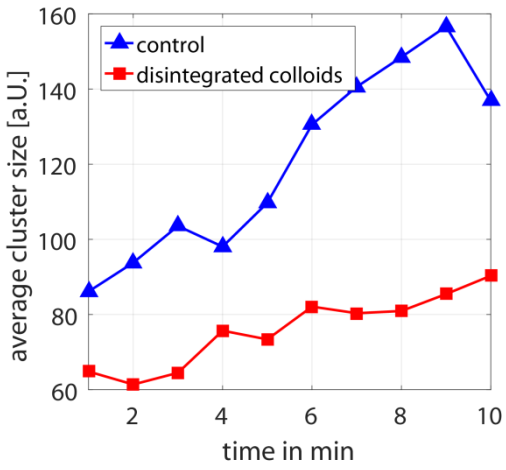

Figure 5.15: Reduced binding affinity. Colloids were linked together with prebuilt RNA. After the disintegration by the *RNAseH,* the colloids were linked a second time via DNA-linker and compared with "new" colloids. The disintegrated colloids show a reduced aggregation.

This “history” of aggregation, which leads to a temporary reduced affinity can be taken into account in the simulation. As a result, a forward propagation of the colloidal disintegration front can be detected (Fig. 5.16), similar to the observation in the experiments. The aggregation propagates into the channel and is followed by a disintegration front, acting as a “traveling wave” of aggregation.

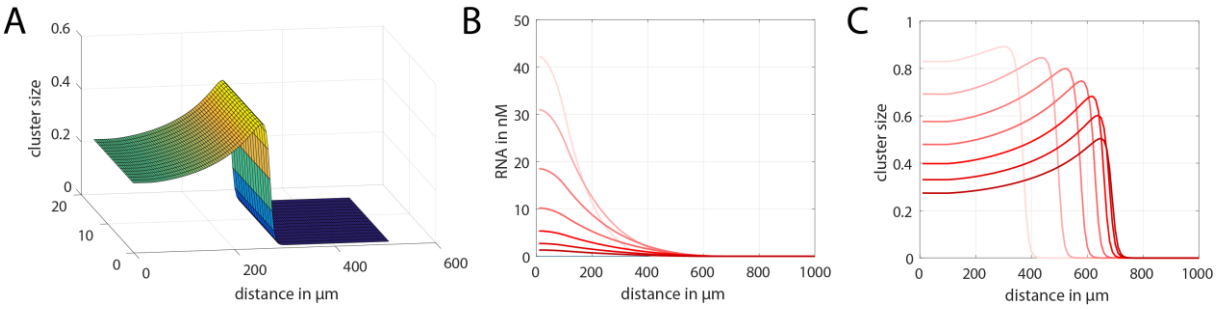

Figure 5.16: Simulation of the diffusion channel with reduced binding affinity of disintegrated colloids. A) Snapshot of the colloidal cluster size demonstrating the travelling wave of aggregation. B) RNA concentration along the middle of the channel at different points in time. It is noticeable, that the profile of the RNA concentration with and without reduced binding affinity (Fig. 5.15B) is identical. C) The maximum of the colloidal cluster sizes travels along the diffusion channel and shows the same behaviour as observed in the experiments.

5.5 Summary and Outlook

In this chapter it was shown that the colloidal self-assembly of DNA-coated colloids can be dynamically controlled by using enzymatic reactions. The colloidal interactions are tuned by producing and degrading RNA-linker, which are able to bridge between two species of colloids and induce the aggregation. The enzymatic activities of the *T7 RNA polymerase* and the *RNaseH* were quantified, in order to obtain a simplified reaction model and make predictions for the reaction kinetics of the enzymes. We showed that the enzymatic reaction speed can be directly coupled to the macroscopic structure formation process. In addition, the interplay of the antagonistic enzymatic reactions enables the autonomous and transient self-assembly of the colloids. Here, tuning the molecular reactions allow to control the time traces of the transient aggregation process in terms of lifetime and cluster size. Since, the colloidal interactions are based on the selectivity of the DNA sequences, competitive hybridisation reactions can be deployed to manipulate the hierarchical organization by inducing aggregation thresholds. Finally, we were able to restrict the enzymatic activity locally within a microfluidic chamber in order to investigate the spatio-temporal behavior. We revealed a temporal reduction of the colloidal binding affinity, which results in a travelling aggregation front unattainable for passive diffusive systems.

In general, mechanisms like time delays are the basis for many nonlinear pattern formation processes. Therefore, we started to expand the reaction network in order to prevent the equilibration of RNA production and degradation, demonstrated in chapter 5.4.1. To this

end, we added an additional enzymatic reaction to the system, capable of regenerating the degraded and monomeric RNA fragments into *NTP*s. This recovery system was realized by *NMP*- and *NDP-Kinases* and was sufficient to create a delay between the degradation and production reaction, resulting in a damped oscillation of RNA-linker production (Fig 5.17A). Besides using reaction-based time delays on the molecular level, we see high potential for the development of non-linear pattern formations, in the coupling of enzymatic activity to the colloidal structure formation. The separation of the different timescales of molecular and macroscopic processes can be exploited to create feedback mechanisms, feasible to create oscillating structure formation.

The presented approach is highly adaptable and versatile, as it is straight forward to use the enzymatic setup with desired DNA sequences. It is possible to tune the colloidal interactions precisely, resulting in a wide range of accessible structures. In addition, the competing hybridization reactions can be used in multi species systems for the hierarchical guided self-assembly leading to aggregation scaffold. As the material properties of the colloidal aggregates are mainly defined by the properties of the single building blocks, many different applications can be addressed. Therefore, we demonstrated that the colloidal aggregation of the polystyrene colloids is capable to tune optical properties, like the transparency (Fig. 5.17B), while plasmonic gold nanoparticles result in the tuning of absorption spectra's[112]. Especially the dynamic and transient control of colloidal organization may prove to be useful to facilitate the development of active and autonomously acting materials[49,113,114].

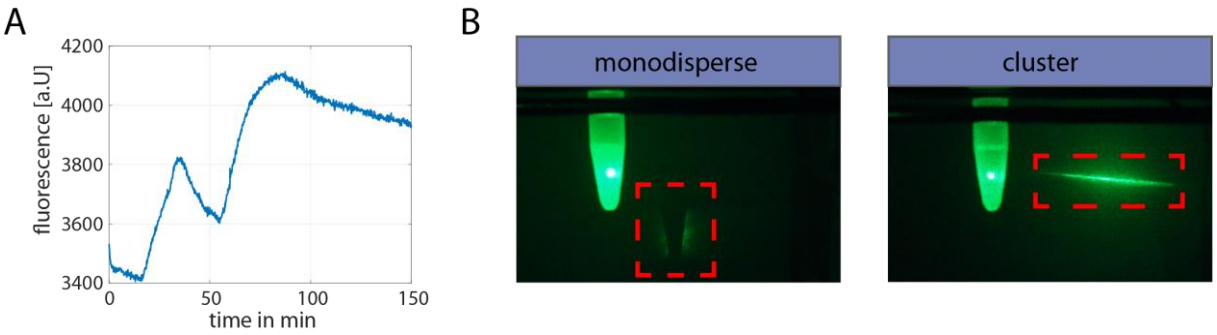

Figure 5.17: Oscillatory RNA production and optical applications. A) Oscillating RNA production, by using a kinase based *NTP* regenerating system. B) Optical properties of the colloidal solution. Colloids are illuminated by a green 1mW laser beam. The sample containing monodispersed colloids absorbs the laser beam, which can be seen by the outline of the sample holder (red dotted line) on the detection wall. The colloidal volume fraction is too high and causes absorption and scattering of the light beam. In contrast, the colloidal gelation leads to the transmission of the laser beam. Here, huge volume fractions arise, where no colloids are present.

6. Oscillating structure formation

Beside the autonomous and transient aggregation, we aim to expand the temporal control of the colloidal binding affinities in order to create a system, which is capable to drive an oscillating structure formation process on the macro scale. Therefore, we coupled the colloidal aggregation to an enzymatic system that is able to generate DNA in an oscillating manner at constant temperature.

Many essential biological processes are driven by biochemical oscillators[115–118]. However, the synthetic reconstitution of an oscillating network is very complex and requires the synchronisation of non-linear reactions, feedback loops and/or time delays[64,119]. Additionally, the expansion of such an oscillating network in order to control a desired mechanism is a major challenge, because it requires the precise understanding of the underlying reactions and the critical mechanisms keeping the system in an oscillating regime. One example of a synthetic oscillator is the molecular predator-prey system[56], which is able to produce sustained oscillations of two distinct DNA strands (chapter 6.1). The regulation mechanisms and the time courses of the single DNA strands are well studied and analysed. However, the characteristics of this system do not allow the control of a macroscopic process so far. The non-linear enzymatic reactions are based on very weak DNA-DNA interactions which are necessary to enable an exponential DNA amplification[120]. Here, we report a new oscillating regime of the predator-prey system facilitating an increased DNA concentration and longer lifetimes of the DNA pulses (chapter 6.2). The DNA concentration peaks during these oscillations are in the range of several hundred nanomolar with lifetimes of up to 5 hours and last over 60 hours of DNA polymerisation. The knowledge of the distinct DNA sequences allows us to expand the system with further enzymatic reactions in order to produce an additional DNA species with higher DNA binding affinities, able to bridge between colloids. Thus, we were able to exploit the peaks of DNA concentration in this oscillatory process to trigger colloidal structure formation. The temporal concentration profile of the short DNA fragments exhibits the exact same temporal behaviour as the lifetime of the colloidal aggregation.

6.1 Enzymatic reactions

The enzymatic reactions used in the system to realize the oscillation of DNA production and degradation have many intersections with the predator–prey population dynamic described by the Lotka-Volterra equations[121]. This analogy helps a lot to understand the underlying processes, hence the nomenclature of the predator-prey system is exploited to describe the enzymatic interplay on the nanoscale. The oscillation of DNA is based on three enzymatic reactions: an exponential DNA amplification, a negative feedback loop and a degradation reaction (Fig. 6.1). Here, the exponential amplification of DNA is realized by a nicking enzyme amplification reaction (NEAR)[122]. By virtue of the exponential reaction characteristics the produced DNA strand is named “prey”. This reaction can be coupled to a negative feedback mechanism which is able to elongate the 10 nucleotide (nT) prey sequence and transform it into the 14 nT sequence “predator”. This transformation corresponds to the consumption of the prey, effectively slowing down the production of prey DNA and results in the stop of DNA amplification. Finally, the degradation reaction is able to restore the initial conditions, leading to the regeneration and the continuation of the DNA amplification cycle. The functionality and characteristics of the single reactions and their interplay are described in the following chapters.

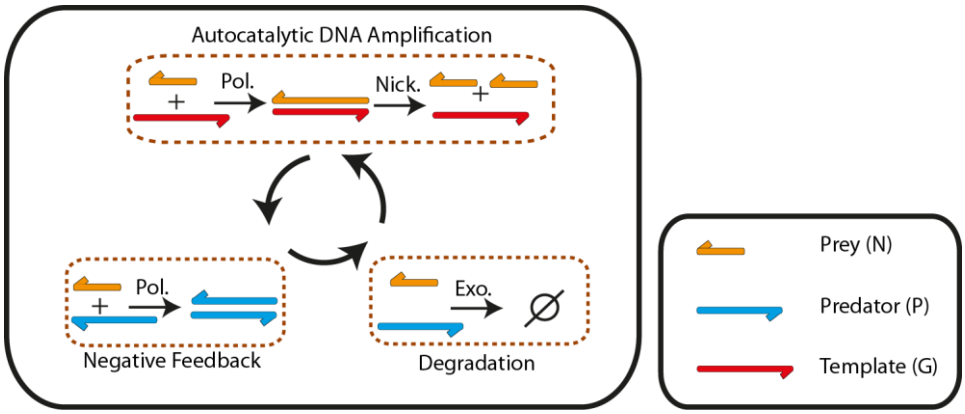

Figure 6.1: Oscillating reaction network. The oscillating DNA production is based on the interplay of three enzymatic reactions. In the autocatalytic DNA amplification, a DNA template with a repetitive DNA sequence is used by the *Bst DNA polymerase* and the nickase *Nb.Bsmi*. The exponential growth of the prey DNA is coupled to a negative feedback, which is based on the palindromic sequence of the predator, effectively transforming the prey into predator DNA. Finally, the exonuclease *Recj* is able to degrade the DNA species prey and predator in order to enable the continuation of the reaction cycle[56].

6.1.1 Exponential DNA amplification (Prey)

The isothermal and exponential amplification of DNA is realized by a nicking enzyme amplification reaction, which results in the autocatalytic self-replication of the prey (Fig. 6.2A). In detail, the prey (N) binds a single stranded DNA template (G) leading to the elongation by the *Bst DNA polymerase* and the formation of the dsDNA complex GG*. The sequence of the template G has a recognition site for the *nickase Nb.Bsmi*. Thus, the G* strand is cut in the middle, resulting in two identical sequences of the prey. By that, an autocatalytic self-replication of the prey sequence is realised, where the product (prey) enhances the speed of the reaction (eq. 6.1). The exponential prey amplification can be visualised by the DNA intercalator *EVA Green* using fluorescence spectroscopy (Fig. 6.2B).

$$G + N \rightarrow G + 2N \tag{6.1}$$

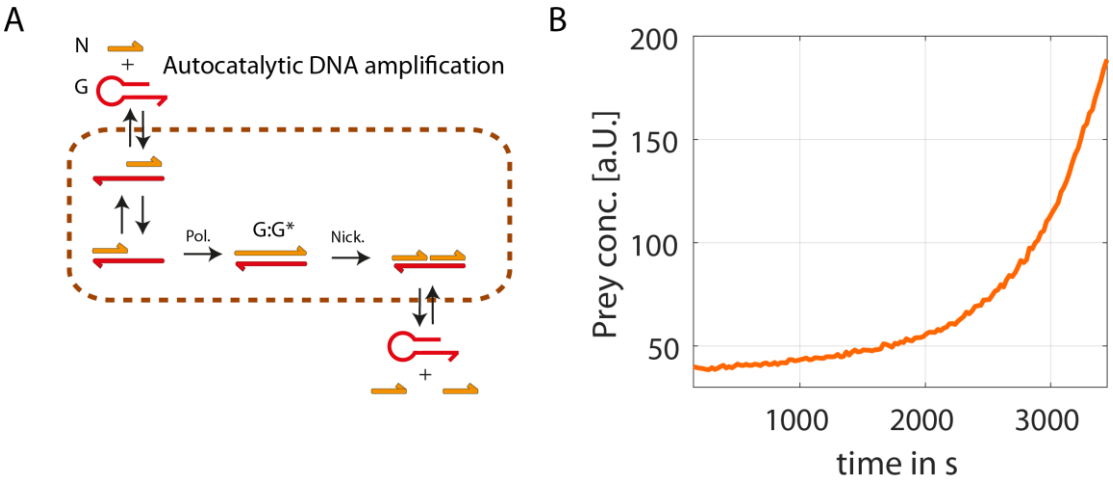

Figure 6.2: Prey amplification. A) The template G forms a DNA hairpin with a short overhang, which is opened by the binding of the prey strand. The prey acts as a primer and is elongated by the *Bst DNA polymerase* along the 5'→3' direction resulting in the double stranded complex GG*. Thus, the recognition sequence for the *nickase Nb.Bsmi* is formed and enables the production of two prey strands, because of the repetitive sequence of G. B) The exponential growth of the prey is monitored using fluorescence spectroscopy.

The speed of production is given by the polymerase and the equilibrium concentration of the G:N complex and can be described by Michaelis-Menten kinetics. The prey amplification can be characterised by an exponential but limited growth process. The limitation of the amplification is given by the upper limit of the enzymatic activity of the *nickase*. In contrast, the saturation of the template-strand by the binding of two prey strands is not limiting the speed of production. The association constant $K_a^{G:N}$ of prey and template is very low ($5 \cdot 10^{-7} nM^{-1}$) leading to a very unstable association of prey and template. Hence, the majority of the template strands is single stranded for reasonable concentrations of N. Therefore, the prey amplification ($N \rightarrow N$) can be described with the following model:

$$N \rightarrow N: \quad \frac{dN}{dt} = k_{bst,1} \cdot pol \cdot \frac{G{:}N}{K_{M,G:N} + G{:}N} \tag{6.2}$$

$$G{:}N = {K_a}^{G:N} \cdot G_{free} \cdot N_{free} \tag{6.3}$$

$$N \rightarrow N: \quad \frac{dN}{dt} = k_n \cdot pol \cdot \frac{G_{free} \cdot N_{free}}{1 + b \cdot G \cdot N} \tag{6.4}$$

With $k_{bst,1}$ the rate of production of the polymerase for a saturated nickase concentration and *pol* the effective polymerase concentration. $K_{M,G:N}$ represents the Michaelis-Menten constant for the prey amplification and $k_n = \frac{{K_a}^{G:N} \cdot k_{bst,1}}{K_{M,G:N}}$ and $b = \frac{{K_a}^{G:N}}{K_{M,G:N}}$.

6.1.2 Negative feedback (Predator)

For the realisation of an oscillating reaction, the prey amplification reaction is coupled to an autocatalytic negative feedback mechanism (Fig. 6.3A).. The predator is able to bind the prey and form a DNA duplex. Subsequently, the prey gets elongated and transformed into a predator, because of the palindromic sequence of the predator. The autocatalytic growth (eq. 6.5) can be visualized for a fixed prey concentration and a small amount of predator strands (Fig. 6.3B).

$$P + N \rightarrow 2P \tag{6.5}$$

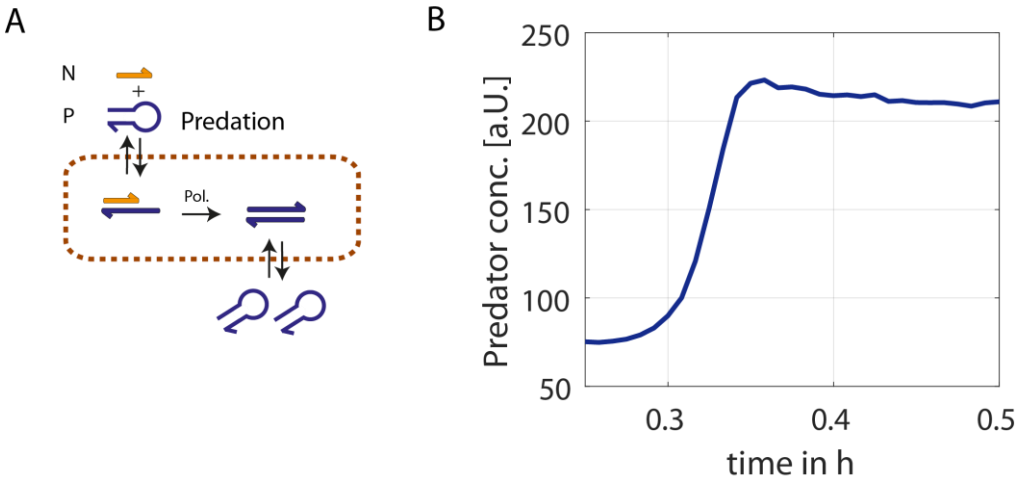

Figure 6.3: Predator amplification. A) The predator strand has a palindromic DNA sequence and is able to form a DNA hairpin. The prey can bind the predator which results in a subsequent elongation by the polymerase. Here, a double stranded complex of two predators is formed, which can dissociate because of the weak interaction. B) The "predation reaction" is visualised in the absence of DNA templates for a fixed amount of prey (50 nM) and predator (~1 nM). The predators grow exponentially as long as a sufficient amount of prey is available.

Once all the prey is consumed by the predator reaction, a stationary phase results. Similar to the prey-template complex, the association constant ${K_a}^{P:N}$ of prey and predator is very low. Thus, the reaction is not limited by the saturation of the P:N complex and can be described by a first order differential equation:

$$N \rightarrow P: \qquad \frac{dP}{dt} = k_{bst,2} \cdot pol \cdot P:N \tag{6.6}$$

$$P:N = {K_a}^{P:N} \cdot P_{free} \cdot N_{free} \tag{6.7}$$

$$N \rightarrow P: \qquad \frac{dP}{dt} = k_p \cdot pol \cdot P_{free} \cdot N_{free} \tag{6.8}$$

with $k_{bst,2}$ the enzymatic rate of the *Bst polymerase* and $k_p = k_{bst,2} \cdot {K_a}^{P:N}$.

6.1.3 Degradation

The properties of the degradation reaction of the prey and predator is another essential part of the network. The degradation is realized by the exonuclease *RecJ*, which is able to degrade single stranded DNA in the $5' \rightarrow 3'$ direction. The property to degrade only single stranded DNA is significant for the kinetics of the reaction. The prey can be approximated as exclusively single stranded, because the interaction of the prey and other occurring DNA is very weak. In contrast, the predator forms stable double stranded duplexes, which protect the predator from degradation. However, the dissociation constant is high enough to prevent a complete inhibition of the predator degradation, resulting in a reduced degradation speed (Fig. 6.4).

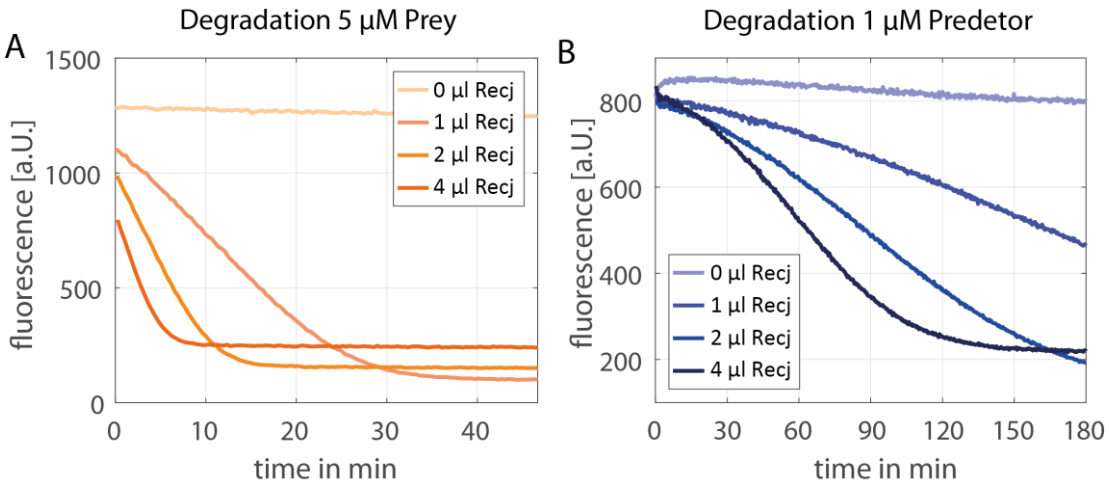

Figure 6.4: Degradation of prey and predator DNA. The degradation of the prey and predator was measured for an identical series of exonuclease concentrations. A) The degradation of 5 µM prey is completed in 30 minutes for the lowest *Rec. j* concentration. Here, prey strands are exclusively single stranded and can be degraded with the optimal enzymatic activity. B) In contrast, the degradation of 1 µM predator DNA is slowed down significantly for the same enzymatic conditions.

The speed of prey degradation is much higher compared to the speed of predator degradation. In addition, the degradation of prey and predator takes place simultaneously in the reaction network. Thus, the degradation is a competing reaction which can be described by Michaelis-Menten kinetics.

$$N \to 0: \quad \frac{dN}{dt} = rec \cdot k_{cat,N} \cdot \frac{N}{K_{m,N} \cdot \left(1 + \frac{N}{K_{m,N}} + \frac{P}{K_{m,P}}\right)} \tag{6.9}$$

$$P \to 0: \quad \frac{dP}{dt} = rec \cdot k_{cat,P} \cdot \frac{N}{K_{m,P} \cdot (1 + \frac{N}{K_{m,N}} + \frac{P}{K_{m,P}})} \tag{6.10}$$

With k_{cat} the catalytic rate and $K_{m,N}$ and $K_{m,P}$ the Michaelis-Menten constants of the exonuclease for prey and predator and *rec* the concentration of *Recj*. Since, the majority of the predator is in a protected double stranded state, the availability for the exonuclease is reduced, leading to saturated predator degradation ($K_{m,N} \gg K_{m,P}$). Thus, following approximations can be made:

$$N \to 0: \frac{dN}{dt} = rec \cdot k_{N2} \cdot \frac{N}{1 + \frac{P}{K_{m,P}}} \tag{6.11}$$

$$P \to 0: \frac{dN}{dt} = rec \cdot k_{P2} \cdot \frac{N}{1 + \frac{P}{K_{m,P}}} \tag{6.12}$$

With $k_{N2} = \frac{k_{cat,N}}{K_{m,N}}$ and $k_{P2} = \frac{k_{cat,P}}{K_{m,P}}$.

6.1.4 Oscillating reaction network

The regime of oscillating DNA amplification is based on the interplay of all three reactions. The kinetic evolution of the prey depends on the prey growth, the predation and the degradation. In addition, the predator reaction depends on the predation and the degradation. By that, the complete system can be described by the set of two coupled ordinary differential equations:

$$\frac{dN}{dt} = \ growth - predation - degradation\_prey \tag{6.13}$$

$$\frac{dN}{dt} = [\ N \to N\ ] - [N \to p] \ - \ \ [N \to 0] \tag{6.14}$$

$$\frac{dN}{dt} = k1 \cdot pol \cdot \frac{G \cdot N}{1 + b \cdot G \cdot N} \ - \ k_2 \cdot pol \cdot P \cdot N \ - rec \cdot k_{cat,N} \cdot \frac{N}{1 + \frac{P}{K_{m,P}}} \tag{6.15}$$

$$\frac{dP}{dt} = predation - degradation\_predator \tag{6.16}$$

$$\frac{dP}{dt} = [N \rightarrow p] \; - \; [p \rightarrow 0\,] \tag{6.17}$$

$$\frac{dP}{dt} = k_2 \cdot pol \cdot P \cdot N \; - \; k_{cat,P} \cdot \frac{N}{1 + \frac{P}{K_{m,P}}} \tag{6.18}$$

Reactions with a limited growth are often characterised by damped oscillation. Here, nonlinearities in the functional response are necessary to create limited cycles within the phase-space. In the molecular predator-prey system, the essential mechanism is the competitive degradation of the two DNA species. The degradation of the predator can be described by Michaelis-Menten kinetics, while the prey degradation can be simplified by a linear degradation at reasonable concentration. This mechanism is one essential property for the existence of sustained oscillations. In a first step we were able to reproduce the oscillation of the molecular predator-prey system[56] (Fig. 6.5). Similar to the reported behaviour, the system has a relative high frequency with one amplitude per hour and a relative short lag phase between the concentration peaks.

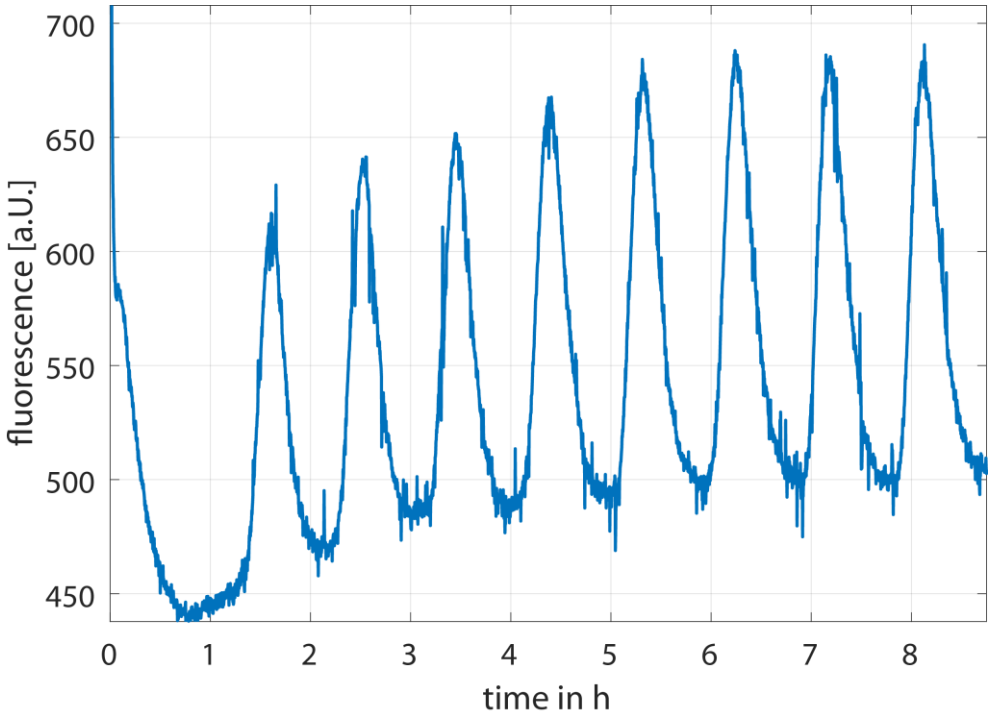

Figure 6.5: Oscillation of the molecular predator-prey system. The interplay of prey amplification, predation and degradation is able to create sustained oscillations of prey and predator production. The prey amplification is limited by the predator reaction, which finally initiates the degradation phase. Once the predator concentration drops below a critical threshold the prey amplification can resume, resulting in sustained oscillations. Here, a template concentration of 160 nM was used.

6.2 Expansion of the predator-prey system

6.2.1 Expansion of the oscillating reaction network

Since the interactions of prey and predator are relative weak, it is essential to expand the predator-prey system with further enzymatic reactions in order to control a macroscopic process (more details in chapter 6.2.2). The expansion of an oscillating biochemical network requires the fulfilment of two major challenges. On the one hand it is necessary to have a robust system, which is capable to endure interferences caused by the interactions of the coupled reaction. On the other hand, the oscillation has to match up with the time-scales of the macroscopic process. Therefore, it is necessary to expand the oscillating regime of the predator-prey system to create amplitudes with longer lifetimes and lower frequencies. In this regime, small interferences have less influence to the system and it is possible to synchronize the aggregation and disintegration of the colloidal structure formation with the peaks of the DNA concentrations. Consequently, we aimed to maximize the DNA amplification by identifying the limitation of the network and the capability of the negative feedback to stop the exponential growth. Here, tuning the enzymatic setup is limited. The rate of the prey amplification and the predation both rely on the polymerase concentration and the nickase is already used at a saturated concentration. Thus, the prey amplification can exclusively be enhanced by increasing the template concentration. It proved to be useful to analyse the amplification reactions in the absence of the degradation (Fig. 6.6).

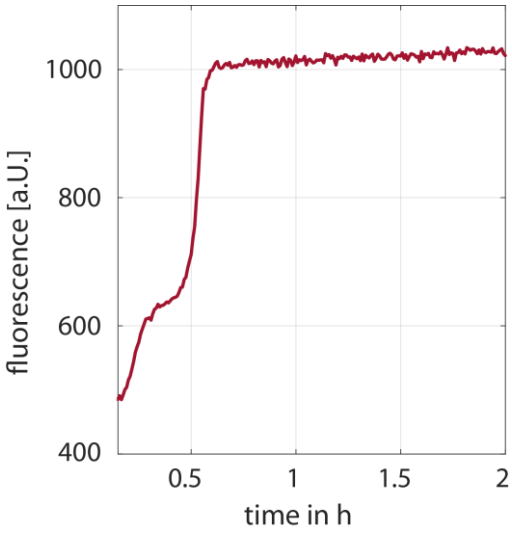

Figure 6.6: Prey amplification for high template concentrations. The prey-amplification is monitored for a template concentration of G=400 nM in the absence of the predator and degradation reaction. However, the amplification stops after 35min of polymerisation and the increase of the signal can be characterised by two growth steps.

The increase of the prey is characterised by a two-step growth process. After a critical time of around 35 min the reaction suddenly stops, even without predator DNA, indicating a further feedback. This mechanism was identified and analysed by gradually increasing the prey concentration in the absence of template strands (Fig. 6.7). It was observed that low prey concentrations (up to 50 nM) stay constant over the entire experiment (25 h).

However, prey concentrations above a critical concentration (100 nM) increase very fast, similar to the reaction seen for the predation.

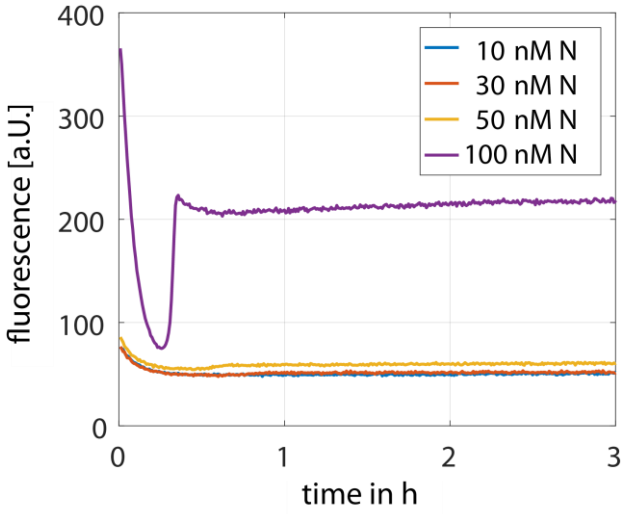

Figure 6.7: Spontaneous predation. A series of prey concentration was measured over time in the presence of exclusively *Bst polymerase*. Prey concentrations below 50 nM stay constant over the entire experiment, while higher concentrated samples (100 nM Prey) result in a fast increase of the signal.

This process can be explained by the "spontaneous predation" and occurs only for high prey concentrations. The interaction between two prey strands is very weak, but they are still partially complementary (Fig. 6.8). Once such an unstable duplex is formed, the DNA overhangs get elongated by the polymerase which leads to the formation of a predator duplex. This event is sufficient to start the autocatalytic production of the predator reaction.

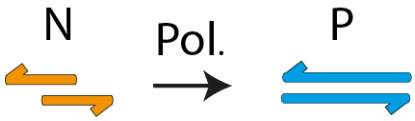

Figure 6.8: Prey-Prey interaction. Two prey strands are partially complementary (5 nT overlap) and are able to form a very unstable complex. However, these temporary duplexes occur at high prey concentration. Hence, the polymerase is able to elongate the prey, resulting in the formation of a predator strand.

This spontaneous predation represents the upper limitation of the system at high template concentration. However, this mechanism didn't play an important role in the previous system, but becomes crucial in the regime of high DNA concentrations and limits the amplification. Therefore, the pure growth process (Fig. 6.6) can be described by three phases. The prey amplification in the beginning, the start of the spontaneous predation and the lag phase, where only predator is present. In a next step, we completed the predator-prey system and gradually increased the exonuclease concentration *Recj* (Fig. 6.9). It is noticeable, that the degradation reduces the upper limit of DNA concentration, however the spontaneous predation is still present. The lifetime and the total height of the pulse can be directly controlled by the degradation reaction and it is possible to shape the first pulse of the reaction.

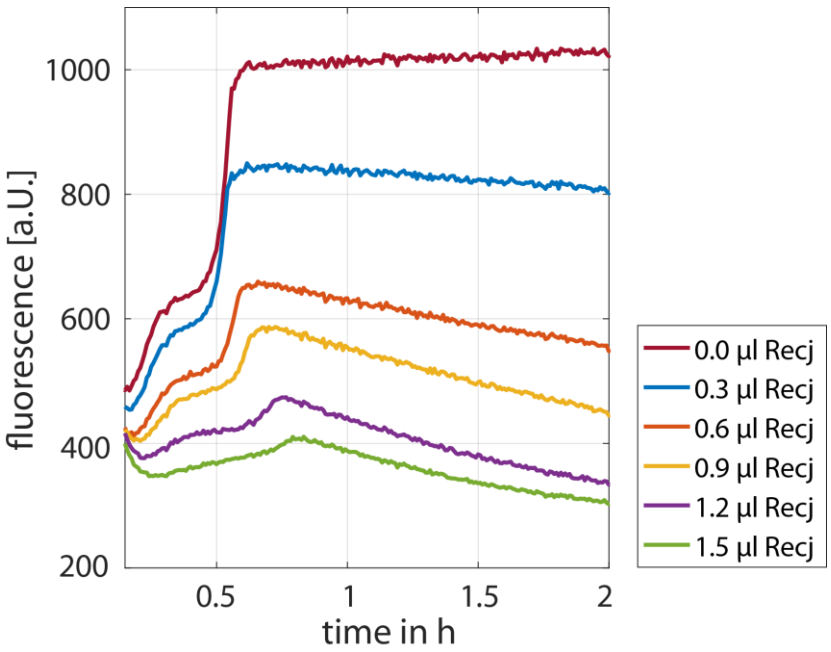

Figure 6.9: Prey-amplification with degradation reaction. The prey amplification is monitored for high template concentration with increasing *Recj* concentration in the absence of predator strands. The sample without exonuclease represents the two step growth process which finally results in a stationary phase, already shown in Fig. 6.6. The peak of the pulse decreases with the *Recj* concentration and the duration of the degradation can be controlled.

The degradation phase is characterized by a high predator concentration which suppresses the prey amplification. Once the predator falls below a critical concentration, the prey amplification is dominating the reactions and the network is able to restart the cycle again (Fig. 6.10). Thus, we were able to increase the lifetime of the amplitudes of up to 5 hours. It is noticeable that the used template concentration is 400 nM and still shows sustained oscillations, while the original system reported sustained oscillation only up to 150 nM templates.

Besides tuning parameters like enzyme and template concentration, the challenge in this "long lifetime" regime, was to prevent nonspecific interactions like the ab initio amplification. The polymerase and the nickase have a negative synergetic effect. The polymerase is able to produce template independent DNA which gets amplified exponentially. This mechanism increases drastically when DNA is present and the polymerase is active. The side reaction can be prevented by stabilizing the single stranded DNA and prevent weak secondary structure using the protein *gp32gene* (details in the materials and methods part 3.4.1).

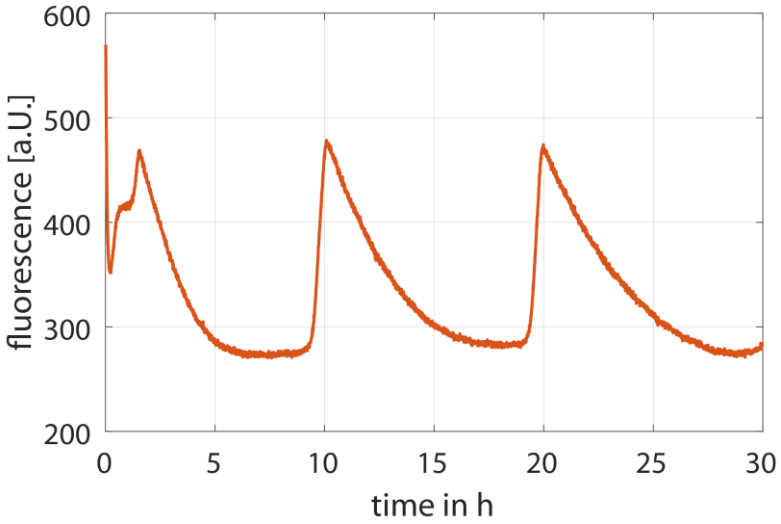

Figure 6.10: Sustained oscillation in the high template regime. The oscillation of DNA can be observed at a template concentration of 400 nM. The amplitudes and lifetimes of the single pulses are significantly increased compared to the original reported oscillations. It is noticeable, that the first pulse is characterised by the two-step growth, while the following pulses don't show this behaviour. Here, predators are already present preventing the occurrence of the spontaneous predation. However, the same amplitude and lifetime compared to the first pulse can be obtained.

In addition, we aimed to tune the profile of the oscillation and achieved to control the frequency and lag phases using different template concentrations. However, damped oscillations occur above 600 nM template concentration representing the upper limit for sustained oscillation at the given enzymatic setup (Fig. 6.11).

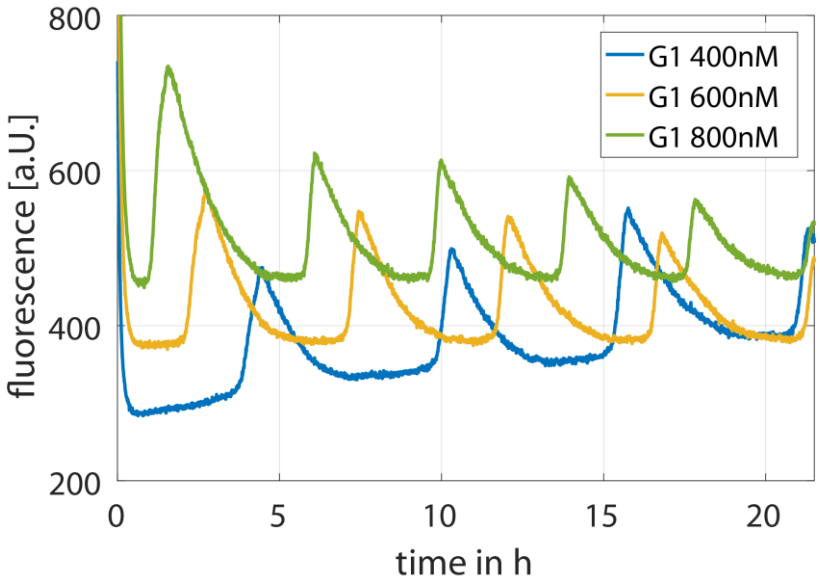

Figure 6.11: Oscillation for different template concentration. Oscillations were monitored for different template concentrations. At 400 nM of templates, sustained oscillations can be obtained, while the increase of the template concentration results in the occurrence of damped oscillations. Here, an increased frequency can be observed, which is due to a reduction of the lag-phase between two pulses.

6.2.2 Converter-reaction

In a next step, we aimed to exploit the oscillation of the predator-prey system in order to drive the macroscopic structure formation of DNA-coated colloids. The high working temperature of 46.5°C and the short length of the DNA strands (10 and 14 nT) result in very low DNA-DNA interactions. It was shown experimentally that the binding affinity of the prey and predator is too low to induce the colloidal aggregation. The minimum length of DNA able to bridge between two colloids at this buffer and temperature conditions was identified to be at least 20 nucleotides long. Hence, it is necessary to expand the system with a further enzymatic reaction which is able to produce a third DNA species. The oscillation of the predator-prey is based on a precise match up of all the single enzymatic reactions and the properties of all the occurring hybridisation reactions. Therefore, an additional reaction should not influence the kinetics of the system by changing the equilibrium of the hybridisation reactions nor consume the prey and predator DNA. However, the activity of the reaction needs to be coupled to the oscillating profile. Therefore, we added a further enzymatic reaction to the system, which is based on the isothermal nicking enzyme amplification reaction (NEAR). In this “converter-reaction” (Fig. 6.12), a primer DNA binds to the complementary part of the converter strand and activates the polymerase to elongate it. Due to the elongation of the primer, the recognition sequence of the nickase is formed, leading to the nicking of the strand. As a result, two DNA strands are produced. The unchanged primer DNA and a second strand, which is complementary to the converter strand and can be designed as desired (linker). The only limitation is the 6 nucleotide long sequence, predefined by the recognition sequence of the nickase. Finally, the converter-reaction can be incorporated in the reaction network by using the prey or predator as the primer DNA (Fig. 6.13)

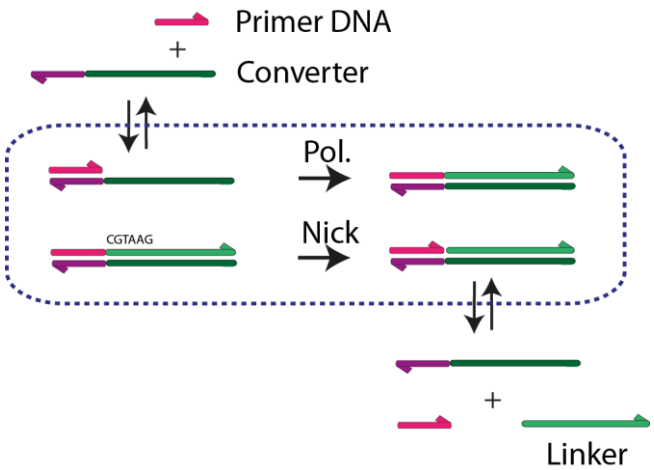

Figure 6.12: Scheme of the converter reaction. The converter strand is composed of two functional parts. The recognition sequence (purple) is complementary to the primer DNA, which catalyses the enzymatic reaction, once it is bound. The subsequent sequence contains the recognition part of the nickase and the DNA sequence, which is complementary to the DNA-linker. Thus, the converter reaction is induced by a primer DNA without consuming it.

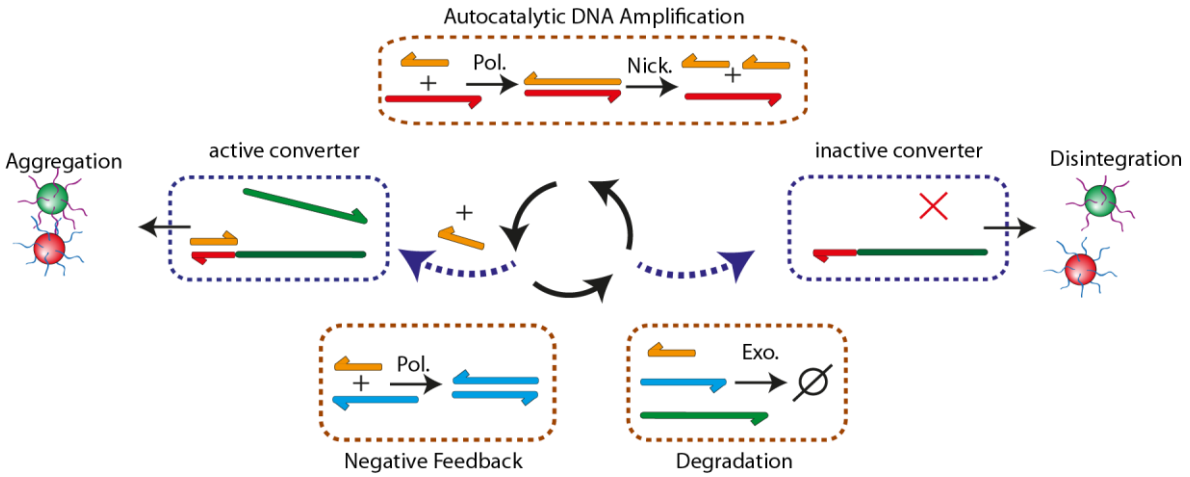

Figure 6.13: Reaction network coupled to colloidal aggregation. The converter-reaction is coupled to the predator-prey reaction network. The primer strands (prey) activate the converter, leading to the production of DNA-linker in order to induce the colloidal structure formation. In addition, the exonuclease degrades single stranded linker in bulk. The reduction of the linker concentration changes the equilibrium of bound and unbound linker strands, effectively resulting in the colloidal disintegration.

In a first step we designed a converter which is activated by the prey and produces a 40 nT long linker. We show that the speed of linker production is controlled by the prey and depends on the total concentration of the prey (Fig. 5.14A). The constant production speed in the beginning indicates that the prey is not consumed during the reaction. However, for high linker concentrations, a saturation and inhibition can be observed. This is due to the binding of the produced linkers to the converter strands, which prevents the further production of linker. To overcome this rate limiting effect, we decreased the total length of the linker from 40 nT to 20 nT, effectively reducing the binding affinity of the linker and the converter. The linear production over 4 hours (Fig. 5.14B) proves the absence of the rate limiting effect caused by the stable converter-linker complex. Hence, free linker above the converter concentration can be produced without consuming the primer DNA. The linker production can be described by the following equation:

$$\frac{dlinker}{dt} = k_{conv} \cdot pol \cdot conv{:}primer \tag{6.19}$$

With k_{conv} the effective rate of the *Bst polymerase* and *conv*:*primer* the concentration of the converter-primer complex, which depends on the association constant ${K_a}^{conv:primer}$.

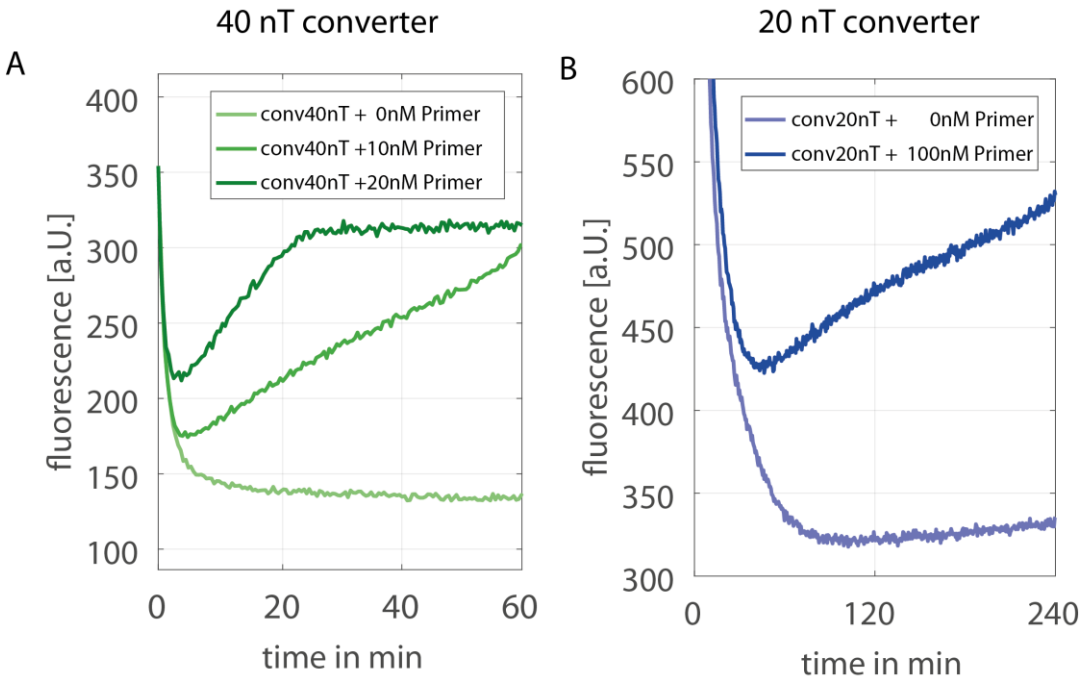

Figure 6.14: Converter reaction for different linker lengths. A) The 40 nT DNA-linker production of the converter reaction is induced and controlled by the amount of primer DNA. A constant production can be observed, which saturates with increasing linker concentration. B) The constant production of a 20 nT linker was monitored over 4 hours of polymerisation. Here, 200 nM of prebuilt DNA-linker were added to 100 nM of converter in order to exclude the negative feedback of the DNA-linker.

6.3 Converter induced structure formation

In a next step, the DNA-converter was used to induce the structure formation of the DNA-coated colloids. Therefore, two different types of DNA converter were designed which differ in the recognition part of the primer DNA. Thus, it is possible to prime the converter reaction either with prey or predator DNA (Fig. 6.15). The predator converter is only partially complementary to the predator in order to prevent the activation by the prey. The elongation of the prey and the subsequent nick would result in the transformation to a predator.

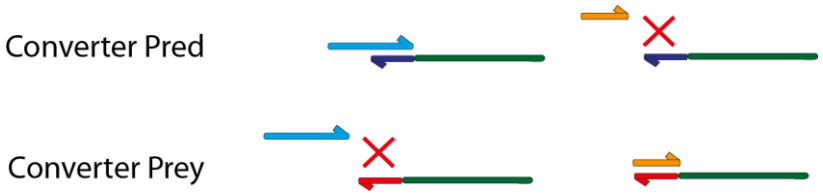

Figure 6.15: Converter strands with prey and predator recognition part. Two kinds of converter strands were designed which differ in the recognition sequence for the primer. The production of a 20 nT linker strand can be induced with the prey and predator DNA, respectively.

The structure formation of the colloids was induced by the two converter reactions using the different primer DNA strands. As expected, only the specific primer results in the colloidal aggregation (Fig. 6.16). It is noticeable, that the predator converter can also be activated by the prey DNA on longer timescales, due to the weak but still present interaction of the prey and the recognition part. In a next step, we incorporated the converter DNA to the oscillatory setup and analysed the interference with the network. At first, we investigated the influence of the predator-converter to the first pulse of the oscillation (Fig. 6.17). The growth process of the reaction is unchanged in the presence of the converter. Once the spontaneous predation begins, the activation of the converter can be observed. The linker are produced during the degradation phase, leading to a slower decrease of the signal.

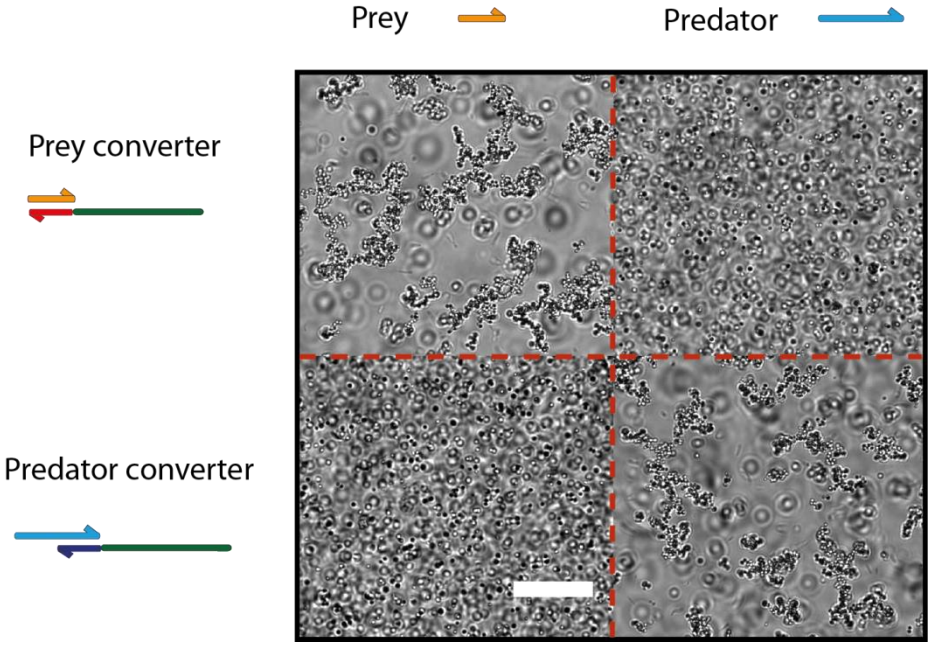

Figure 6.16: Converter-reaction coupled to the colloidal structure formation. The colloidal structure formation was monitored after one hour of polymerisation for the different converter strands and primer DNA. As expected, each converter is only activated by the corresponding primer DNA, resulting in a selective colloidal aggregation. Here, 50 nM of primer and 100 nM of converter were used (scalebar=70 µm).

In addition, the enzymatic setup seen in Fig. 6.17 was transferred to the colloidal system containing the prey and the predator-converter, respectively. Transient aggregation of the colloids can be observed for both converters (Fig. 6.18), corresponding to the DNA profile of the underlying reaction. The sample containing the prey-converter shows a direct start of colloidal aggregation, since the prey amplification takes place in the beginning. In contrast, the colloidal aggregation caused by the predator-converter is delayed by approximately one hour. This fits well with the duration till the spontaneous predation starts. Thus, it is possible to use the different amplification steps to induce the colloidal aggregation at different points in time using different converters.

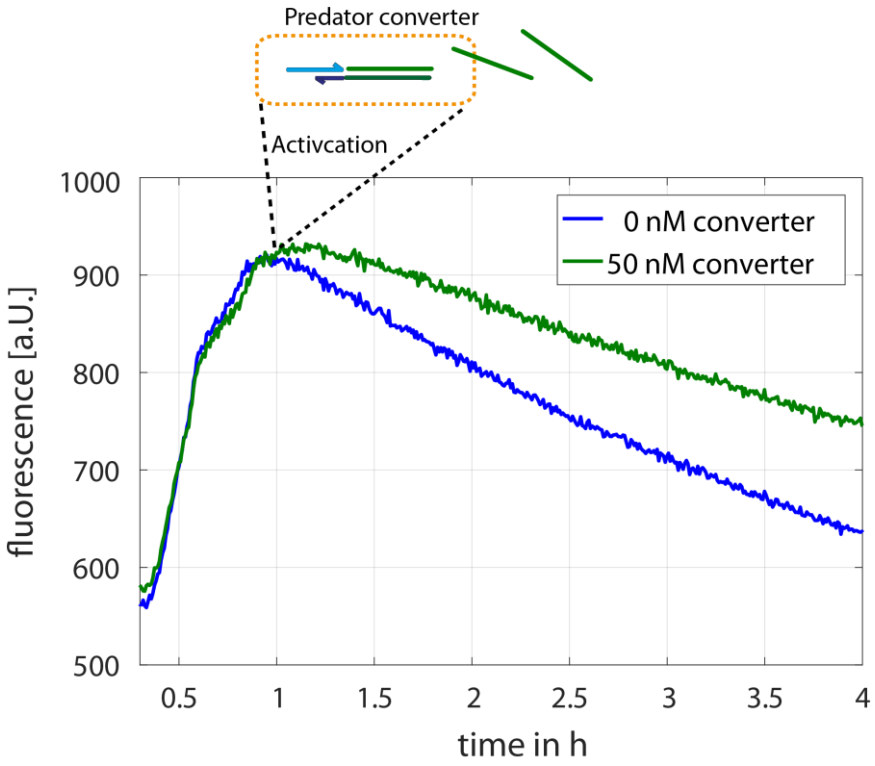

Figure 6.17: Oscillatory reaction network coupled to the predator-converter. The interference of the predator-converter on the predator-prey system was observed. Therefore, 50 nM of predator-converter was added to the predator-prey network (400 nM G). The growth processes of both samples are identical. After the spontaneous predation initiates (60 min) an increase of the signal can be observed for the sample containing the converter, indicating the production of linker DNA.

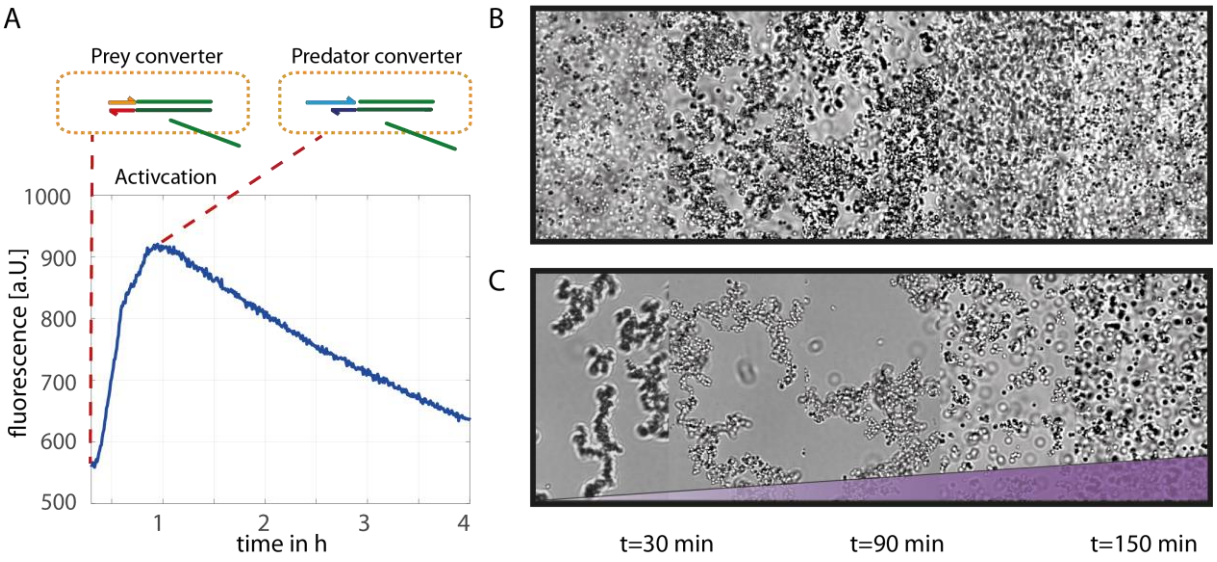

Figure 6.18: Colloidal structure formation induced by the prey- and predator-converter. A) Activation of the prey- and predator-converter during the first pulse. B) The aggregation of the sample containing the predator-converter starts after 60 min, which is in accordance with the predator amplification. C) In contrast, the prey-converter induces the structure formation after several minutes and is much more effective. Here, larger clusters are formed, which are more stable over time.

6.4 Oscillating structure formation

In the previous chapter, we already showed that the aggregation of the colloids can be directly coupled to the profile of the predator/prey DNA and both converters didn't interfere with the first pulse of the oscillations. However, the converters do have an influence on the remaining reaction, but behave differently. The predator-converter does interfere with the oscillating reaction already at pretty low concentrations (Fig. 6.19A). In the beginning, reduced concentration peaks can be observed, which start to increase with every period (Fig. 6.19B). At high converter concentrations, which are necessary to observe colloidal structure formation (50 nM), long lag phases arise (Fig. 6.20). This behaviour can be explained by the binding of the predator DNA and the converter. The DNA duplex results in a reduced degradation speed of the predator, which causes a stronger inhibition of the prey amplification.

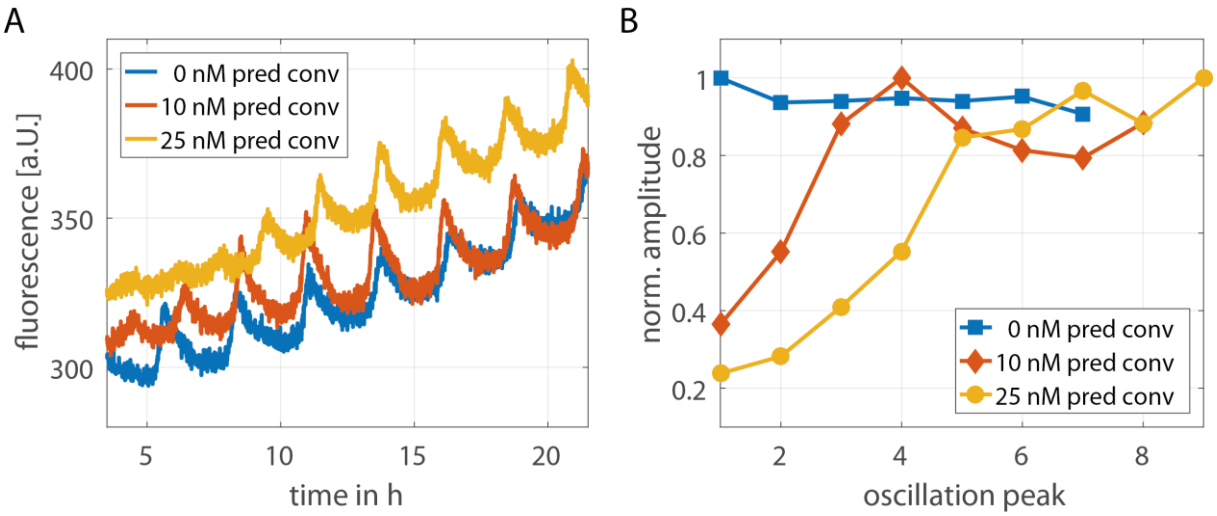

Figure 6.19: Interference of the predator-converter at low concentrations. A) Different concentrations of predator-converter were added to the oscillatory network. Already 10 nm of the predator-converter are sufficient to interfere with the amplitudes of the first peaks. B) The amplitudes of the different peaks were determined and plotted in an ascending order. A damping of the oscillations caused by the converter can be seen. However, after around five cycles the system recovers, resulting in sustained oscillations

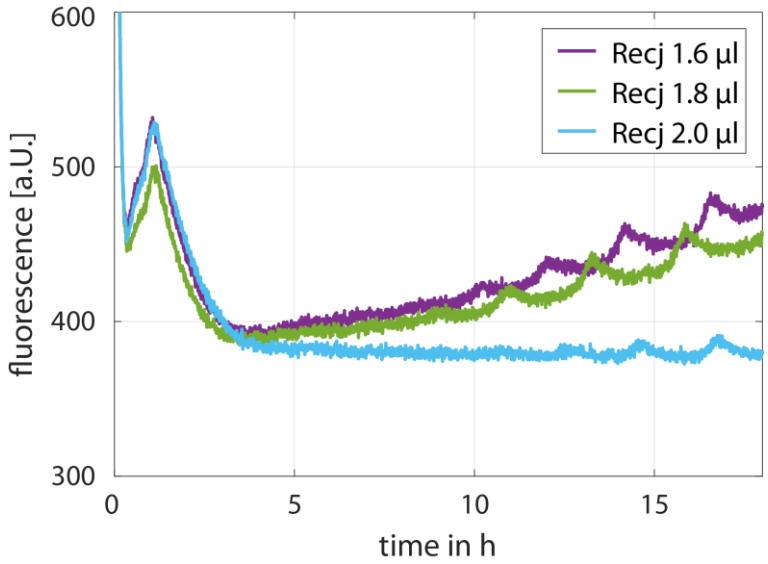

Figure 6.20: Interference of the predator-converter. The oscillatory reaction network containing 50 nM of predator-converter was observed for different degradation reactions. The amount of converter represents the concentration which is necessary to induce colloidal structure formation. Long lag times arise after the first pulse (15 hours), proving the negative interference already demonstrated in Fig. 6.19.

In contrast, the prey-converter proved to be useful to reduce the lag time of the oscillatory network (Fig. 6.21A). This can be demonstrated for an enzymatic setup with a relative high exonuclease concentration. In this regime, the samples without prey-converter are characterised by a long lag phase after the first pulse. However, the increase of prey-converter leads to a reduction of the lag phase. This was quantified by calculating the delay between the first and the second pulse (Fig. 6.21B). Similar to the predator-converter, the prey-converter is able to protect the primer DNA from degradation. Thus, the reduced prey degradation results in a shorter lag phase.

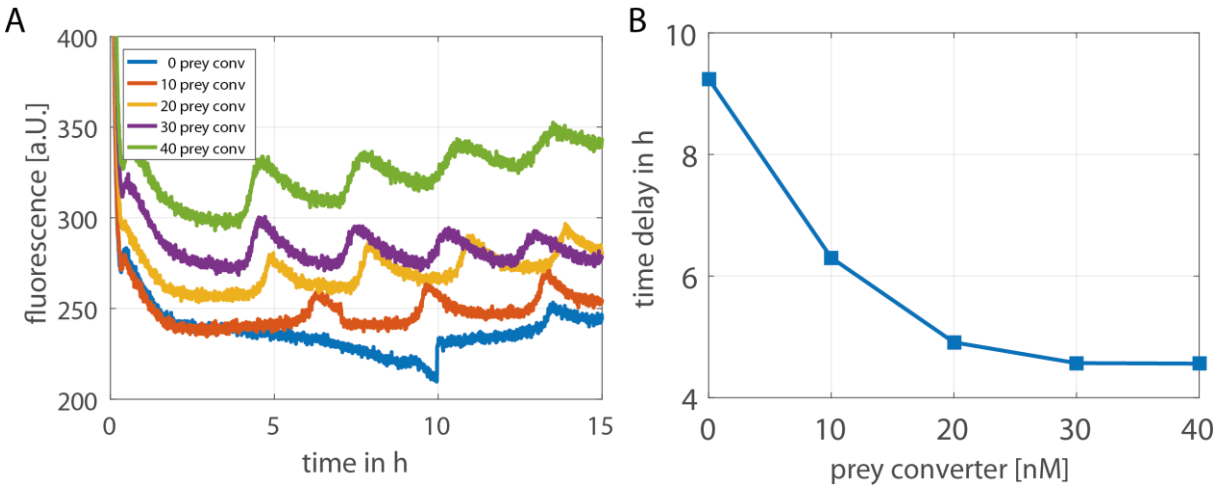

Figure 6.21: Interference of the prey-converter. A) The oscillatory reaction network was observed for different concentrations of the prey-converter. The prey-converter reduces the lag-phase successively, leading to more robust oscillations. B) The lag-times between the first and second pulse were determined and plotted for the different converter concentrations.

The prey-converter proved to be useful in order to achieve sustained oscillations, which are coupled to the linker production. Thus, the oscillatory setup containing the prey-converter was observed on longer timescales (Fig. 6.22). At different points in time (red circle), DNAcc were added to the solution and the structure formation was observed. At this configuration, the colloidal structure formation obeys the exact same profile as the oscillating DNA profile. The peak to peak amplitudes of the oscillatory network can be exploited to switch the macroscopic structure formation between colloidal aggregation and disintegration.

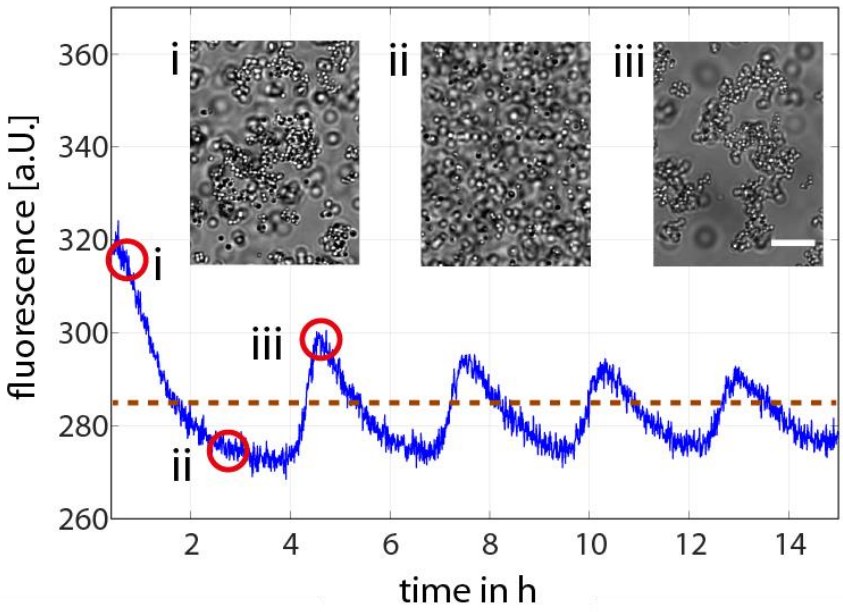

Figure 6.22: Oscillatory structure formation. The oscillatory network containing 50 nM of prey-converter was monitored over time. At different points in time (red circles), DNA-coated colloids were added to a sample and imaged (scale bar 30 µm). The colloidal aggregation fits perfectly with profile of the oscillating DNA. The brown dotted line represents the aggregation threshold between the aggregated and the disintegrated state.

6.5 Summary and Outlook

In this chapter it was shown that the macroscopic structure formation of DNA-coated colloids can be controlled by an oscillating reaction network of DNA amplification and degradation. An autocatalytic amplification of a 10 nucleotide “prey” strand is realized by an isothermal nicking enzyme amplification reaction, which is based on the repetitive sequence of the DNA template. The self-replication of the prey DNA leads to an exponential growth at constant temperature. This reaction is coupled to a negative feedback loop, which transforms the prey DNA into a 14 nT “predator” strand. The DNA species has a palindromic DNA sequence, which leads to an autocatalytic consumption of the shorter prey strand and

to the inhibition of the prey amplification. Finally, the competitive degradation of prey and predator leads to regeneration of the reaction network and results in sustained oscillations. Overall, the nonlinear interactions are based on very weak DNA interactions. Thus, the reaction network was expanded with a further enzymatic reaction in order to produce DNA strands with higher binding affinities able to induce colloidal aggregation. A “converter” reaction was coupled to the network, which can be activated by either prey or predator strands depending on the recognition site of the “converter” template. Therefore, it is possible to activate the colloidal aggregation at different points in time during the reaction cycle. For the realization of the oscillating structure formation, the regime of the sustained oscillations was expanded in order to synchronize the reaction with the macroscopic process. The pulse-lifetimes were increased by identifying the limiting reactions like the “spontaneous predation” and the prevention of the non-specific ab initio amplification. Thus, colloidal structure formation was realized which obeys the exact same profile as the oscillating reaction network.

Based on the advanced manipulation of DNA molecules, the presented approach is highly versatile and can be adapted to a variety of colloidal systems. The converter-reaction is able to produce different linker strands with a desired sequence and tuneable binding affinities. Moreover, the reaction can be activated by different primer DNA strands and consequently at different points in time. This feature can be used in multicomponent systems in order to realise autonomous and hierarchical self-assembly with the potential to create aggregation scaffolds, which guide the subsequent assembly. As discussed in chapter 2.1.2, the choice of the colloidal building blocks and structure formation targets a variety of material properties. Thus, the presented system may prove to be useful to broaden the spectrum of available applications and facilitate the realisation of versatile and switchable materials.

Appendix

A1 Simulation of the reaction-diffusion system

```
clear all
close all

global simlength simhigh
simlength    = 16;
simhigh      = 128;
```

Diffusionskernel

```
hsize      = [3 3];

sigma_RNA  =  0.47;

Hdiff_RNA  = fspecial('gaussian', hsize, sigma_RNA);

hsize      = [3 3];
sigma_Bead =  0.1;
Hdiff_Bead = fspecial('gaussian', hsize, sigma_Bead);
```

Matrices

```
RNA          = zeros(simlength,simhigh);

Temp         = zeros(simlength,simhigh);

Temp(:,1:10) = 1;

Bead_A       = ones(simlength,simhigh);

Bead_B       = ones(simlength,simhigh);

Cluster      = zeros(simlength,simhigh);
```

Rates

```
NTP         = 1;                % in mM
t7          = 10;               % in U
time        = 4;                % in h

polymerase = NTP*0.03*t7/3.7;
RNAse      = 1.5*0.3*10^-3;

t           = 3600*time;

NTP         = zeros(1,t);
NTP(1)      = NTP;
kAB         =.1;
```

Simulation

```
for i=2:t
RNA          = RNA + Temp*polymerase*NTP(i-1) - RNA*RNAse;
NTP(i)       = NTP(i-1) - polymerase*NTP(i-1)*0.005;
RNA          = imfilter(RNA, Hdiff_RNA,'replicate') ;

Bead_A       = imfilter(Bead_A, Hdiff_Bead,'symmetric') ;

Bead_B       = imfilter(Bead_B, Hdiff_Bead,'symmetric') ;

X            = kAB * (Bead_A .* Bead_B.*RNA);
Bead_A       = Bead_A  - X + Cluster*RNAse;
Bead_B       = Bead_B  - X + Cluster*RNAse;
RNA          = RNA     - X;
Cluster      = Cluster + X - Cluster*RNAse;

vid1(:,:,i) = Cluster;
vid2(:,:,i) = RNA;
end
```

A2 Protocol: Expression of cc-ttRecj

The cloning of *cd-ttRecJ* (45,9kda) was performed by *genescript*. The gene codon was optimized and cloned into *pET28b(+)* vector via *NdeI/XhoI*, the N-terminal *6xHis* tag for purification in *E.coli BL21*.

Expression:

- Preculture 200 mL 2xYT, containing 100 µg/ml Kanamycin at 37°C over night
- Inoculate 5l 2xYT, containing 100 µg/ml Kanamycin and let it grow at 30°C until it reaches OD600=0.4
- Start expression with 0.4 mM IPTG (200 µl IPTG 1M for 500ml) and shake 3h at 30°C
- Harvest by centrifugation and store at -20°C

Purification:

Buffer:

A	**C**
20 mM Tris pH7,9	20 mM Tris pH7,5
500 mM NaCl	0,1 mM EDTA
5 mM Imidazole	100 mM NaCl
10% Glycerol	10% Glycerol
0,5 mM PMSF	

Thaw frozen cells, suspend in 80 ml of buffer A + protease inhibitor(complete) and disrupt by french press. Centrifuge at 48000g, 60min, 4°C. Add filtered supernatant to wash and equilibrate 1h with Ni-NTA Beads. Fill an empty column with the beads and wash with 50ml buffer A and 50 ml A + 20 mM Imidazole. Elute with A + 200 mM Imidazole. Measure the protein concentration with Bradford. Purification with Gelfiltration Sephacryl S200 HR equilibrated with buffer C.

A3 List of publications

- Dehne, H., Hecht, F. M. & Bausch, A. R. The mechanical properties of polymer–colloid hybrid hydrogels. *Soft Matter* **13,** 4786–4790; (2017).
- Dehne, H., Reitenbach, A. & Bausch, A. R. Transient self-organisation of DNA coated colloids directed by enzymatic reactions. *Sci Rep* **9,** 1–9; (2019).

List of figures

Bibliography

1. Dequan, A. L. ed. *Molecular Self-Assembly. Advances and Applications* (Pan Stanford Publishing; Taylor & Francis Group [distributor], Singapore, Florence, 2012).
2. Whitesides, G. M. & Boncheva, M. Beyond molecules: self-assembly of mesoscopic and macroscopic components. *Proceedings of the National Academy of Sciences of the United States of America* **99,** 4769–4774; 10.1073/pnas.082065899 (2002).
3. Jacob N. Israelachvili. *Intermolecular and Surface Forces.* 3rd ed. (Academic Press, 2011).
4. McManus, J. J., Charbonneau, P., Zaccarelli, E. & Asherie, N. The physics of protein self-assembly. *Current Opinion in Colloid & Interface Science* **22,** 73–79; 10.1016/j.cocis.2016.02.011 (2016).
5. Chhabra, R., Sharma, J., Liu, Y., Rinker, S. & Yan, H. DNA self-assembly for nanomedicine. *Advanced drug delivery reviews* **62,** 617–625; 10.1016/j.addr.2010.03.005 (2010).
6. Li, Z., Wang, J., Li, Y., Liu, X. & Yuan, Q. Self-assembled DNA nanomaterials with highly programmed structures and functions. *Mater. Chem. Front.* **2,** 423–436; 10.1039/C7QM00434F (2018).
7. Nagata, K. & Handa, H. eds. *Real-time analysis of biomolecular interactions. Applications of BIACORE* (Springer, Tokyo, New York, 2000).
8. Rothemund, P. W. K. Folding DNA to create nanoscale shapes and patterns. *Nature* **440,** 297–302; 10.1038/nature04586 (2006).
9. Hong, F., Zhang, F., Liu, Y. & Yan, H. DNA Origami: Scaffolds for Creating Higher Order Structures. *Chemical reviews* **117,** 12584–12640; 10.1021/acs.chemrev.6b00825 (2017).
10. Xu, L. *et al.* Nanoparticle assemblies: dimensional transformation of nanomaterials and scalability. *Chemical Society reviews* **42,** 3114–3126; 10.1039/c3cs35460a (2013).
11. Redl, F. X., Cho, K.-S., Murray, C. B. & O'Brien, S. Three-dimensional binary superlattices of magnetic nanocrystals and semiconductor quantum dots. *Nature* **423,** 968–971; 10.1038/nature01702 (2003).
12. Howes, P. D., Chandrawati, R. & Stevens, M. M. Bionanotechnology. Colloidal nanoparticles as advanced biological sensors. *Science (New York, N.Y.)* **346,** 1247390; 10.1126/science.1247390 (2014).
13. Durniak, K. J., Bailey, S. & Steitz, T. A. The Structure of a Transcribing T7 RNA Polymerase in Transition from Initiation to Elongation. *Science* **322,** 553–557; 10.1126/science.1163433 (2008).
14. Sharma, P. Self-Assembly of Colloidal Particles. *Reson* **23,** 263–275; 10.1007/s12045-018-0616-0 (2018).

15. Hoath, S. D. ed. *Fundamentals of inkjet printing. The science of inkjet and droplets* (Wiley-VCH Verlag GmbH & Co. KGaA, Weinheim, 2016).

16. Torres-Carbajal, A., Herrera-Velarde, S. & Castañeda-Priego, R. Brownian motion of a nano-colloidal particle: the role of the solvent. *Physical chemistry chemical physics : PCCP* **17,** 19557–19568; 10.1039/c5cp02777b (2015).

17. Mehta, A. ed. *Granular Matter. An Interdisciplinary Approach* (Springer New York, New York, NY, 1994).

18. Bartlett, P. & van Megen, W. in *Granular Matter. An Interdisciplinary Approach,* edited by A. Mehta (Springer New York, New York, NY, 1994), pp. 195–257.

19. Alder, B. J. & Wainwright, T. E. Phase Transition for a Hard Sphere System. *The Journal of Chemical Physics* **27,** 1208–1209; 10.1063/1.1743957 (1957).

20. Pusey, P. N. & van Megen, W. Observation of a glass transition in suspensions of spherical colloidal particles. *Phys. Rev. Lett.* **59,** 2083; 10.1103/PhysRevLett.59.2083 (1987).

21. Li, B., Di Zhou & Han, Y. Assembly and phase transitions of colloidal crystals. *Nat Rev Mater* **1,** 249; 10.1038/natrevmats.2015.11 (2016).

22. Maranzano, B. J. & Wagner, N. J. The effects of interparticle interactions and particle size on reversible shear thickening: Hard-sphere colloidal dispersions. *Journal of Rheology* **45,** 1205–1222; 10.1122/1.1392295 (2001).

23. Brown, E. & Jaeger, H. M. Shear thickening in concentrated suspensions: phenomenology, mechanisms and relations to jamming. *Reports on progress in physics. Physical Society (Great Britain)* **77,** 46602; 10.1088/0034-4885/77/4/046602 (2014).

24. *Modern Aspects of Bulk Crystal and Thin Film Preparation* (Intech, s.l., 2012).

25. Murray, Cherry A., and David G. Grier. Colloidal Crystals. *American Scientist* **1995,** 238–245.

26. Lazzari, S., Nicoud, L., Jaquet, B., Lattuada, M. & Morbidelli, M. Fractal-like structures in colloid science. *Advances in colloid and interface science* **235,** 1–13; 10.1016/j.cis.2016.05.002 (2016).

27. HUTCHINSON, J. E. Fractals and Self Similarity. *Indiana University Mathematics Journal,* 713–747 (1981).

28. Buczkowski, S., Hildgen, P. & Cartilier, L. Measurements of fractal dimension by box-counting: a critical analysis of data scatter. *Physica A: Statistical Mechanics and its Applications* **252,** 23–34; 10.1016/S0378-4371(97)00581-5 (1998).

29. Sorensen, C. M. The Mobility of Fractal Aggregates: A Review. *Aerosol Science and Technology* **45,** 765–779; 10.1080/02786826.2011.560909 (2011).

30. Lin *et al.* Universal reaction-limited colloid aggregation. *Physical review. A, Atomic, molecular, and optical physics* **41,** 2005–2020; 10.1103/physreva.41.2005 (1990).

31. Verwey, E.J.W. and Overbeek, J.Th.G. Theory of the Stability of Lyophobic Colloids. The Interaction of Sol Particles Having an Electric Double Layer. *Elsevier* **1948**.

32. Kovalchuk, N. M. & Starov, V. M. Aggregation in colloidal suspensions: Effect of colloidal forces and hydrodynamic interactions. *Advances in colloid and interface science* **179-182,** 99–106; 10.1016/j.cis.2011.05.009 (2012).

33. González García, Á., Nagelkerke, M. M. B., Tuinier, R. & Vis, M. Polymer-mediated colloidal stability: on the transition between adsorption and depletion. *Advances in colloid and interface science* **275,** 102077; 10.1016/j.cis.2019.102077 (2020).

34. Banerjee, D., Yang, J. & Schweizer, K. S. Entropic depletion in colloidal suspensions and polymer liquids: role of nanoparticle surface topography. *Soft Matter* **11,** 9086–9098; 10.1039/C5SM02072G (2015).

35. Evander, M. & Nilsson, J. Acoustofluidics 20: applications in acoustic trapping. *Lab on a chip* **12,** 4667–4676; 10.1039/c2lc40999b (2012).

36. Alivisatos, A. P. *et al.* Organization of 'nanocrystal molecules' using DNA. *Nature* **382,** 609–611; 10.1038/382609a0 (1996).

37. Mirkin, C. A., Letsinger, R. L., Mucic, R. C. & Storhoff, J. J. A DNA-based method for rationally assembling nanoparticles into macroscopic materials. *Nature* **382,** 607–609; 10.1038/382607a0 (1996).

38. Angioletti-Uberti, S., Mognetti, B. M. & Frenkel, D. Theory and simulation of DNA-coated colloids: a guide for rational design. *Physical chemistry chemical physics : PCCP* **18,** 6373–6393; 10.1039/c5cp06981e (2016).

39. Varilly, P., Angioletti-Uberti, S., Mognetti, B. M. & Frenkel, D. A general theory of DNA-mediated and other valence-limited colloidal interactions. *The Journal of Chemical Physics* **137,** 94108; 10.1063/1.4748100 (2012).

40. Biancaniello, P. L., Kim, A. J. & Crocker, J. C. Colloidal interactions and self-assembly using DNA hybridization. *Physical review letters* **94,** 58302; 10.1103/PhysRevLett.94.058302 (2005).

41. Wang, Y. *et al.* Crystallization of DNA-coated colloids. *Nat Commun* **6,** 1–8; 10.1038/ncomms8253.

42. Wang, Y. *et al.* Colloids with valence and specific directional bonding. *Nature* **491,** 51–55; 10.1038/nature11564 (2012).

43. Di Michele, L. *et al.* Multistep kinetic self-assembly of DNA-coated colloids. *Nat Commun* **4,** 1–7; 10.1038/ncomms3007.

44. Villadsen, J., Nielsen, J. & Lidén, G. *Bioreaction Engineering Principles.* 3rd ed. (Springer Science+Business Media LLC, Boston, MA, 2011).

45. Panda, S., Hogenesch, J. B. & Kay, S. A. Circadian rhythms from flies to human. *Nature* **417,** 329–335; 10.1038/417329a (2002).

46. Nakajima, M. *et al.* Reconstitution of circadian oscillation of cyanobacterial KaiC phosphorylation in vitro. *Science (New York, N.Y.)* **308,** 414–415; 10.1126/science.1108451 (2005).

47. Stricker, J. *et al.* A fast, robust and tunable synthetic gene oscillator. *Nature* **456,** 516–519; 10.1038/nature07389 (2008).

48. Elowitz, M. B. & Leibler, S. A synthetic oscillatory network of transcriptional regulators. *Nature* **403,** 335–338; 10.1038/35002125 (2000).

49. Boekhoven, J., Hendriksen, W. E., Koper, G. J. M., Eelkema, R. & van Esch, J. H. Transient assembly of active materials fueled by a chemical reaction. *Science (New York, N.Y.)* **349,** 1075–1079; 10.1126/science.aac6103 (2015).

50. Satnoianu, R. A., Menzinger, M. & Maini, P. K. Turing instabilities in general systems. *J Math Biol* **41,** 493–512; 10.1007/s002850000056 (2000).

51. Gelens, L., Anderson, G. A. & Ferrell, J. E. Spatial trigger waves: positive feedback gets you a long way. *Molecular biology of the cell* **25,** 3486–3493; 10.1091/mbc.E14-08-1306 (2014).

52. Chang, J. B. & Ferrell, J. E. Mitotic trigger waves and the spatial coordination of the Xenopus cell cycle. *Nature* **500,** 603–607; 10.1038/nature12321 (2013).

53. Dani, J. W., Chernjavsky, A. & Smith, S. J. Neuronal activity triggers calcium waves in hippocampal astrocyte networks. *Neuron* **8,** 429–440; 10.1016/0896-6273(92)90271-E (1992).

54. Montagne, K., Plasson, R., Sakai, Y., Fujii, T. & Rondelez, Y. Programming an in vitro DNA oscillator using a molecular networking strategy. *Molecular systems biology* **7,** 466; 10.1038/msb.2010.120 (2011).

55. Kim, J. & Winfree, E. Synthetic in vitro transcriptional oscillators. *Molecular systems biology* **7,** 465; 10.1038/msb.2010.119 (2011).

56. Fujii, T. & Rondelez, Y. Predator-prey molecular ecosystems. *ACS nano* **7,** 27–34; 10.1021/nn3043572 (2013).

57. Eu, B. C. & Al-Ghoul, M. *Chemical Thermodynamics* (WORLD SCIENTIFIC, 2018).

58. Mikhailov, A. S. & Ertl, G. in *Chemical complexity. Self-organization processes in molecular systems,* edited by A. S. Michajlov & G. Ertl (Springer, Cham, Switzerland, 2017), pp. 89–103.

59. Franck, U. F. Chemical Oscillations. *Angew. Chem. Int. Ed. Engl.* **17,** 1–15; 10.1002/anie.197800013 (1978).

60. Ross, J., Castleman, A. W., Toennies, J. P., Yamanouchi, K. & Zinth, W. *Thermodynamics and Fluctuations far from Equilibrium* (Springer, Berlin, Heidelberg, 2008).

61. Qian, H. Open-system nonequilibrium steady state: statistical thermodynamics, fluctuations, and chemical oscillations. *The journal of physical chemistry. B* **110,** 15063–15074; 10.1021/jp061858z (2006).

62. Semenov, S. N. *et al.* Autocatalytic, bistable, oscillatory networks of biologically relevant organic reactions. *Nature* **537,** 656–660; 10.1038/nature19776 (2016).

63. Glass, L., Beuter, A. & Larocque, D. Time delays, oscillations, and chaos in physiological control systems. *Mathematical Biosciences* **90,** 111–125; 10.1016/0025-5564(88)90060-0 (1988).

64. Novák, B. & Tyson, J. J. Design principles of biochemical oscillators. *Nature reviews. Molecular cell biology* **9,** 981–991; 10.1038/nrm2530 (2008).

65. Boissonade, J. & Kepper, P. de. Transitions from bistability to limit cycle oscillations. Theoretical analysis and experimental evidence in an open chemical system. *J. Phys. Chem.* **84,** 501–506; 10.1021/j100442a009 (1980).

66. Kinoshita, S. ed. *Pattern formations and oscillatory phenomena* (Elsevier; Elsevier Science, Amsterdam, Burlington, 2013).

67. Oscillatory Rheology. *G.I.T. Laboratory Journal,* 69–70 (2007).

68. Sujit S. Datta. Tutorial: Rheology of Materials. *Derpartmment of Physics, Harvard University*.

69. Chen, Y. C. & Jeng, S. T. Binding affinity of T7 RNA polymerase to its promoter in the supercoiled and linearized DNA templates. *Bioscience, biotechnology, and biochemistry* **64,** 1126–1132; 10.1271/bbb.64.1126 (2000).

70. Anand, V. S. & Patel, S. S. Transient state kinetics of transcription elongation by T7 RNA polymerase. *The Journal of biological chemistry* **281,** 35677–35685; 10.1074/jbc.M608180200 (2006).

71. Kanaya, S. & Crouch, R. J. DNA sequence of the gene coding for Escherichia coli ribonuclease H. *J. Biol. Chem.* **258,** 1276–1281 (1983).

72. Biswas, B. B. & Roy, S. *Proteins: Structure, Function, and Engineering* (Springer US, 2013).

73. Dobosy, J. R. *et al.* RNase H-dependent PCR (rhPCR): improved specificity and single nucleotide polymorphism detection using blocked cleavable primers. *BMC Biotechnol* **11,** 1–18; 10.1186/1472-6750-11-80 (2011).

74. Hogrefe, H. H., Hogrefe, R. I., Walder, R. Y. & Walder, J. A. Kinetic analysis of Escherichia coli RNase H using DNA-RNA-DNA/DNA substrates. *J. Biol. Chem.* **265,** 5561–5566 (1990).

75. Kopecek, J. Hydrogels: From soft contact lenses and implants to self-assembled nanomaterials. *Journal of Polymer Science Part A: Polymer Chemistry* **47,** 5929–5946; 10.1002/pola.23607 (2009).

76. Yahia, L. *et al.* History and Applications of Hydrogels. *Journal of Biomedical Sciences* **4**; 10.4172/2254-609X.100013 (2015).

77. Caló, E. & Khutoryanskiy, V. V. Biomedical applications of hydrogels: A review of patents and commercial products. *European Polymer Journal* **65,** 252–267; 10.1016/j.eurpolymj.2014.11.024 (2015).

78. Slaughter, B. V., Khurshid, S. S., Fisher, O. Z., Khademhosseini, A. & Peppas, N. A. Hydrogels in regenerative medicine. *Advanced materials (Deerfield Beach, Fla.)* **21,** 3307–3329; 10.1002/adma.200802106 (2009).

79. Zhao, F. *et al.* Composites of Polymer Hydrogels and Nanoparticulate Systems for Biomedical and Pharmaceutical Applications. *Nanomaterials (Basel, Switzerland)* **5,** 2054–2130; 10.3390/nano5042054 (2015).

80. Annabi, N. *et al.* 25th anniversary article: Rational design and applications of hydrogels in regenerative medicine. *Advanced materials (Deerfield Beach, Fla.)* **26,** 85–123; 10.1002/adma.201303233 (2014).

81. Hoffman, A. S. Hydrogels for biomedical applications. *Advanced drug delivery reviews* **54,** 3–12; 10.1016/s0169-409x(01)00239-3 (2002).

82. Merino, S., Martin, C., Kostarelos, K., Prato, M. & Vazquez, E. Nanocomposite Hydrogels: 3D Polymer-Nanoparticle Synergies for On-Demand Drug Delivery. *ACS nano* **9,** 4686–4697; 10.1021/acsnano.5b01433 (2015).

83. Bonanno, L. M. & Segal, E. Nanostructured porous silicon-polymer-based hybrids: from biosensing to drug delivery. *Nanomedicine (London, England)* **6,** 1755–1770; 10.2217/nnm.11.153 (2011).

84. Gaharwar, A. K., Peppas, N. A. & Khademhosseini, A. Nanocomposite hydrogels for biomedical applications. *Biotechnology and bioengineering* **111,** 441–453; 10.1002/bit.25160 (2014).

85. Dehne, H., Hecht, F. M. & Bausch, A. R. The mechanical properties of polymer–colloid hybrid hydrogels. *Soft Matter* **13,** 4786–4790; 10.1039/C7SM00628D (2017).

86. Loh, X. J. *In-Situ Gelling Polymers: For Biomedical Applications* (Springer Singapore, 2014).

87. Xu, S., Deng, L., Zhang, J., Yin, L. & Dong, A. Composites of electrospun-fibers and hydrogels: A potential solution to current challenges in biological and biomedical field. *Journal of biomedical materials research. Part B, Applied biomaterials* **104,** 640–656; 10.1002/jbm.b.33420 (2016).

88. FM, H. & AR, B. Kinetically guided colloidal structure formation. *Proc Natl Acad Sci U S A* **113,** 8577–8582; 10.1073/pnas.1605114113 (2016).

89. MacKintosh, F. C., Käs, J. & Janmey, P. A. Elasticity of Semiflexible Biopolymer Networks. *Phys. Rev. Lett.* **75,** 4425; 10.1103/PhysRevLett.75.4425 (1995).

90. Mermet-Guyennet, M.R.B. *et al.* Size-dependent reinforcement of composite rubbers. *Polymer* **73,** 170–173; 10.1016/j.polymer.2015.07.041 (2015).

91. Di Michele, L., Zaccone, A. & Eiser, E. Analytical theory of polymer-network-mediated interaction between colloidal particles. *PNAS* **109,** 10187–10192; 10.1073/pnas.1202171109 (2012).

92. Rueb, C. J. & Zukoski, C. F. Viscoelastic properties of colloidal gels. *Journal of Rheology* **41,** 197–218; 10.1122/1.550812 (1997).

93. Shih, W.-H. *et al.* Mechanical Properties of Colloidal Gels. *MRS Online Proceedings Library Archive* **155**; 10.1557/PROC-155-83 (1989).

94. Zhou, Y. *et al.* Unusual multiscale mechanics of biomimetic nanoparticle hydrogels. *Nat Commun* **9,** 1–11; 10.1038/s41467-017-02579-w.

95. Kamp, S. W. & Kilfoil, M. L. Universal behaviour in the mechanical properties of weakly aggregated colloidal particles. *Soft Matter* **5,** 2438–2447; 10.1039/B814975E (2009).

96. Park, J.-G. *et al.* Full-spectrum photonic pigments with non-iridescent structural colors through colloidal assembly. *Angewandte Chemie (International ed. in English)* **53,** 2899–2903; 10.1002/anie.201309306 (2014).

97. Fan, J. A. *et al.* Self-assembled plasmonic nanoparticle clusters. *Science (New York, N.Y.)* **328,** 1135–1138; 10.1126/science.1187949 (2010).

98. Y, L., N, H., P, L. & V, S. Interaction forces between colloidal particles in liquid: theory and experiment. *Adv Colloid Interface Sci* **134-135,** 151–166; 10.1016/j.cis.2007.04.003 (2007).

99. Meakin, P. Formation of Fractal Clusters and Networks by Irreversible Diffusion-Limited Aggregation. *Phys. Rev. Lett.* **51,** 1119; 10.1103/PhysRevLett.51.1119 (1983).

100. Masuda, Y., Itoh, T. & Koumoto, K. Self-assembly patterning of silica colloidal crystals. *Langmuir : the ACS journal of surfaces and colloids* **21,** 4478–4481; 10.1021/la050075m (2005).

101. Chen, Q., Bae, S. C. & Granick, S. Directed self-assembly of a colloidal kagome lattice. *Nature* **469,** 381–384; 10.1038/nature09713 (2011).

102. Lu, P. J. *et al.* Gelation of particles with short-range attraction. *Nature* **453,** 499–503; 10.1038/nature06931 (2008).

103. Dreyfus, R. *et al.* Aggregation-disaggregation transition of DNA-coated colloids: Experiments and theory. *Phys. Rev. E* **81,** 41404; 10.1103/PhysRevE.81.041404 (2010).

104. Angioletti-Uberti, S., Mognetti, B. M. & Frenkel, D. Re-entrant melting as a design principle for DNA-coated colloids. *Nature materials* **11,** 518–522; 10.1038/nmat3314 (2012).

105. Maltzahn, G. von *et al.* Nanoparticle Self-Assembly Directed by Antagonistic Kinase and Phosphatase Activities. *Advanced Materials* **19,** 3579–3583; 10.1002/adma.200701183 (2007).

106. Angioletti-Uberti, S., Varilly, P., Mognetti, B. M. & Frenkel, D. Mobile Linkers on DNA-Coated Colloids: Valency without Patches. *Phys. Rev. Lett.* **113,** 128303; 10.1103/PhysRevLett.113.128303 (2014).

107. McGinley, J. T., Wang, Y., Jenkins, I. C., Sinno, T. & Crocker, J. C. Crystal-Templated Colloidal Clusters Exhibit Directional DNA Interactions. *ACS nano* **9,** 10817–10825; 10.1021/acsnano.5b03272 (2015).

108. Park, S. Y. *et al.* DNA-programmable nanoparticle crystallization. *Nature* **451,** 553–556; 10.1038/nature06508 (2008).

109. Weitz, D. A., Huang, J. S., Lin, M. Y. & Sung, J. Dynamics of Diffusion-Limited Kinetic Aggregation. *Phys. Rev. Lett.* **53,** 1657; 10.1103/PhysRevLett.53.1657 (1984).

110. Zaccarelli, E. Colloidal gels: equilibrium and non-equilibrium routes. *J. Phys.: Condens. Matter* **19,** 323101; 10.1088/0953-8984/19/32/323101 (2007).

111. Dehne, H., Reitenbach, A. & Bausch, A. R. Transient self-organisation of DNA coated colloids directed by enzymatic reactions. *Sci Rep* **9,** 1–9; 10.1038/s41598-019-43720-7.

112. Buchmann, B., Hecht, F. M., Pernpeintner, C., Lohmueller, T. & Bausch, A. R. Controlling Non-Equilibrium Structure Formation on the Nanoscale. *Chemphyschem : a European journal of chemical physics and physical chemistry* **18,** 3437–3442; 10.1002/cphc.201700844 (2017).

113. Park, N., Um, S. H., Funabashi, H., Xu, J. & Luo, D. A cell-free protein-producing gel. *Nature materials* **8,** 432–437; 10.1038/nmat2419 (2009).

114. Roh, Y. H., Ruiz, R. C. H., Peng, S., Lee, J. B. & Luo, D. Engineering DNA-based functional materials. *Chem. Soc. Rev.* **40,** 5730–5744; 10.1039/C1CS15162B (2011).

115. Chance, B., Ghosh, A. K. & Pye, E. K. *Biological and Biochemical Oscillators.* 1st ed. (Elsevier Reference Monographs, s.l., 1973).

116. Fall, C. P., Marland, E. S., Wagner, J. M. & Tyson, J. J. eds. *Computational Cell Biology* (Springer-Verlag New York Inc, New York, NY, 2004).

117. Qin, X. *et al.* A biochemical network controlling basal myosin oscillation. *Nat Commun* **9,** 1–15; 10.1038/s41467-018-03574-5.

118. Goldbeter, A. Dissipative structures and biological rhythms. *Chaos: An Interdisciplinary Journal of Nonlinear Science* **27,** 104612; 10.1063/1.4990783 (2017).

119. Börsch, A. & Schaber, J. How time delay and network design shape response patterns in biochemical negative feedback systems. *BMC Syst Biol* **10,** 1–10; 10.1186/s12918-016-0325-9 (2016).

120. Reid, M. S., Le, X. C. & Zhang, H. Exponential Isothermal Amplification of Nucleic Acids and Assays for Proteins, Cells, Small Molecules, and Enzyme Activities: An EXPAR Example. *Angewandte Chemie (International ed. in English)* **57,** 11856–11866; 10.1002/anie.201712217 (2018).

121. Weiling, F. Lotka, A. J.: Elements of Mathematical Biology. Dover Publications Inc., New-York 1956; XXX + 465 S., 72 Abb., 36 Tabellen und 4 Übersichtstabellen im Anhang, Preis $ 2,45. *Biometrische Zeitschrift* **7,** 208; 10.1002/bimj.19650070323 (1965).

122. Ménová, P., Raindlová, V. & Hocek, M. Scope and limitations of the nicking enzyme amplification reaction for the synthesis of base-modified oligonucleotides and primers for PCR. *Bioconjugate chemistry* **24,** 1081–1093; 10.1021/bc400149q (2013).